# Europa Lander Docking and Sample Transport System

**MEIE 4701/4702**

**Technical Design Report**

**Europa Lander Docking and Sample Transport System**

**Final Report**

**Academic Advisor: Prof. Randall Erb**
**Industry Advisor: Christopher Yahnker**

**Design Team**
**Eileen Butler, Colin Davis**
**Christopher Kerr, Leo Stolov**
**Kathryn Sweeney**

**December 5, 2017**

**Department of Mechanical and Industrial Engineering**
**College of Engineering, Northeastern University**
**Boston, MA 02115**

## Europa Lander Docking and Sample Transport System

**Design Team**

**Eileen Butler, Colin Davis**

**Christopher Kerr, Leo Stolov,**

**Kathryn Sweeney**

**Design Advisor** **Randall Erb**

**Industry Advisor** **Christopher Yahnker**

# Abstract

Europa, one of Jupiter's moons, may harbor extraterrestial life; proof of which may exist within its icy crust. In the hopes of investigating this potential, the NASA Jet Propulsion Laboratory (JPL) – the industry sponsor for this project – is investigating the concept of sending a lander to Europa that is capable of both collecting surface samples via a robotic arm and conducting analyses of those samples with various scientific instruments located within the lander body. The envisioned lander currently lacks a design for delivering the collected samples from the excavation arm to the instruments. This Capstone project fills that gap by offering a solution termed the Europa Lander Docking and Sample Transfer system (ELDST). The ELDST system can dock the robotic arm, collect samples from the arm via transfer cups, measure sample volumes, transport samples to internal instruments, and resupply the robotic arm with new transfer cups. Docking occurs by mating three hemispherical features on the arm with three radial grooves on a docking platform that has six spring-loaded "legs" and is capable of adjusting in six degrees of freedom. The samples are then transferred from the arm to ELDST using a linear actuator with a passive spring-loaded gripper. After transfer, these samples are transported along the lander body using a lead screw. The sample volume is measured using an infrared proximity sensor. Samples of sufficient volume shall be transported to the scientific instruments in the lander body, while samples of insufficient volume shall be returned to the robotic arm for additional sample collection. Upon the succesful delivery of a round of samples, ELDST shall provide new sample containers to the robotic arm. All these subsystems shall function while withstanding the harsh environment of Europa. A physical prototype based on this design is built and tested to show functionality in an ambient Earth environment. Heat transfer analysis, mechanical analysis, and a particle simulation are used to provide insight into the system's performance in a Europan environment.

# Table of Contents

# List of Figures

# List of Tables

## Acknowledgements

The capstone group would like to thank its academic advisor, Randy Erb, who has been indispensable in helping and offering insight into the design process. Special thanks are also extended to Chris Yahnker for being the lead industry advisor from JPL. Additionally, the team would like to thank Andrew Gouldstone for assisting in the collaboration with the JPL advisors and helping to make this project a viable capstone.

# 1. Introduction

## 1.1. *Europa Mission Summary*

NASA is planning an upcoming mission to explore Europa, a moon of Jupiter. Europa is characterized by its probable large amount of water. Though this water takes the form of ice on the surface, scientific investigations including flyby mission Galileo and imaging from the Hubble Space Telescope suggest a subsurface liquid water ocean. This oceanic subsurface has resulted in Europa being identified as a location potentially suitable for sustaining life. NASA seeks to explore this possibility by sending a lander to the surface of Europa, where it will gather surface samples to examine for signs of past or present life. An artist depiction of this lander is shown in Figure 1.

Figure 1: Artist depiction of lander on Europa surface [1]

This search for life constitutes the main goal of the mission. Of secondary importance is assessing the habitability of Europa, as well as characterizing its surface conditions. Of tertiary importance is determining if Europa has the ability to support life forms. Characterizing the surface conditions will aid in planning any future missions to Europa.

Upon its delivery to Europa, a robotic arm located on the outside of the lander shall extract and package surface samples. These samples will be gathered from 10 cm below the surface of Europa, most likely using a saw excavation tool, and directed into three containers to be transported back to the lander for analysis. The analysis of the surface samples will be carried out by three instruments: an organic compositional analyzer (OCA), a microscope for life detection (MLD), and a vibrational spectrometer (VS). The vital link between the robotic excavation arm and the scientific instruments has yet to be designed [1].

## *1.2. The Three Main Goals of the Europa Lander Mission*

As mentioned in the preceding section, there are three main goals that NASA hopes to achieve during this mission. The goals are (1) to search for the evidence of life, (2) to assess the habitability of Europa and (3) to characterize the surface conditions.

The search for the evidence of life can be characterized by four objectives. The first objective is to detect and characterize any organic indicators of past or present life. The presence of life affects the local ecosystem by creating biomolecules, organic substrates, and end products. Picking up signs of these on the surface of Europa would suggest that life was present and at one point left its chemical mark. This evidence would be found using the OCA. The second objective would be to identify and characterize morphological, textural, or other indicators of life. This would be done by identifying cells or other features connected to biological processes. This would be detected by the MLD. The third objective

would be to detect and characterize any inorganic indicators of past or present life such as biominerals and fossils. These structures must contain chemical and structural attributes uniquely indicative of microbial cells or extracellular processes. The fourth and final objective is to determine the provenance of sampled materials. This is to further understand where the evidence of life comes from and how it can be categorized. This is also to gather supporting evidence to determine if the surface sample is indicative of a potential subsurface ocean.

The second main goal is to assess the habitability of Europa. This encompasses two main objectives, the first of which is to characterize the non-ice composition. Although there is evidence of salts on the surface, it is important to identify exactly those chemicals are. The second is to determine the proximity of subsurface ocean to the surface of Europa. The VS will be the scientific instrument dedicated to this analysis.

The third and final goal of the Europa lander mission is to characterize the surface and subsurface properties. This goal is sub characterized by two objectives, characterize the physical properties of the surface, and to investigate the dynamic processes on and below the surface. This goal is primarily to aid NASA's applied science and engineering technology groups, by providing useful data to be used when developing future missions to Europa [1]. A summary of the three main goals can be seen below in Figure 2.

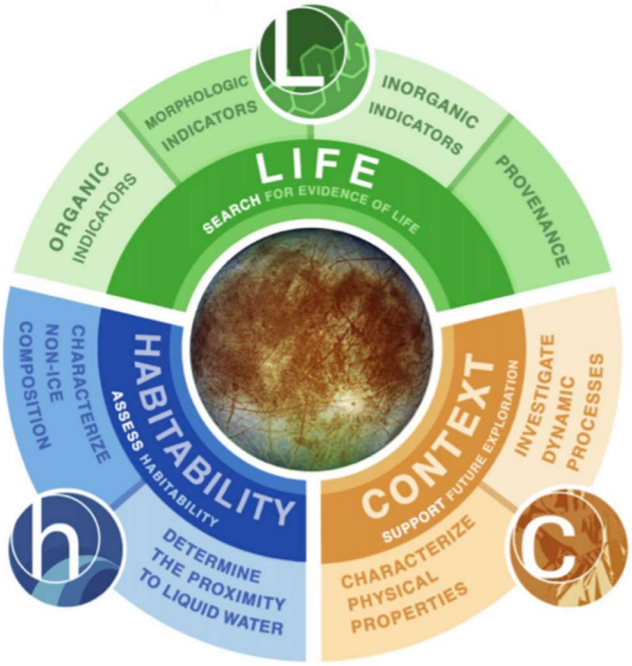


Figure 2: Science Goals and Objectives of the Europa Lander Mission Concept [1]

### *1.3. Mission Specifics*

Before the lander can carry out its tasks, the launch and landing present their own challenges. An overview of the planned timeline from launch to land is illustrated in Figure 3.

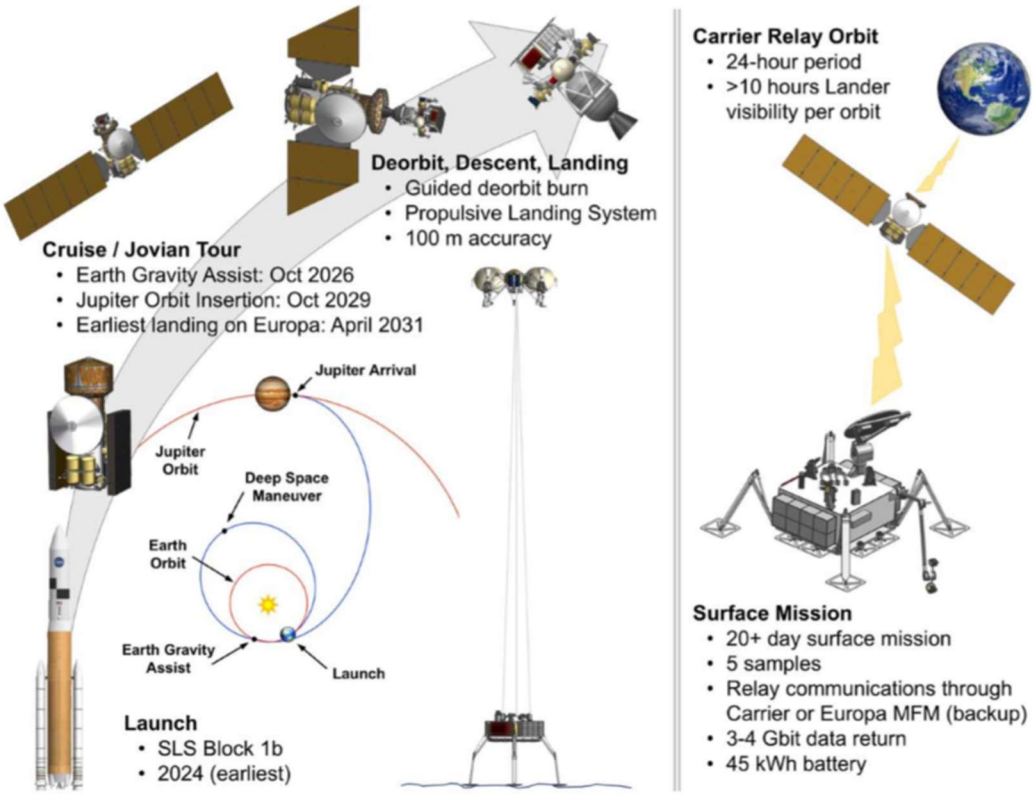


Figure 3: Europa Timeline from Launch to Land [1]

Beginning with the launch tentatively planned for 2024, vibrations created during ascent will shake the module. Landing, currently projected for 2031, also offers a challenge from the expected impact forces and vibrations. Current descent plans include a "sky crane" assisted landing system that will gently lower the lander upon the surface, minimizing impact. Although the effects of ascent and descent are not to be ignored, at JPL's behest they will not be considered a high priority for this project.

Once the lander is stably on the surface, its 20+ day surface mission shall begin, during which five samples will be collected. To do this, the docking and transfer system will have to complete its specified functions in less than 90 minutes. This allotted time begins when the robotic arm presents a sample and ends when the sample is delivered to the scientific instruments.

While there will be communication relay between operators on Earth and the lander, the connection will be intermittent and only occur once per day. Therefore, it is imperative that the system carries out its functions autonomously. There will also be a 45 kWh battery onboard the lander, of which 5% shall be allotted to the system [1].

### *1.4. The Problem Statement*

As mentioned previously, the connection between the excavation arm and scientific instruments is where this Docking and Transport System (henceforth referred to as the "system") is concerned. The placement of this system is shown in Figure 4. In addition to transporting the sample from arm to instruments, it is also necessary to verify that the amount of sample collected is sufficient for use by the instruments. This requires a volume measurement of the sample; a volume outside of the operating range of the instruments would call for additional actions to be taken. An insufficient volume might require the arm to collect more material, while a partial purge might be in order to lower the volume to a specified range. This requirement leads to a refined problem statement, which is: **Design a system for the Europa Lander mission capable of receiving a surface sample from a robotic arm, then verifying and delivering the**

**proper sample volume to the lander's scientific instruments.** The specifics of the individual parts of the problem statement will be explored in the *Requirements* section later in this report.

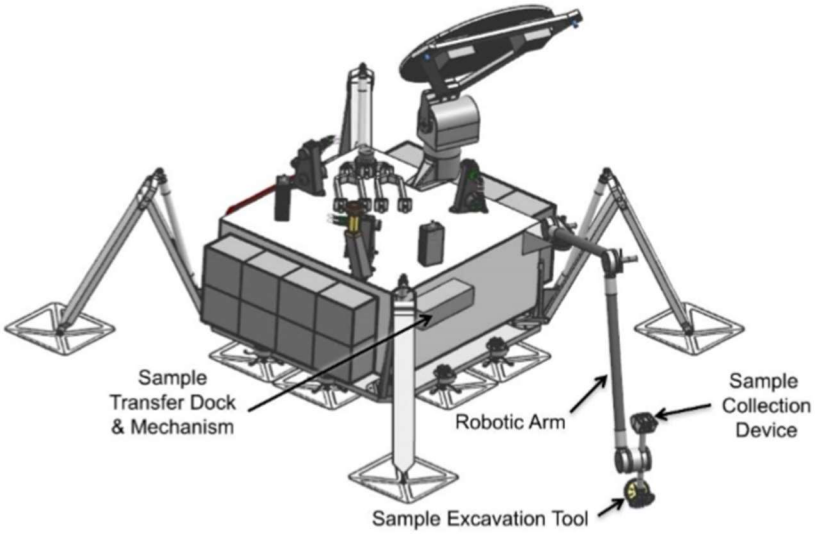


Figure 4: Lander Concept with labeled components [1]

From a macro perspective, the aim of this capstone project is to create a system that will perform its role of docking and material transfer in the harsh environment of space and Europa. Due to time and cost limitations, JPL has advised that rather than create a "flight ready" system, energy should be focused on creating a working prototype with readily available materials and components. Aspects that would be included in a "flight ready" system but will not be included in the prototype shall be comprehensively examined with various analysis techniques, and be offered as a suggestion to JPL.

### *1.5. Introduction to Design*

Now that the context of the Europa lander mission has been introduced, an overview of the current design follows. Figure 5 shows the completed CAD of the prototype design and its home on the lander body. A more detailed and labeled CAD design of the system is shown in Figure 6. All following representations of the system in the section will be simplified to highlight the components of focus, with unrelated parts hidden. This section serves as an outline of the basics of the system; all components will be explored in further detail in later sections.

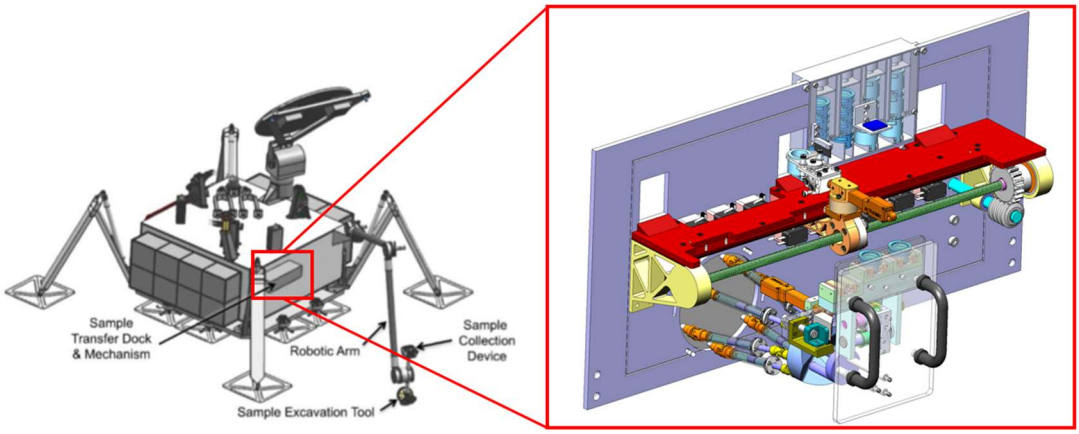


Figure 5 Final prototype CAD and location on lander body

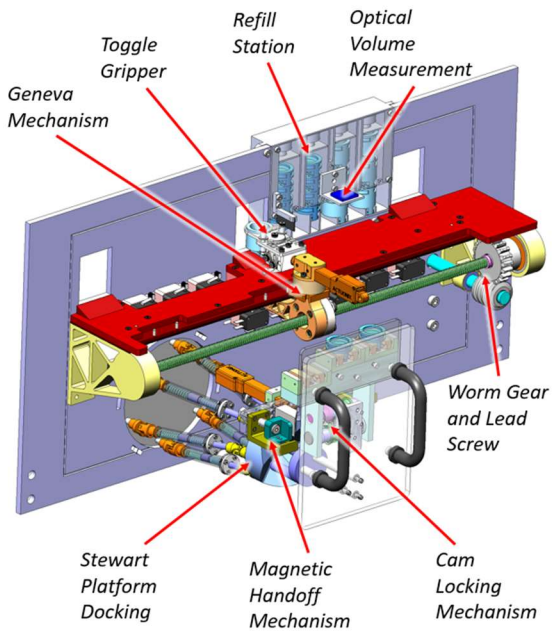


Figure 6: Current System Design

As mentioned in the problem statement, the first major capability of the system is that it must be able to dock the robotic arm and collect the excavated samples. This will be done with the mechanisms highlighted in Figure 7.

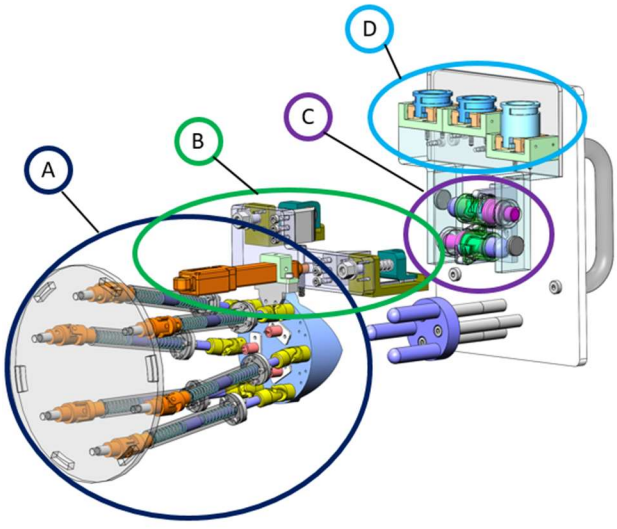


A) Kinematic Coupling and Stewart Platform Docking
B) Magnetic Handoff Mechanism
C) Cam Locking Mechanism
D) Container Tray with Sample Containers

Figure 7: Simplified System - Docking and Locking Mechanism

For docking and aligning the robotic arm, the system uses a kinematic coupling, where three hemispherical features on the arm mate with three radial grooves on the docking platform, in conjunction with a Stewart platform, which has six spring-loaded "legs" and can adjust in six degrees of freedom. This Stewart platform and kinematic coupling are labeled "A" in Figure 7. Once the arm is docked, the

magnetic handoff mechanism, labeled “B” moves toward the cam locking mechanism, labeled “C”, by use of a linear actuator. The cam locking mechanism mounts the container tray with three sample containers, labeled “D”. Two containers hold 1 cc of excavated sample volume while the third holds 5cc. They are mounted to the container tray with passive, spring loaded grippers. The magnet handoff mechanism grabs this container tray and unlocks it from the robotic arm by interacting with the cam locking mechanism. Once the sample container tray has been securely transferred, the robotic arm will move away from the docking platform. This will allow the Stewart platform to move back into its equilibrium position. From this position, the transport mechanisms will come into action.

Figure 8 shows the mechanisms used for transporing the sample containers. Each container is picked up individually with the use of a toggle gripper, labeled “E”. It is attached to a linear actuator, which moves the gripper forward to contact the sample container. With enough force, the toggle gripper triggers, grabs the sample container, and removes it from the bottom gripper.

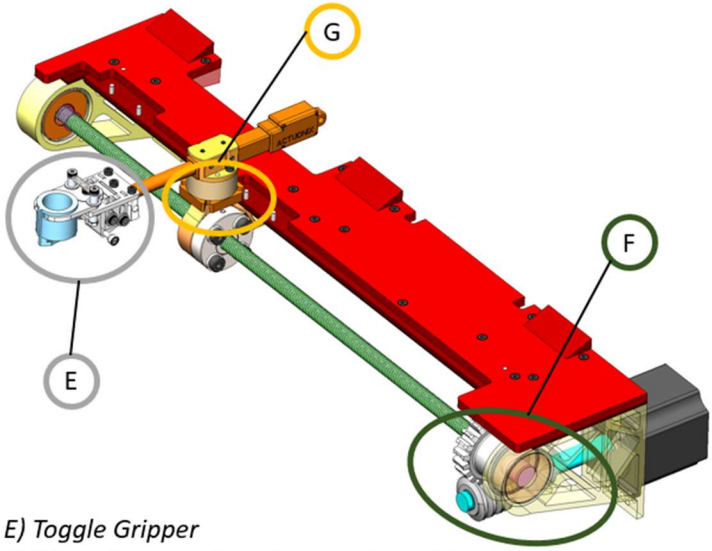


*E) Toggle Gripper*
*F) Worm Drive and Lead Screw Assembly*
*G) Geneva Mechanism*

Figure 8: Transport Assembly

Once the toggle gripper has the sample container, it can be moved across the length of the system. This is done through rotation of the lead screw, which translates the lead nut that the toggle gripper is mounted on. The rotation is provided through a worm gear and worm, which is powered by a stepper motor. This subassembly is labeled “F” in Figure 8. As the container translates, the Geneva mechanism, labeled “G”, interacts with pins on the red platform to passively rotate 180° so that the sample container can face the vault wall. Once the sample container is facing the vault wall, it can be taken to the volume measurement station. The volume measurement station is labeled as “H” Figure 9.

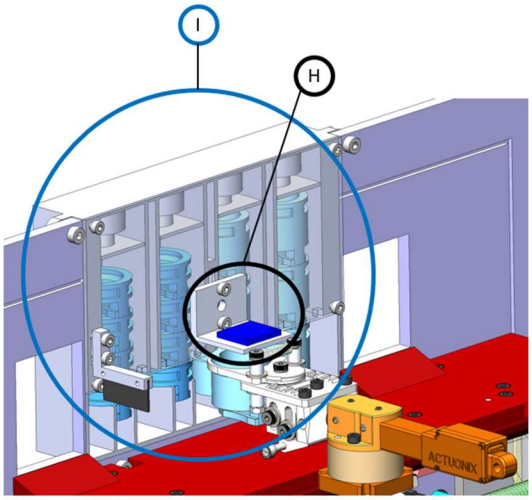


*H) Optical Volume Measurement*
*I) Sample Refill Station*

Figure 9: Volume Measurement and Sample Container Refill

Here, the volume of the sample in the container will be verified using an IR sensor, which measures the distance from the surface of the sample. A container with insufficient sample is returned to the container tray, a container with sufficient sample is transported through the openings to the vault wall, where it is received by a scientific instrument.

Once a sample container is passed to a scientific instrument, a replacement container will need to be brought to the robotic excavation arm. The replacement container will be stored in the refill station, shown in the pink circle labeled "I". When the gripper has a replacement container, another will fall and take its place. The gripper will take the container back to the container tray, allowing the robotic arm to redock, and grab the container tray to collect the next sample.

As mentioned above, more in-depth explorations of the specific components shown in this section will be shown later in this report. This section serves as an introductory view of the presented design concept.

# 2. Background

## *2.1. Europa*

### 2.1.1. Overview

Europa is an icy moon of Jupiter roughly the size of Earth's moon. Its surface gravity is 1.314 m/s$^2$, or about 13% of Earth's gravity. Europa's orbital period matches its rotational period, meaning it is tidally locked with Jupiter and the same side faces the planet at all times [2]. The orbit around Jupiter is elliptical, which means the gravity exerted on Europa by the planet fluctuates during a trip around the planet. This fluctuation creates tidal forces in the moon, which causes it to flex and relax, a phenomenon known as tidal flexing.

Tidal flexing is a source of heat that is thought to be enough to warm the interior of the planet, resulting in a liquid ocean several kilometers beneath the icy surface. Evidence from past missions has resulted in a scientific agreement of the likelihood of a subsurface saltwater ocean, and has elevated Europa to one of the highest priority targets to look for signs of life [3].

### 2.1.2. Surface

The surface environment is most relevant to the lander mission. Perhaps the most challenging condition is the low temperature, which can be anywhere from 130 Kelvin near the equator to 80 Kelvin near the

poles. Since Europa is tidally locked, the surface temperature does not significantly fluctuate at any one point [1].

On the geological scale, Europa is the smoothest body in the Solar System, lacking large mountains and craters. An image collected by NASA is shown in Figure 10.

Figure 10: Image of Europa based on data from NASA's Galileo mission [4]

However, the surface does have large cracks most likely due to tidal flexing, and has been observed to have water vapor plumes jetting out from the subsurface ocean. On the smaller scale, the topography is generally unknown and has the possibility to contain chaotic features due to the active, geological motion of the icy surface on top of the ocean [5]. An artist's depiction of a potential cross-section is shown in Figure 11.

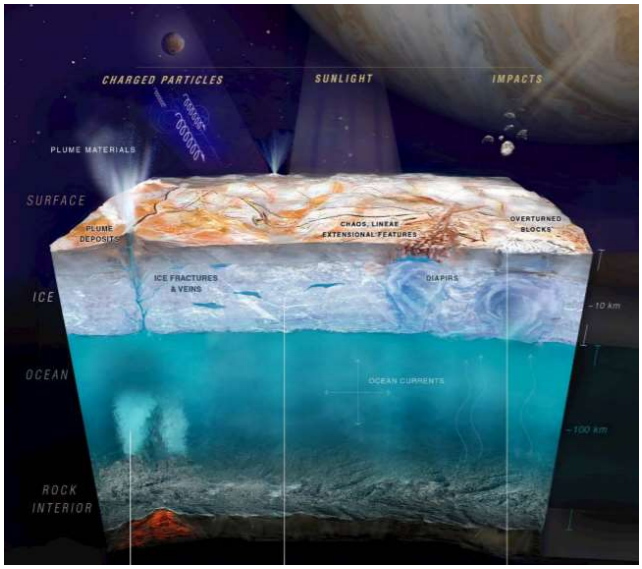


Figure 11: Artist's depiction of a not-to-scale cross section of Europa [1]

One example of such a feature is a penitent, which is a bizarre icy spike structure that has been hypothesized to exist on the surface [6]. The possibility of these features is a major reason why investigations into an excavation tool have thus far favored a saw over a coring drill like the one used for the Mars 2020 mission, since a drill will be more challenged interacting with such chaotic structures [1].

Europa's proximity to Jupiter also means that the moon experiences high amounts of radiation coming from the planet's magnetosphere. This high radiation can damage any technology near the moon and is especially detrimental to electronics. One of the justifications for a lander mission life of around 20 days

is that the lifetime of Carrier Relay Orbiter (CRO), or the orbiter meant transmit data from the lander to Earth, is limited to around 30 days due to the harsh radiation environment [1].

### 2.1.3. Surface Composition

Radiation also affects the composition of the Europan surface. The high-energy particles that constantly bombard the surface can create other chemicals. It is estimated that the surface material on the moon is heavily irradiated down to depths of about 10 cm [1].

However, infrared spectra data has shown that the moon is composed primarily of an ice-salt mixture. The temperature and pressure conditions on the surface also allow for the possibility of amorphous ice, which may behave differently than crystalline ice depending on the time scale of observation. Table 1 shows some of the materials identified on the surface [7].

Table 1: Europan surface composition [7]

| Identification | Method | Wavelength or Region | Comments |
|---|---|---|---|
| $H_2O$ ice | Solar reflectance | 1.5, 2, 3 μm | Amorphous and crystalline |
| Hydrate or hydronium | " | 1.3, 1.5, 2 μm | Salts and/or acid |
| $S_\mu$, $S_4$, $S_8$ | " | 0.3–0.6, 0.53 μm | Trailing/leading-side differences |
| $SO_2$ | " | 0.25–0.32, 4 μm | Trailing-side enhancement |
| $O_2$ | " | 0.577, 0.628 μm | Radiolytic, surface and atmosphere |
| $H_2O_2$ | " | 3.5 μm, 0.2–0.3 μm | Radiolytic |
| $CO_2$ | " | 4.26 μm | |
| Possible transient $NH_3$ $H_2O$* | " | 2.21, 2.32 μm | Possibly spurious* |
| Possible amide features $-NH_2$† | " | 2.05, 2.17 μm | |
| Na, K | Atmospheric resonance scattering | 0.589, 0.590, 0.766, 0.770 μm | In sputter atmosphere and escaping from Europa. |
| $H_2O^+$ | Plasma mass spectra | M/Z = 18 | Pickup ions‡ |
| $H_3O^+$ or $K^{2+}$ | " | M/Z = 19 | § |
| $O_2^+$ | Ion cyclotron waves | | Possible trace pickup ions¶ |
| $Cl^+$, $Cl^-$ | " | | " |
| $Na^+$ or $Ca^+$, $Mg^+$ or $K^+$ | " | | " |
| $SO^+$, $Si^+$ | " | | " |
| Water group atoms and molecules (inferred) | Energetic Neutral Atoms (H) | $H^+$ charge exchange | In gas torus around Jupiter** |
| H†† | Emission spectra | 0.12 μm | " |

Some of the compounds that may also exist on the surface, such as magnesium sulfate and sulfuric acid, can also be corrosive and more difficult to interact with. The size of the particles can also be small and hard to deal with. Table 2 shows the grain size for some non-ice chemicals observed on the surface. The smallest grain size observed with confidence on Europa is 5 μm [8].

Table 2: Europan surface chemicals and corresponding grain size [8]

| Chemical Formula | References | Temperature | Grain Size |
|---|---|---|---|
| **$H_2SO_4.8(H_2O)$** | Carlson et al. (1999b) | 140 K | ~50 $\mu$m |
| **$MgCl_2.2(H_2O)$** | Hanley et al. (2014) | 80 K | / |
| $MgCl_2.4(H_2O)$ | Hanley et al. (2014) | 80 K | / |
| $MgCl_2.6(H_2O)$ | Hanley et al. (2014) | 80 K | / |
| **$Mg(ClO_3)_2.6(H_2O)$** | Hanley et al. (2014) | 80 K | / |
| **$Mg(ClO_4)_2.6(H_2O)$** | Hanley et al. (2014) | 80 K | / |
| $MgSO_4$ brine | Dalton et al. (2005) | 100 K | 50–150 $\mu$m |
| **$MgSO_4.6(H_2O)$** | Dalton & Pitman (2012) | 120 K | 100–200 $\mu$m |
| **$MgSO_4.7(H_2O)$** | Dalton & Pitman (2012) | 120 K | 100–200 $\mu$m |
| $MgSO_4.12(H_2O)$ | Dalton et al. (2005) | 100 K | ~50 $\mu$m |
| $Na_2CO_3.10(H_2O)$ | McCord et al. (2001) | ~100 K | 355–500 $\mu$m |
| **$Na_2Mg(SO_4)_2.4(H_2O)$** | Dalton & Pitman (2012) | 120 K | 125–150 $\mu$m |
| **NaCl** | Hanley et al. (2014) | 80 K | / |
| $NaClO_4$ | Hanley et al. (2014) | 80 K | / |
| **$NaClO_4.2(H_2O)$** | Hanley et al. (2014) | 80 K | / |
| $Na_2SO_4.10(H_2O)$ | Dalton et al. (2005) | 100 K | 100–150 $\mu$m |

### *2.2. Past Missions*

NASA often utilizes spaceflight-proven technology from previous missions, which allows a reduction in the cost of production and an improvement from the overall quality of results, due to the technology being tried and verified via prior applications.

#### 2.2.1. NASA Apollo Missions to Earth's Moon

The first sample collection missions conducted by NASA were the Apollo missions to Earth's moon. The mechanism for the collection and transfer of sample material (in this case, moon rocks) was not very technologically developed, as the astronauts would load a case, called the Apollo Lunar Sample Return Container (ALSRC) with sample specimens by hand [2]. The hinged ALSRC box was made of 7075 AA aluminum alloy and featured a triple seal, which consisted of a knife edge on one side of the box that would cut into the soft metal sealing surface (consisting of 90% indium and 10% silver) on the other side, Teflon covers to protect the seal, and two o-rings made of fluorosilicone [9]. Though relying solely on human power as a transfer application is restricted due to limitations in manned space travel, investigating these missions proved valuable in establishing primary materials used for aerospace applications, and also introduced the concept of using metal seals.

#### 2.2.2. NASA Stardust Mission to Comet Wild 2

NASA's Stardust mission investigated the comet Wild 2. Its sample collection and transfer system consisted of an array of aerogel cells arranged in a two-sided "tennis-racket" shape, which was then directly attached to its sample return canister with a retracting robotic arm [10].

This mission provided the introduction of aerogel as a potential material insulation material. Though in Stardust it was used to capture hypervelocity dust particles from Wild 2, its low density and low thermal conductivity make it an ideal insulator, as it has been used as insulation for the Mars rovers.

#### 2.2.3. NASA OSIRIS-REx Mission to Bennu Asteroid

The Origins, Spectral Interpretation, Resource Identification, Security, Regolith Explorer (OSIRIS-REx) is a NASA sample acquisition mission that launched in September 2016. It is set to investigate the near-Earth asteroid Bennu and collect a regolith sample of at least 60 g for return to Earth. To collect the sample, OSIRIS-REx is equipped with a system, called the Touch-and-Go Sample Acquisition Mechanism (TAGSAM), which consists of an articulated positioning arm that has one plane of motion and sampler head that is designed to retrieve upwards of 150 g of sample to provide margin for the mission requirement. Once OSIRIS-REx reaches Bennu, TAGSAM contacts the surface of the asteroid for a period of up to five seconds, during which it mobilizes the loose top layer with a burst of nitrogen gas, causing sediment passes through the sampler head's filters into storage. After the sample is collected, TAGSAM returns the sampler head to the sample return canister, where one of the cameras from its camera suite, referred to as SamCam, verifies that a sufficient amount of sample has been collected, and once sample acquisition is confirmed, potentiometers in conjunction with another camera, called StowCam, are used to verify the alignment between the sampler head and the sample return canister capture ring (Figure 12) [11, 12].

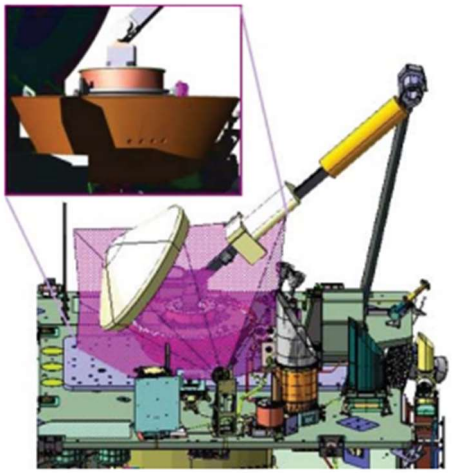

Figure 12: OSIRIS-Rex camera suite inspects for collected sample and help align sampler head into sample return canister capture ring [11]

This mission helped introduce potential solutions to controls challenges, such as using optical imaging for sample verification, as well as combining cameras with sensors such as potentiometers for positioning of sampler head in the capture ring of the sample return container.

### *2.3. Materials*

Selecting potential materials for use in the sample conveyance system are significantly limited due to the extreme environment they will be required to operate in. Not only do the materials need to operate at the cryogenic temperatures found at the surface of Europa, but they must also withstand NASA's standard bake-out procedure, where the system is held at 125°C for 56 days in order to ensure the outgassing of components, Also, due to the very low mass requirement of the system imposed by JPL (2kg), the usage of very low-density materials is crucial, while still maintaining effective material properties.

#### 2.3.1. Structures

Aluminum is the standard material used for aerospace applications, however lower density aerospace materials are available. Promising materials for structural applications include aluminum-lithium (Al-Li) alloys, which offer excellent fatigue and cryogenic toughness properties in addition to low density, as seen in Figure 13. [13, 14]. Li is the lightest elemental metal, and in Al-Li alloys each 1 percent of Li reduces the density of an aluminum alloy by 3%, and increases the elastic modulus by 6 percent [13]. Though currently the applications are very problem specific, they become useful when weight reduction

is a necessity [15]. Several commercial alloys exist, including AA 2090, AA 8090, and AA 8091, which are compared with other metals and alloys in Figure 14 and Figure 15.

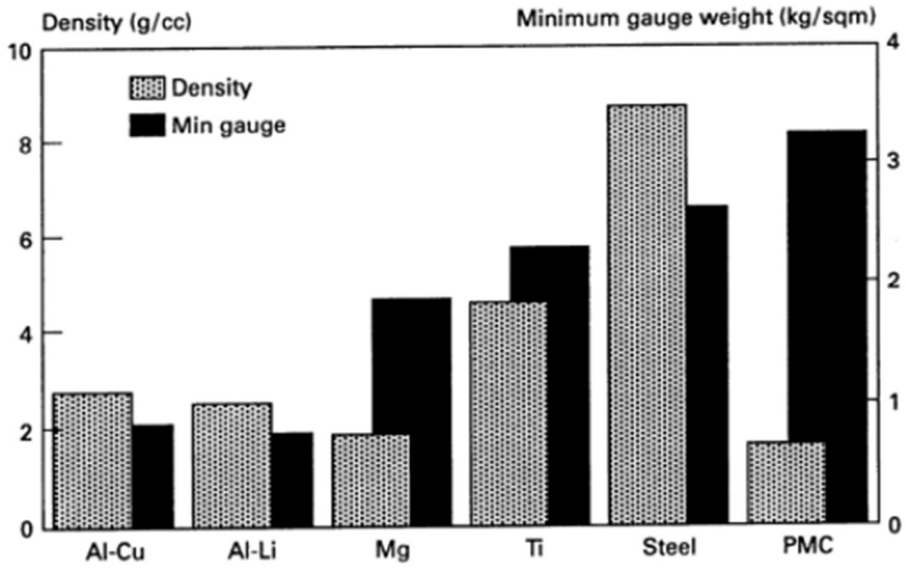


Figure 13: Comparison of the densities and the weight of the minimum gauge for various aerospace metals and alloys [16].

AA 2090 was developed to match the high-strength AA 7075-T6, and has the highest strength of all Al-Li alloys. Its tensile strength is almost 20 percent greater than that of conventional alloys, such as AA 2019 and AA 2014. Meanwhile, AA 8090 has 15 to 20 percent lower strength than AA 2090, but has improved damage tolerance and short-transverse toughness [14].

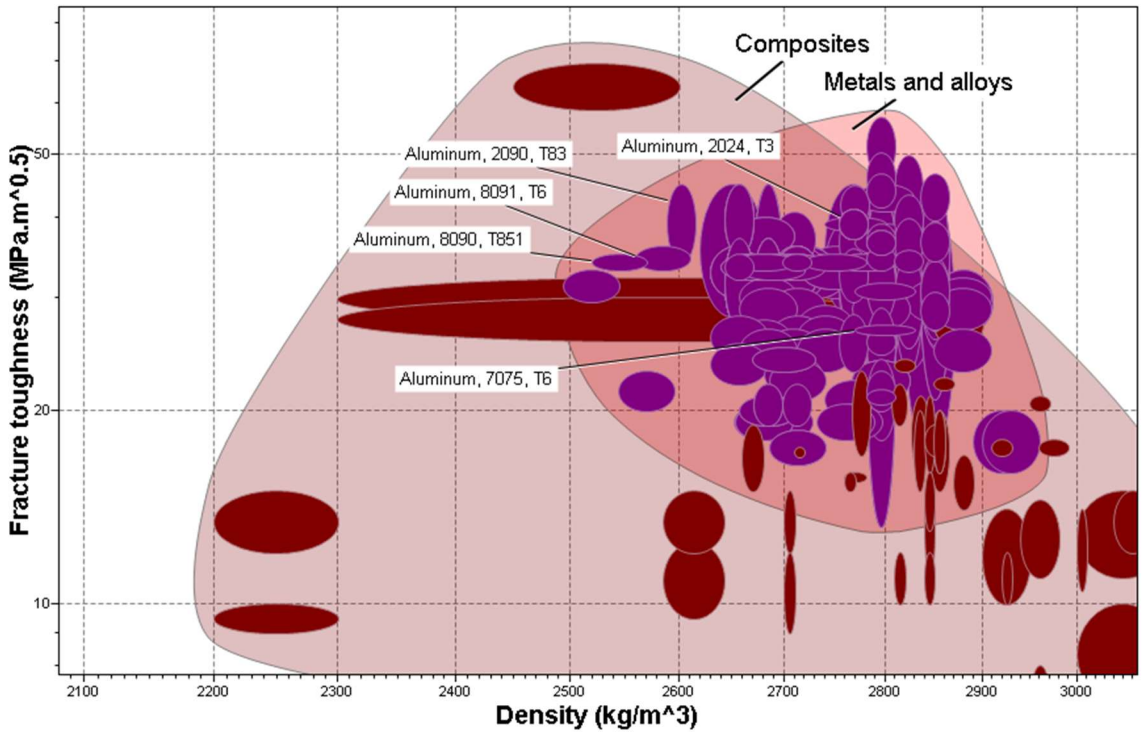


Figure 14: Density vs fracture toughness of aluminum alloys

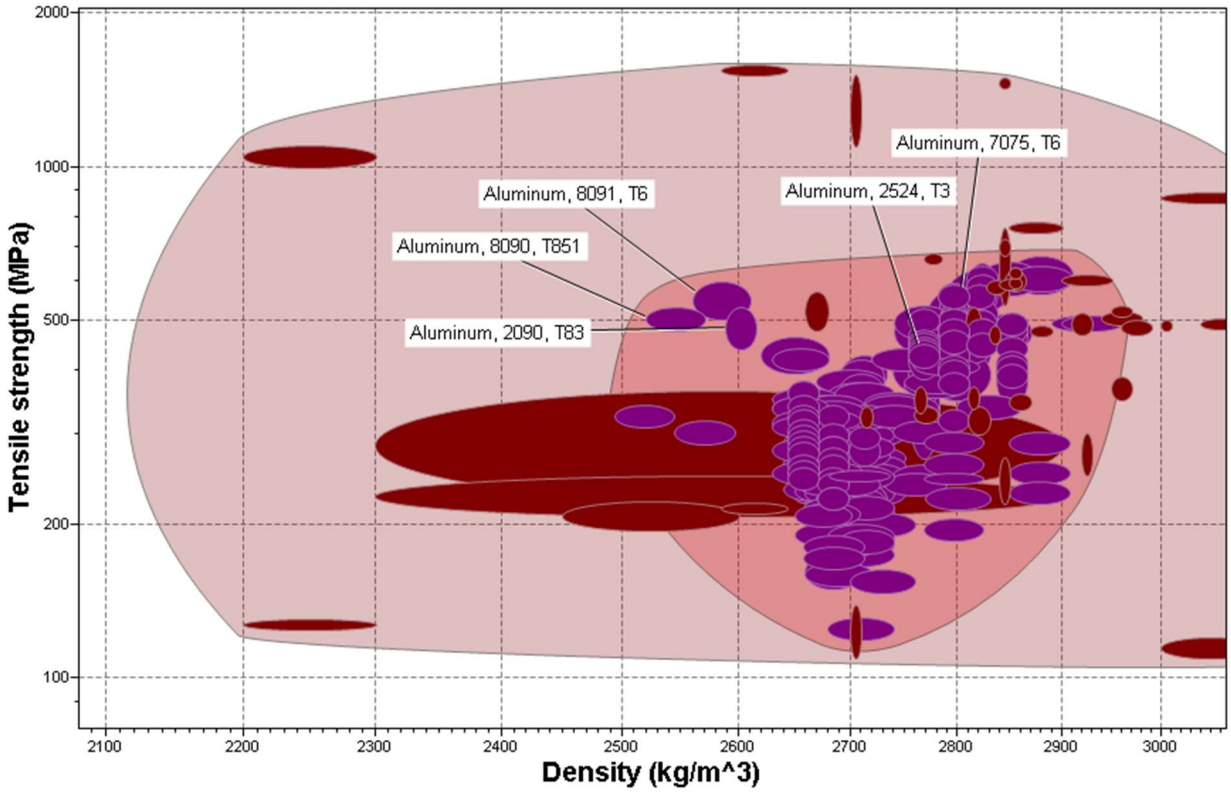


Figure 15: Density vs tensile strength for aluminum alloys

### 2.3.2. Aerogel

Most aerogels are silica-based, similar to glass, however they exhibit a variety of unique physical properties as seen in Table 3**.** By volume, they are 99.8 percent air and 0.2 percent silicon dioxide, and because they are mostly air, they have extremely low densities (as low as 0.001 g cm-3), and thermal conductivities (as low as 10 mW/m*K), as the heat conduction of the gas phase is very poor [17, 18, 19]. Those are very strong and can support up to 4000 times their own weight, though historically they have low fracture toughness and relatively low compressive strength. However, innovations such as reinforcing silica-aerogels with polymers can result in an aerogel that maintains its low density, but is two orders of magnitude stronger, while creating aerogels made entirely of polymers can be made into bendable thin films [19].

Table 3: Physical Properties of Silica Aerogel [18]

| Property | Silica Aerogel | Silica Glass |
|---|---|---|
| Density ($kgm^3$) | 5-200 | 2300 |
| Specific Surface Area ($m^3/g$) | 500-800 | 0. 1 |
| Refractive Index at 632.8 nm | 1.002 – 1.046 | 1.514 – 1.644 |
| Optical Transmittance at 632.8 nm | 90% | 99% |
| Coefficient of Thermal Expansion 1/C at 20-80 °C | $-2 \times 10^{-6}$ | $10 \times 10^{-6}$ |
| Thermal Conductivity (W/mK) at 25 °C | 0.016 – 0.03 | 1.2 |
| Sound Velocity (m/s) | 70 - 1300 | 5000 - 6000 |
| Acoustic Impedance ($kg/m^2/s$) | $10^4$ | $10^7$ |

| | | |
|---|---|---|
| Electric Resistivity (ohm-cm) | $1 \times 10^{18}$ | $1 \times 10^{15}$ |
| Dielectric Constant at 3 – 40 GHz | 1.008 – 2.27 | 4.0 – 6.75 |

### 2.3.3. Material Properties at Cryogenic Temperatures

Although it is often not considered in most everyday applications, many material properties can vary with temperature. Due to the extreme cryogenic temperatures of Europa, it cannot be assumed that all materials used in the system design will exhibit the same properties during the mission as they do in an ambient Earth environment. Because of this, special considerations and analysis must be taken to ensure that the system design will perform as intended in the Europan environment.

The material properties of greatest concern that will vary with temperature are material strength, ductility, elasticity, and thermal conductance. For most materials, the yield strength, tensile strength, elasticity modulus, hardness and fatigue resistance all increase as temperature lowers. Many metals and alloys lose ductility as temperature decreases, making them more susceptible to fractures and failures at low stress levels. Some metals remain ductile at extreme cryogenic temperatures, such as aluminum, nickel, titanium, lead, copper and silver while other materials exhibit more complex behaviors [20]. Many of these relationships have been empirically measured and documented in detail, such as in Figure 16. Thermal conductance can also vary greatly with decreasing temperature, as shown for aluminum in Figure 17.

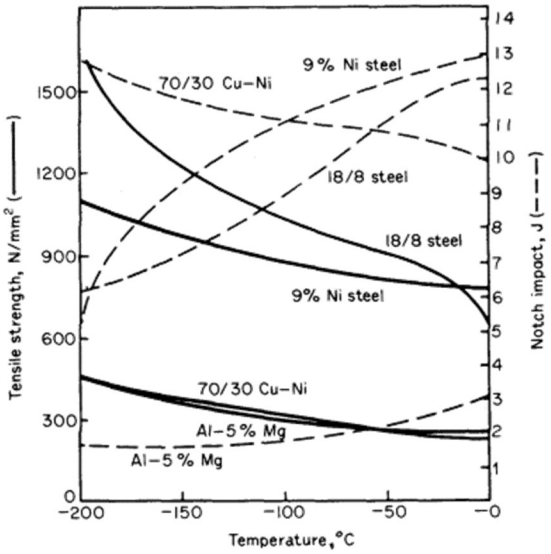


Figure 16: Tensile Strength of steel at cryogenic temperatures [21]

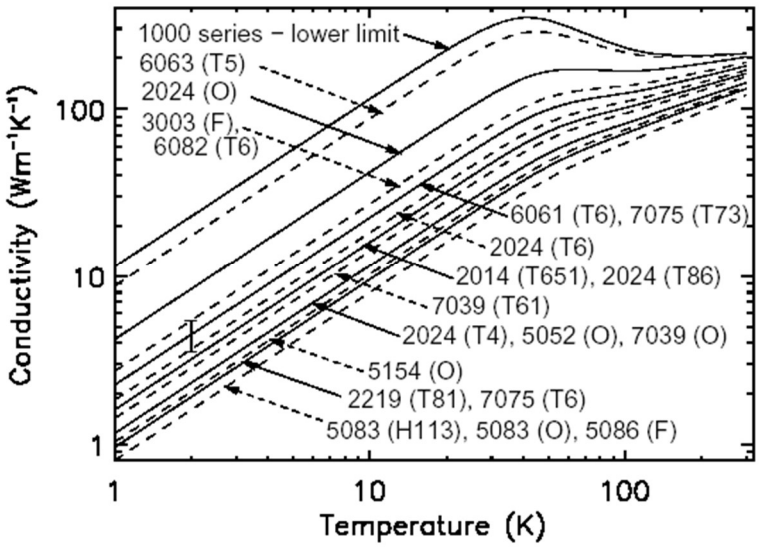


Figure 17: Thermal conductivity of aluminum at cryogenic temperatures [22]

Also of concern is thermal expansion and contraction of components. When materials are heated they expand and when they are cooled they contract in a manner driven by the material's thermal expansion coefficient, seen in Figure 18. This can lead to compatibility and tolerance issues between two parts of an assembly. Components that once fit together and operated smoothly may be too close or too far away at significantly lower temperatures. When two materials with different thermal expansion coefficients are constrained together in a design, it is possible that one will contract or expand faster than the other, resulting in thermal expansion induced stress. Unchecked, this can result in the excessive deformation or failure of a component.

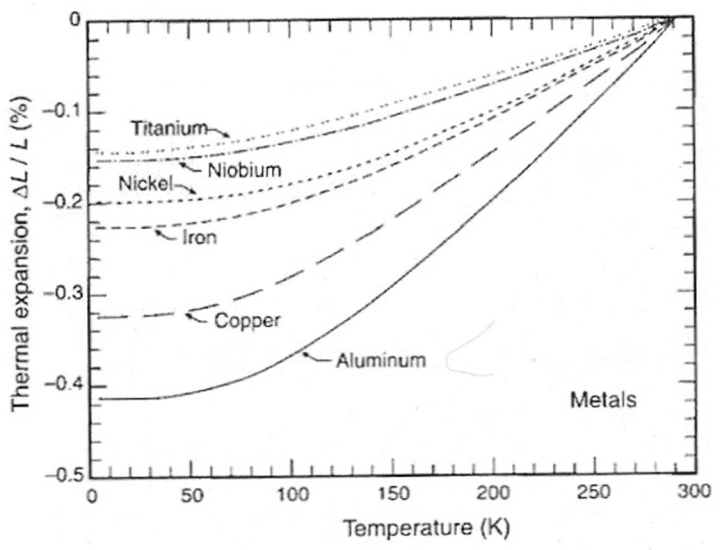


Figure 18: Thermal expansion coefficients of metals at cryogenic temperatures [23]

Two approaches can be taken to ensure that the system will operate properly at low temperatures. First, the system can be constructed out of materials that show little variance with temperature in important material properties, such as choosing materials with low coefficients of thermal expansion. Second,

analysis can be done to account for the change in material properties due to temperature and show that the system will function as required in a mission environment.

## *2.4. Handling of Fine Powders in Industry*

### 2.4.1. Volume Measurement

As stated in the Europa Background section, the surface will likely consist of fine ice crystals and salts. This combined with JPL's probable use of a saw for surface sample collection, the team concluded that there is a strong possibility that the sample will be a fine, powder-like material. This means that there is a chance the system may have to interface with fine powders. The team looked to the pharmaceutical industry for inspiration regarding the handling of fine powders, as in virtually every step of the manufacturing process for solid drugs, powders must be handled securely and in known quantities.

In a paper written by pharmaceutical scientists Deliang Zhou and Yihong Qiu, various techniques for measuring properties of fine powders are compared [24]. This entails knowing very accurately the volumes, and masses being dealt with, which in turn requires knowledge of the relationship between powder flow and compaction. Powder flow and powder compaction are dependent on material and mechanical properties of the sample. At small enough grain sizes, fine powders can exhibit fluid-like flows, opening up otherwise difficult to understand situations to fluid dynamics analysis. These flows are typically examined under the influence of the Earth's gravity however; their fluid-like properties would not hold true in the low gravity environment of Europa. Additionally, the exact nature of the powder is as of yet unknown, making it difficult to translate powder behavior to understandable analysis.

In a paper authored by Joseph D Lewis, several methods are outlined for measuring levels of bulk solids in bins, hoppers, and silos. The outlined methods include weights and cables, ultrasonic and guide wave radar, thru-air radar, lasers, load cells, and strain gauges. To use a weight and cable for surface level measurement, the weight is dropped to the surface of the material and distance to it measured. Translating this method to a smaller scale was not considered because particle simulation, discussed in section 5.3, showed that on Europa particles could be highly responsive to any agitation (possibly escaping the container) and sample contamination was likely. Using ultrasonic waves to measure sample height relative to its container is not possible in a vacuum; the negligible atmosphere of Europa would result in inaccurate results. Load cells and strain gages can be used to determine forces such as mass, however the very low gravity on Europa meant gravity could not be use to facilitate any movement or measurement. Additionally, using mass to determine volume requires significant knowledge about material composition; the sample to be found on Europa is an unknown. [25]

One other industry that works with fine powders is the food industry. When it comes to measuring the volume of the powders they work with, it was mostly based on either the weight of the powder or the container they were filling. For the purposes of this project, a volume measurement is required, and not a weight measurement, and what is incorporated in the project is the sample container volume. By making the internal volume of the sample container the required volume for the instruments to use, the upper limit of the sample range is eliminated, because the container cannot physically hold more volume than the required sample volume.

### 2.4.2. Transportation

The pharmaceutical industry also has a number of transportation processes that move and separate powders. One common technique for transporting these powders is granulation, that being the transformation of fine powders into larger grains or granules, and transporting that. In a paper by Srinivasan Shanmugam, various granulation techniques are discussed, most of which include adding material to a powder that changes its consistency, and then removing the added material later. Figure 19 below shows one example of a granulation technique used in the transport of fine powders [26]. The figure also shows that gravity plays a large role in the transportation of the powders. This is evident in

both the conveyer belt system, and the blend/roller system. The food industry also primarily uses conveyor belts for transporting powders. Because the lander will be operating in Europan gravity, and possibly at an angle of up to 30 degrees to the normal of the surface, gravity is not a reliable force to design the system around. This is one example out of a number of granulation techniques, all of which require a number of process to transform fine powders into easily maneuverable substances.

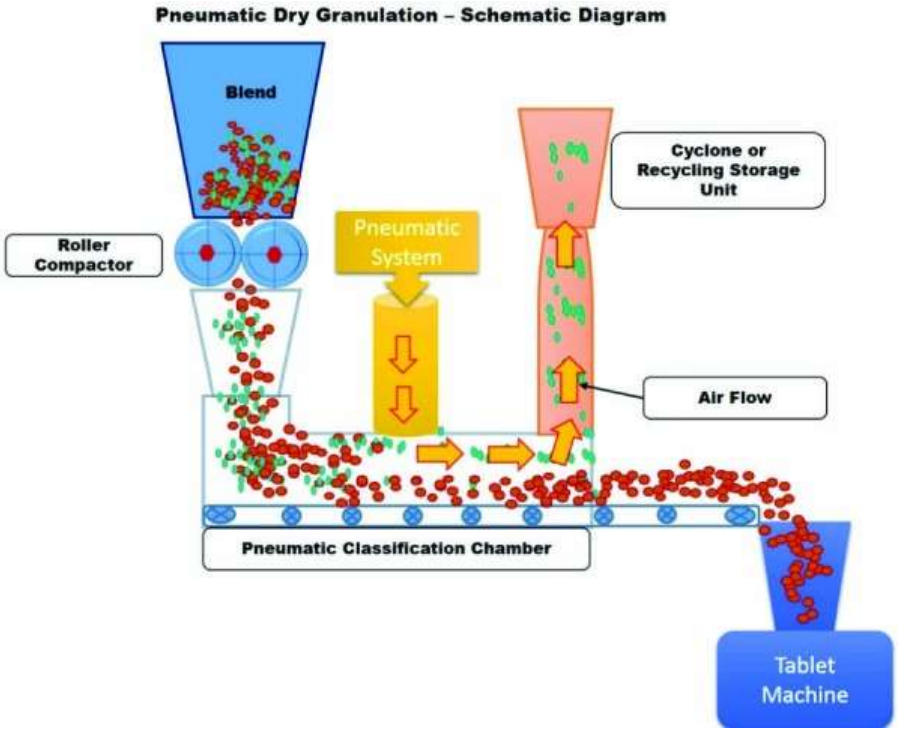


Figure 19: Example of Granulation Process in Pharmaceutical Industry [26]

## 2.5. ***Component Industry Research***

### 2.5.1. Docking Literature Review

When considering the docking of robotic arms in industry, there were few examples to draw from. The most prominent usage of docking technology came from past space exploration and sample retrieval missions. A popular form of docking for satellites is a docking ring. Figure 20 depicts a basic docking ring.

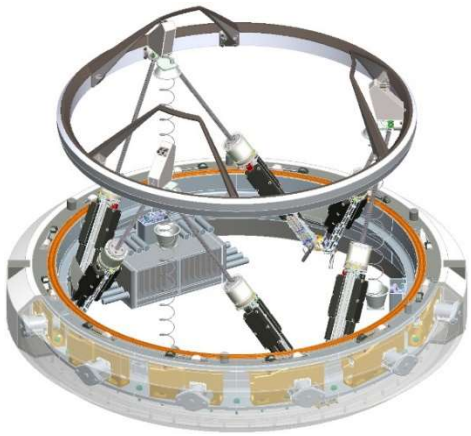

Figure 20: Example of a docking ring [27]

Although docking rings are primarily used for satellite docking, the basics of docking can be considered the same for the purposes of this project. The International Docking System Standard (IDSS) Interface Definition Document (IDD) shows the fundamentals of docking [28]. The article suggests that having a soft capture mechanism, which is a mechanism that does not hold the mating feature but guides it, should lead into a hard capture mechanism, which is mechanism that physically locks and holds the mating feature. This would be a good mechanism for the subsystem, because of the limited precision of the robotic arm. The soft capture would guide the robotic arm into the hard capture mechanism. This protects the arm and the module from any potential damage from collision. Once the arm is guided into the hard capture mechanism, the subsystem will be able to know the exact spatial location of the arm and sample. The most useful aspect of this design is that it promotes little to no energy input. Depending on the choice of hard locking, the power required to lock the arm could be little to none.

Another docking mechanism explored was the Mars 2020 rover sample handling system. Depicted on the NASA website, the robotic arm that collects the surface sample docks using a docking ring with posts on it [29]. With the added posts, this significantly increases the accuracy and repeatability of the subsystem. The posts allow for multiple degrees of freedom as opposed to just a docking ring, but the ring is a good hard capture mechanism. Because the mission has yet to be launched, its usefulness is still unknown. This is something the team will keep in mind while looking into more docking mechanisms.

### 2.5.2. Gripping Literature Review

Methods of gripping can be broken into four categories: impactive, ingressive, astrictive, and contigutive. An impactive grip on the end effector would entail the sample being securely grasped, most likely by a multi-fingered “claw” or chuck. The security of the retention depends on the geometry of the interfacing components, as well as the number of contact points generated by said geometry. Generally, the more contact points between and end effector and its target, the more secure the grip. Figure 21 below illustrates a standard two claw grip outfitted with a controls system, used to pick up a variety of objects.

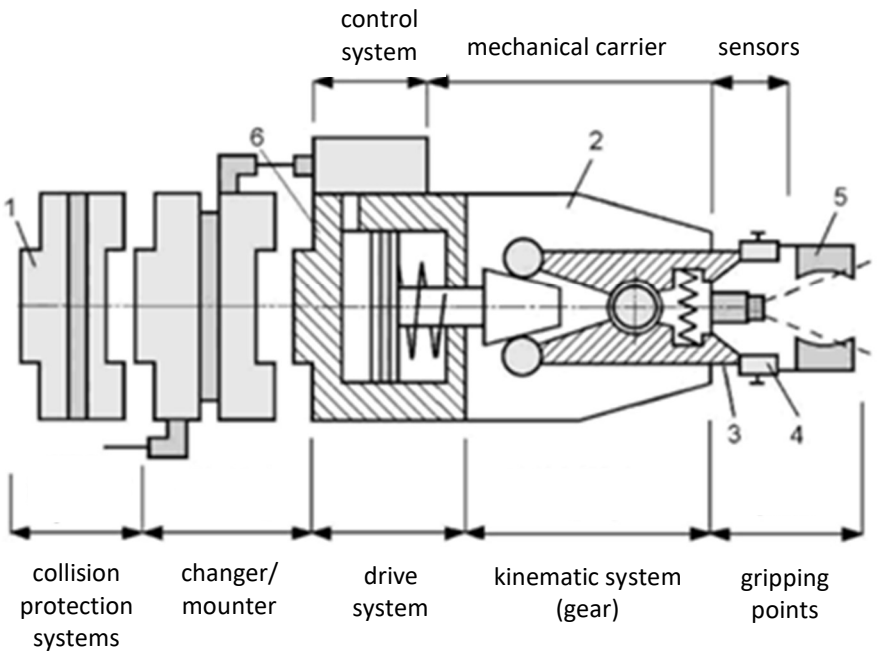


Figure 21: Two claw grip with control system [30]

An ingressive end effector is similar to an impactive one in that its success is dependent upon the geometry of both grip and sample; a penetrative mating feature on either one allows for the securing of the container. Success of this end effector would be highly reliant upon the orientation of the container.

Astrictive grippers offer an exciting solution to picking up objects; a field produces a binding force capable of supporting the gripped load. There are several ways to accomplish this, such as through air movement, magnetism, or electrostatic charge. The force temporarily connects the container to the grip so long as it is applied.

A contigutive grip is one that relies on adhesion between two touching surfaces to be viable. Chemical and thermal adhesion are validated forms of contigutive gripping, however both solutions would complicate the release of the sample as well as present thermal challenges [30].

### 2.5.3. Volume Measurement Literature Review

One solution to determining the amount of sample material present is optical volume measurement. In this method, laser or radar scanners directed at an open face of a container of known dimensions determine the level of material with respect to its container. An artist's rendering of this technology can be seen below, in Figure 22.

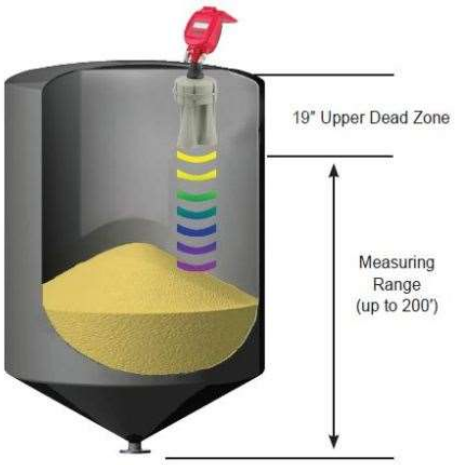


Figure 22: Artist depiction of optical volume measurment [31]

The level of the surface is mapped out over the area in question; the average of this is determined and when compared with the container volume, an accurate volume measurement can be provided. This technology is particularly useful in high-dust, low-dielectric situations. At present, however, optical volume measurements are used primarily in large-scale, industrial applications [31].

Capacitive sensing offers another potentially non-contact solution. One or more sensors measure the capacitance between either the ground and sensor, or the transmitting and receiving sensors. One common application of this technology today is water level monitoring in personal coffee machines. As seen in Figure 23 below, change in sample height creates a change in the amount of signal reaching an array of sensors. Calibrating the sensors for the dielectric constant of the material measured allows for a high degree of accuracy. This technology could even perhaps be incorporated into the containers themselves [32].

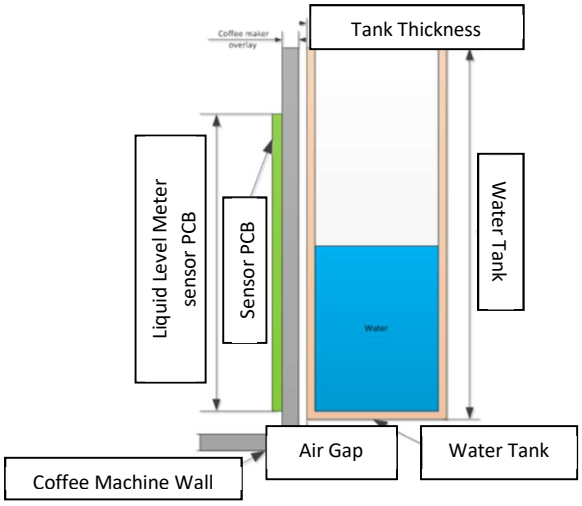


Figure 23: Capacitive Sensing of Water Level

Although typical mass scales would not be particularly useful in this mission situation, JPL is currently developing their piezoelectric mass-sensing technology. Piezoelectric materials emit an electric charge in response to applied mechanical stress. When using flextensional actuators to both measure the piezoelectric balance via voltage produced across the piezoelectric and the frequency change with respect

to a fundamental resonance of the piezoelectric material, two independent calculations for mass could be made and verified against each other [33]. Figure 24 below demonstrates how two measurements could be conducted at once.

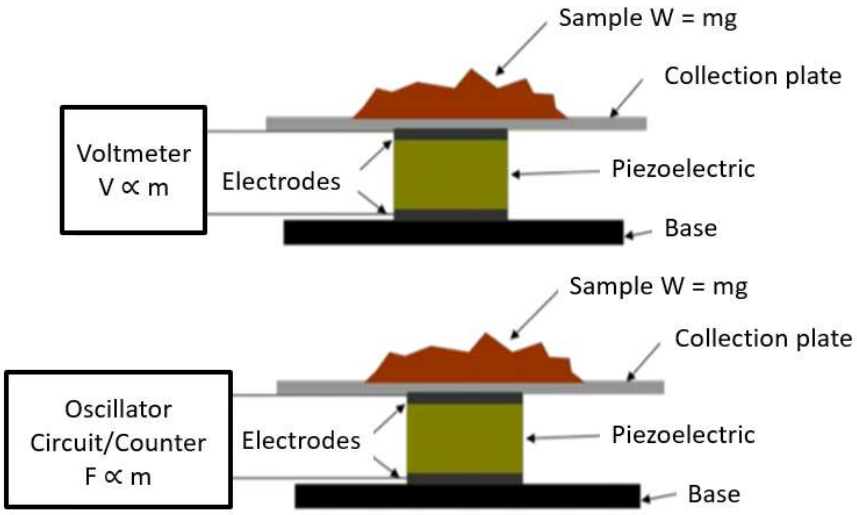


Figure 24: Piezoelectric dual measurement capabilities [33]

One other concept proposed during group brainstorm is to determine the level of sample via calibrated contact with sample, and using the known sample container dimensions to determine volume. A rough sketch of the idea can be seen below in Figure 25.

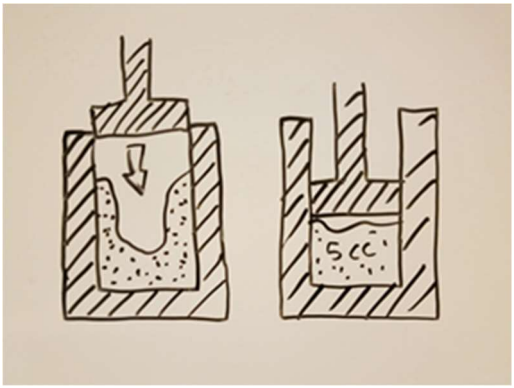


Figure 25: Volume Measurement Through Calibrated Contact Sketch

### 2.5.4. Sample Transfer Literature Review

One of the first concepts developed for the movement of the sample containers was a robotic arm. A robotic arm could offer high mobility depending on the degrees of freedom, allowing for the samples to be delivered quickly and smoothly. NASA is currently developing a smaller robotic arm to assist a larger, sample-collecting arm for the Mars 2020 project, suggesting a robotic arm might be a viable option for this situation. Concerns have been raised, however, about the potential weight of such a mechanism [34].

Simpler mechanisms for transferal have also been investigated. Linkages, systems of rigid links connected at joints via bearings, are mechanisms that manage force and movement. Depending on the geometry and degrees of freedom found in the kinematic chain, linkages can be designed to follow set

paths given a known or predetermined input. Designing a linkage is of interest as it can be constructed to be low weight yet strong, and be highly tailored to follow a desired path [35].

Even simpler mechanisms are belt and chain drives, which use a motor and either a belt or chain to drive a load along a linear pathway. These are also under high consideration, as they can be made quite strong and light. These drives could possibly be coupled with an end effector in a manner bestowing a high degree of maneuverability to the transfer event [36].

In all concepts, the issue of timing will be a concern. The fewer controls required to operate the transfer, the more robust the system will be, and better equipped to deal with as of yet unforeseen issues. Many forms of mechanical timing have been considered, from cams and timing belts to specialized gear drives such as a Geneva Wheel and sample carousel [37].

# 3. Requirements

The requirements of the Docking and Sample Transfer System come from detailed discussions with industry advisor Christopher Yahnker of NASA Jet Propulsion Laboratory and from the NASA Europa Lander Science Report [1]. Here, all requirements have been separated into three categories to be discussed in detail. For a requirements summary table, see Appendix A.

## *3.1 Basic Functional Capabilities*

To fulfill the problem statement, the following four basic functional capabilities must be met.

### 3.1.1. Robotic Arm Docking

As the lander robotic arm transfers the sample container to the lander vault, the system shall provide a docking subsystem to receive and secure the robotic arm and sample cup. This requires a device to mechanically lock the robotic arm to the system before any further operations take place. An electromechanical sensor is necessary to detect the incoming robotic arm and to alert the lander's computer that the sample has docked and is ready to proceed. The docking mechanism shall be compatible with a 4-DOF robotic arm and shall be capable of tolerating an accuracy of ±3 cm and ±2° from the robotic arm. The docking mechanism shall also have the ability to release the container back to the robotic arm in the case where additional sample must be retrieved before further processing can continue.

### 3.1.2. Container Prehension and Retention

While the robotic arm has been docked, the system shall securely grasp and hold the sample both in tandem with and independent of the robotic arm. The system shall maintain secure control of the container until it is delivered to the appropriate scientific instrument.

### 3.1.3. Volume Measurement Device

The system shall determine if the volume of sample in the delivered container is acceptable to within ±5% accuracy and if it eligible to be delivered to the three scientific instruments. The lander will deliver three samples per excavation site of the following volumes: one (1) 5 cc sample and two (2) 1 cc samples. It is expected that the excavation and packaging process will fill the sample containers within a tolerance of +10%/-0%, however the volume measurement device should be capable of measuring the fault cases where there is less than or more than the required sample volume in the container.

In the event that there is not enough sample, a decision shall be returned to the robotic arm for further collection.

### 3.1.4. Sample Transfer and Delivery

After the sample container is gripped, the sample volume is deemed acceptable and the robotic arm releases the sample, the sample transfer mechanism shall deliver the three containers to their respective scientific instruments. The doors to these scientific instruments shall be linearly arranged on the vault wall and spaced approximately 20 cm apart.

#### 3.1.5. A Note on Containers

While this capstone project does not focus on the container aspect of sample collection, the design and delivery of the containers is inherently important to the feasibility of the proposed system. Container development is still in the early design stages at the time of this writing, and so assumptions and/or recommendations about the containers must be made.

It is assumed the system shall receive three containers of uniform dimensions per excavation site. For the collection to be considered successful, the containers shall contain one (1) sample of 5 cc and two (2) samples of 1 cc. These containers will be delivered to and processed by the system one container at a time. To avoid contamination between excavation sites, sample containers shall not be reused for multiple samples. While successful design of a sample container is not an explicit goal of this capstone project, a geometrically representative prototype will likely be required for system testing purposes.

### *3.2 Performance Capabilities*

In addition to the main functional capabilities detailed above, the system must also meet the following performance capabilities.

#### 3.2.1. Environment

The system shall be able to perform in the environment of Europa. To do this, the system shall be capable of operating in an environment where the temperature ranges between 80 K-130 K, the acceleration due to gravity is 1.35 $m/s^2$, and there is a high vacuum (0.1 μPa). All electronics shall be tolerant of high radiation and shall be rated to 300 kRad. System materials shall be resistant to corrosion from $H_2SO_4$ and $MgSO_4$. The system shall also be tolerant of challenging terrain and therefore functional at an orientation of ±30° from the gravity vector. It should also be noted that the system shall survive the standard NASA bakeout procedure on Earth prior to launch of 56 days above 125°C.

#### 3.2.2. Thermal Management

The system shall not alter the material properties of the samples before they are delivered to the scientific instruments. There is major concern that heating the samples above the surface temperature of Europa may begin the process of melting and vaporization. If any gas is released to the atmosphere before the samples are delivered to the analytical instruments, the samples will be improperly characterized.

Because of this, thermal management shall be required for the system. The sample shall be insulated from internal radiation from the lander vault openings. The lander vault internal temperature is at 313 K. The system shall also prevent the sample from reaching the maximum of either (1) greater than 150 K or (2) greater than 10 K above surface temperature.

#### 3.2.3. Sample Material Independence

The system shall be able to interact with samples possessing a wide range of material properties. This means that any mechanism that interacts directly with the sample shall be tolerant to the sample resembling a powder or displaying a sticky characteristic. It shall also be tolerant to a range of sample particulate size, the diameter of which can be less than 2 mm or greater than 5 μm. The system shall also be capable of successfully interacting and measuring sample of an unknown density.

#### 3.2.4. Autonomy

A signal sent from Earth takes approximately an hour to reach Europa and the Europa Lander will only be in communication with Earth once every 24 hours. Therefore, the system shall function with autonomy during mission operation. The system shall make use of inherently fault resistant mechanisms in its design and shall have a control system to make decisions and guide the sample from the robotic arm to the scientific instruments.

#### 3.2.5. Purge Capability

If the Europa Lander determines that there is a need to discard the current excavated sample, the system shall have the capability to purge the sample from the container either in part or in full. No sample shall be purged within the vault of the Europa Lander.

#### 3.2.6. Sample Container Storage

The system shall provide storage for all necessary sample collection containers. The Europa Lander has a goal of attaining five (5) excavated samples over the mission lifetime. With the current assumptions that there will be three (3) containers for each excavated sample and that the containers will not be reused for multiple samples; the system shall have to provide storage for fifteen (15) containers.

#### 3.2.7. Mission Time

The system shall complete the processing of one excavated sample in less than 90 minutes. The system shall survive the mission length of at least 20 days.

### *3.3. Physical Requirements*

The following requirements refer to the physical mechanical and electrical constraints of the system.

#### 3.3.1. Mass

System shall not have a mass that exceeds 2 kg. This mass requirement includes the functioning subsystem components and all necessary containers, however it does not include the plate that will be used to mount the system to the lander.

#### 3.3.2. Volume Envelope

The system shall fit inside a volume envelope extruded from the vault wall of 50 cm x 25 cm x 25 cm as depicted in Figure 26.

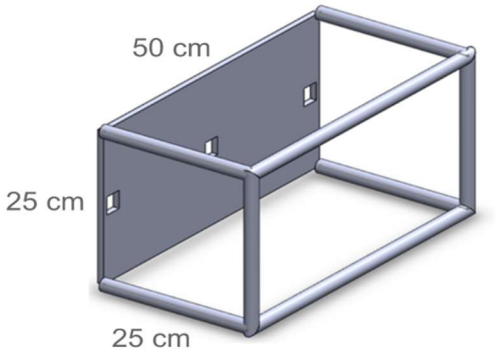


Figure 26: Team developed CAD of System Envelope

#### 3.3.3. Structural

The system shall survive loads and vibrations from flight ascent and descent. This requirement should be satisfied by providing rigid holds for all moving parts during flight that can be released upon landing. The

system shall be mounted to a metal plate that will be mounted to the vault wall. This plate shall not be included in the volume or mass requirements of the system.

#### 3.3.4. Electrical

The system shall perform within the electrical operating range of the Europa Lander. The system shall perform with either 24 VDC or 48 VDC. The system shall operate at less than 1 A always. Over the mission lifetime, the system shall utilize no more than 5% of the lander battery's energy (2.25 kWh). It should be noted that because the electronic system is not the focus of this capstone project, all prototype electronics and control systems shall be constructed in a breadboard and microcontroller fashion and should not be thought of as flight representative.

### *3.4. Mission Success Requirements*

#### 3.4.1. NASA Technology Readiness Level Standards

NASA uses a tier of Technology Readiness Level (TRL) standards to categorize various projects on a scale of 1-9 (See Figure 27). TRL 1 technologies are at a basic investigatory research level while TRL 9 projects have been proven through successful missions [38]. The subcomponents of the Europa Lander are currently at a TRL 3-4. This means that development efforts are focused on creating a proof of concept that can perform all of the necessary functions in an ambient Earth environment while providing analysis to show that it is feasible to meet requirements specific to the Europa environment.

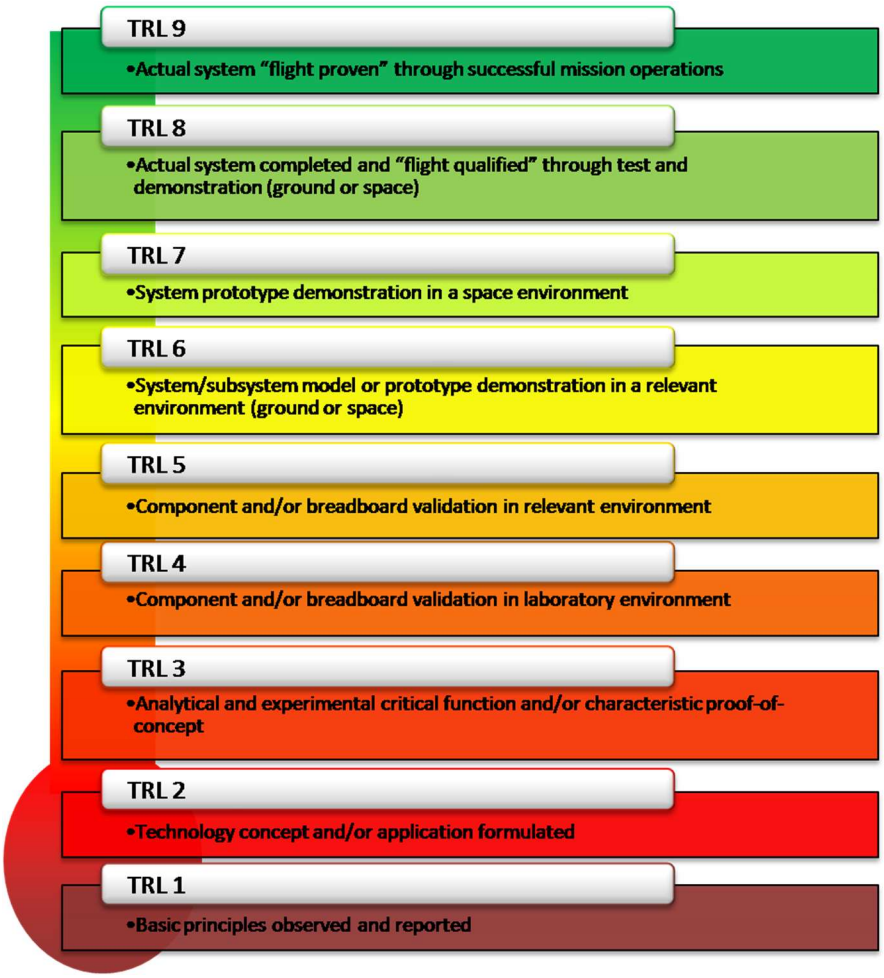


Figure 27: NASA Technology Readiness Level (TRL) Standards [38]

#### 3.4.2. Capstone Project Success

Success for this Capstone Project shall be judged by NASA JPL and by Northeastern University based on the degree to which the following tasks have been achieved:

**1.** Prototype shall perform all functional capabilities in ambient Earth environment.

> This includes docking of the robotic arms, grasping and holding the samples, measuring the sample volumes, transporting and delivering the samples, purging the samples, holding the empty sample containers, and demonstrating autonomy as well as material independence.

**2.** Requirements untestable due to resources shall be shown to be feasible through analysis.

> This includes the performance of materials at cryogenic temperatures, the heat transfer from the lander vault to the sample and particle settling behavior of the sample.

**3.** Requirements that cannot be met due to cost, time or available technology shall be addressed by making future design recommendations.

> This includes meeting constraints such as weight, structural and heat transfer requirements that would require cost prohibitive aerospace materials, building a prototype with temperature compatible motors that are still in development, or including a flight capable radiation resistant electronics system.

# 4. Design

## *4.1 Initial Designs*

One of the major design challenges of this project was to determine what mechanism could best accomplish a range of tasks at an individual component level. The next major design challenge was to understand how each of the selected components would interact in an integrated system. Discussed below are the two potential system-level designs considered by the group.

#### 4.1.1. Linear Concept

The main differentiating feature of the linear concept was the use of a lead screw to transport each sample container along a linear path. The layout of this concept can be seen in Figure 28.

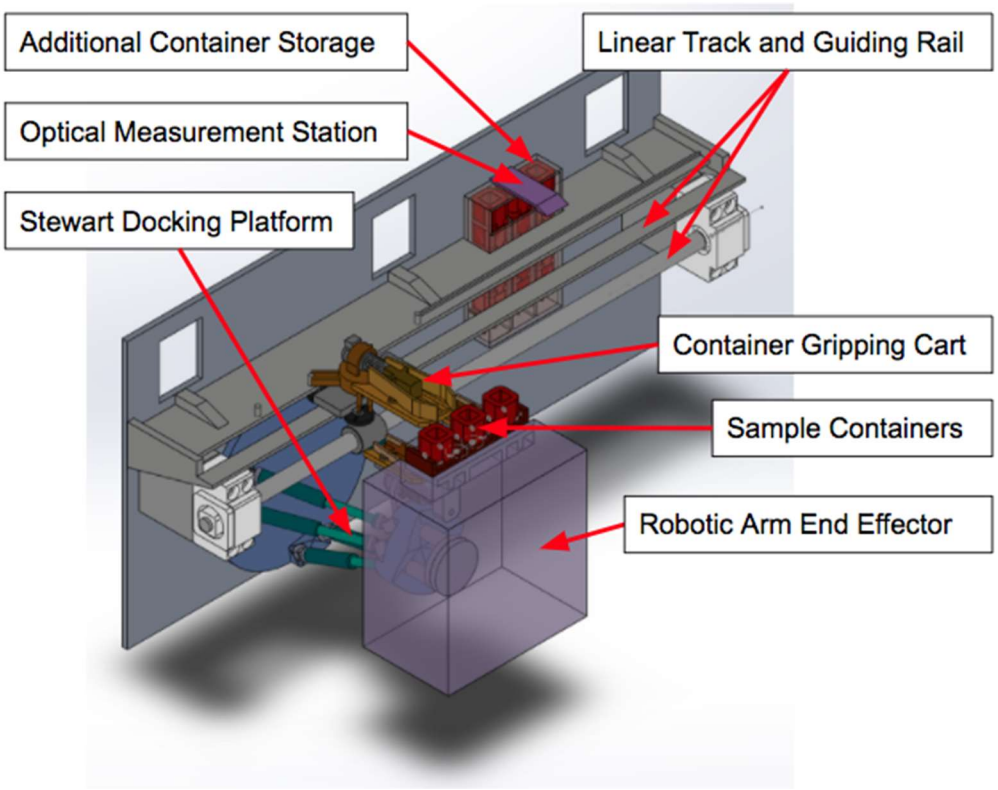


Figure 28: Initial Linear Design with Labeled Components

First, the robotic arm approaches the system and interfaces with the docking platform, which can freely move in all degrees of freedom and respond to any inaccuracy of the arm. An actuated subassembly attached to the docking platform would then translate towards the arm and passively grip the container tray, which holds all three sample containers. Once the container tray is retained by the system, the robotic arm moves away to allow the docking platform to spring back to its original, known position. The container gripping cart would then be actuated toward the sample containers and grip one sample container at a time. The cart is on a lead screw, which translates it towards the volume measurement station. As the cart is translated, it would engage with posts along the track that rotate it passively to face the vault wall. The sample would then be measured optically for volume.

If the sample volume be sufficient, it would be transferred to the inside of the lander body. The cart would then reverse its path and return to the container tray to repeat the process with another sample container. If the sample volume is not sufficient, the cart will return it back to the container tray for refilling.

### 4.1.2. Carousel Concept

The carousel concept consisted of two rotating mechanisms that worked in tandem to transport the sample from the dock to delivery through the vault wall. Unlike the linear concept, the carousel system was oriented on top of the lander body, as opposed to the side. Overall, the system consists of the robotic arm end effector, the docking platform, a station for the storage of additional refill containers, a rotating and actuating container gripping cart, an optical measurement station, a rotating gripper in a transport carousel, and ports for scientific instruments. The layout of these mechanisms can be seen in Figure 29.

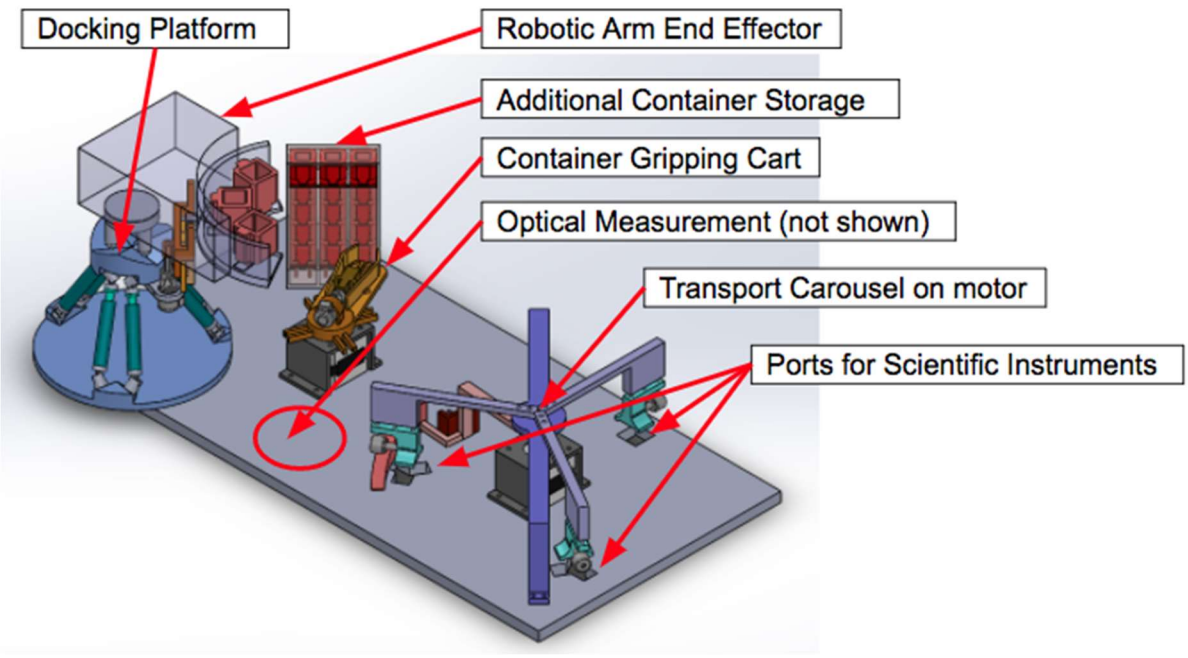


Figure 29: Initial Carousal Concept with Labeled Components

A closer look at the docking and first gripper handoff mechanisms specifically can be seen in Figure 30 on the following page. The docking process between the carousel and linear designs are similar, with the robotic arm end effector docking to a Stewart platform at the docking platform. An actuator, acting vertically, would bring the container tray down to the surface of the lander body, where each container would be taken one by one by the rotating container gripping cart, shown in yellow in Figure 30.

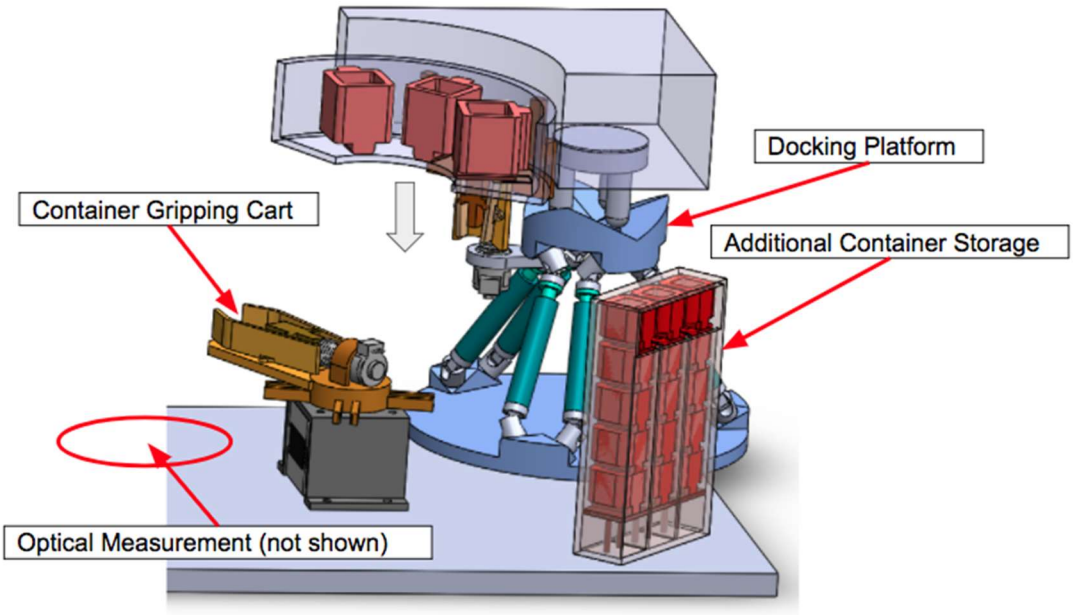


Figure 30: Zoom View of Docking, Container Cart, and Refill Station in Initial Carousal Concept

First, the gripping cart would rotate to an optical measurement and verification station. If the sample failed the optical measurement, the cart would return it to the container tray. However, if the sample contained a sufficient amount of material, the cart would continue rotating until the sample container

lined up with the transport carousel. The container gripping cart would then actuate radially, transferring the sample container to the gripper in the transport carousel. After this handoff, the cart continues to rotate until it passes the additional container refill station. If a round of three samples was successfully delivered to the transport carousel, then the container gripping cart would actuate radially to grab three new containers and deliver them back to the now empty container tray, one by one.

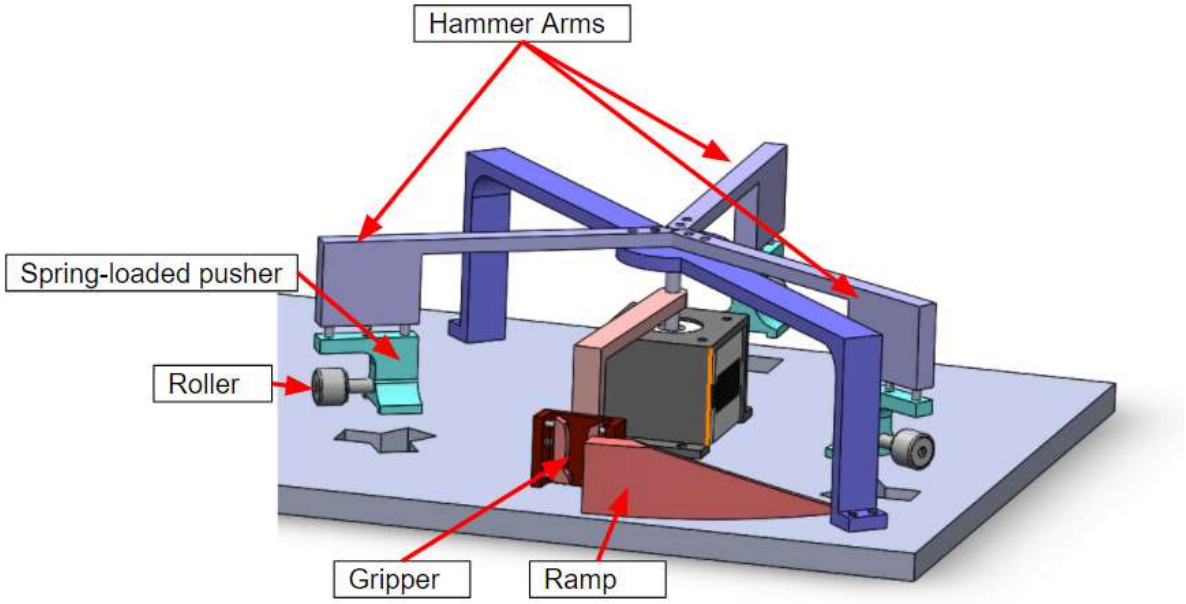


Figure 31: Zoom View of Transport Carousel in Carousel Concept

After the sample left the gripping cart and entered the transport carousel, the carousel's motor would then drive it to rotate. The transport carousel itself, shown in more detail in Figure 31, consists of a rotating gripper, driven by a motor, and three stationary "hammer arms," fixed above each scientific instrument port. The rotating gripper is attached to a ramp feature, and the hammer arms have a spring-loaded pusher feature (shown in teal in Figure 31) that act downwards (toward the vault wall), as well as a roller (gray feature attached to spring-loaded pusher in Figure 31). As the gripper and ramp rotate, when they encounter a hammer arm the roller rolls up the ramp to gain potential energy, and then once it goes over the ramp's edge, the spring-loaded pusher pushes the sample container into the port below the hammer arm. To ensure that the correct sample amount is delivered to an instrument, the ports each have a unique shape, which corresponds to a complementary container shape. That way, a container can only be delivered through a port if they have the same profile.

### *4.2. Decision Matrices*

To arrive at a decision between the two concepts, a list of concerns was created. These concerns do not include all the factors that are needed for a design concept to be a successful one. Instead, they are some important metrics that the final design should address, and by ranking these concerns and then comparing how each design concept fulfills it relative to the other, a winning design can be more objectively chosen. To properly weigh each concern, they were compared against each other in a piecewise comparison chart, which is seen in Table 4.

Table 4: Concern Importance Table

| ***Concerns*** | **Mass** | **Power** | **Sample Security Risk** | **Precision** | **Environmental (Dust)** | **Threat to Timeline** | **Sample Temperature** |
|---|---|---|---|---|---|---|---|
| *Mass* | - | 0 | 1 | 0 | 0 | 1 | 1 |
| *Power* | 1 | - | 1 | 0 | 0 | 1 | 1 |
| *Sample Security Risk* | 0 | 0 | - | 0 | 0 | 0 | 0 |
| *Precision* | 1 | 1 | 1 | - | 1 | 1 | 1 |
| *Environmental (Dust)* | 1 | 1 | 1 | 0 | - | 1 | 1 |
| *Threat to Capstone Timeline* | 0 | 0 | 1 | 0 | 0 | - | 0 |
| *Sample Temperature* | 0 | 0 | 1 | 0 | 0 | 1 | - |
| *Column Sum* | 3 | 2 | 6 | 0 | 1 | 5 | 4 |
| ***Weight with respect to total points*** | 0.1429 | 0.0952 | 0.2857 | 0 | 0.0476 | 0.2381 | 0.1905 |

After comparison, sample security risk was identified as the most important concern, since any sample received from the arm is considered precious. This can be characterized for each concept by how many handoffs and possible points of failure there are in the design. Second most important was the threat to timeline, which captures the effort and time needed to develop and fabricate each design. The importance of this concern stemmed from the acknowledgement that the system being designed is very complex and will be very challenging to create in the limited time that the team has. Third is sample temperature, which is a descriptor for shielding the sample from any heat, the source of which could be heaters on the motors, heat from running the motors, or radiation from the inside of the Lander body through the opening. This is important to address in order to make sure that the samples are kept at the temperature limit of ten degrees above the temperature at Europa's surface. Next in the ranking is mass, which has been identified as one of the most challenging quantifiable requirements to meet. The power concern refers to the wattage needed for each concept to function, which can be characterized by the amount of motors and the expected outputted torque. Environment (Dust), refers to the danger of debris particulates getting into the system and jamming or damaging mechanisms. The least important concern was identified to be precision, which refers to how precise each mechanism must be designed in order to function correctly. While this concern does reflect the merits of each design, it can be more easily addressed with careful tolerances and machining.

Once the concerns were weighted, how well each design concept addressed that concern was evaluated on a scale from 1 to 5, 1 being terrible, 2 being bad, 3 being neutral, 4 being good, and 5 being excellent. These rankings, as well as the resulting weighted totals, are shown in Table 5.

Table 5: Weight Comparison Between Both Concepts

| Final Decision | Sample Security Risk | Threat to Timeline | Sample Temperature | Mass | Power | Environmental (Dust) | Precision | Weighted Totals |
|---|---|---|---|---|---|---|---|---|
| Concern weights | 0.2857 | 0.2381 | 0.1905 | 0.1429 | 0.0952 | 0.0476 | 0 | - |
| Linear Concept | 4 | 4 | 3 | 3 | 4 | 3 | 3 | **3.6190** |
| Carousel Concept | 2 | 2 | 3 | 4 | 2 | 4 | 2 | **2.5714** |

When evaluating how the designs compare to each other for the most important metric, sample security, the linear concept was deemed better because it has fewer handoffs than the carousel concept. For the threat to timeline, at the time of final decision the carousel was less developed than the linear concept. Both concepts handled maintaining sample temperature similarly, especially if the driving motors were embedded in the vault. For mass, the carousel concept had more potential to have less mass than the linear concept, however, using a Stewart platform for docking contributes a lot of mass to both. The carousel design involves more actuators and motors than the linear design, and therefore would have a higher power requirement. For handling the environment and potential dust that could get caught in the system, though the carousel concept mechanisms were more sealed, the linear concept could implement shielding and guards to protect the mechanisms. Finally, both concepts require precision in the interaction between neighboring systems in order to operate, but because the carousel involves more handoffs, its precision is more difficult to achieve. Ultimately, the linear system was chosen as the final design. Examining the weighted point totals for each concept, the linear version won by a factor of nearly 150%.

### *4.3. Final Design*

After extensive research, discussion, and iteration, the design team determined that the integrated design displayed in  and Figure 32, herein referred to as the “Linear Concept” was the strongest candidate for further development. Some design highlights include a passive Stewart docking platform, a toggle

gripper, a Geneva drive, a lead screw linear transport system and an optical volume measurement station.

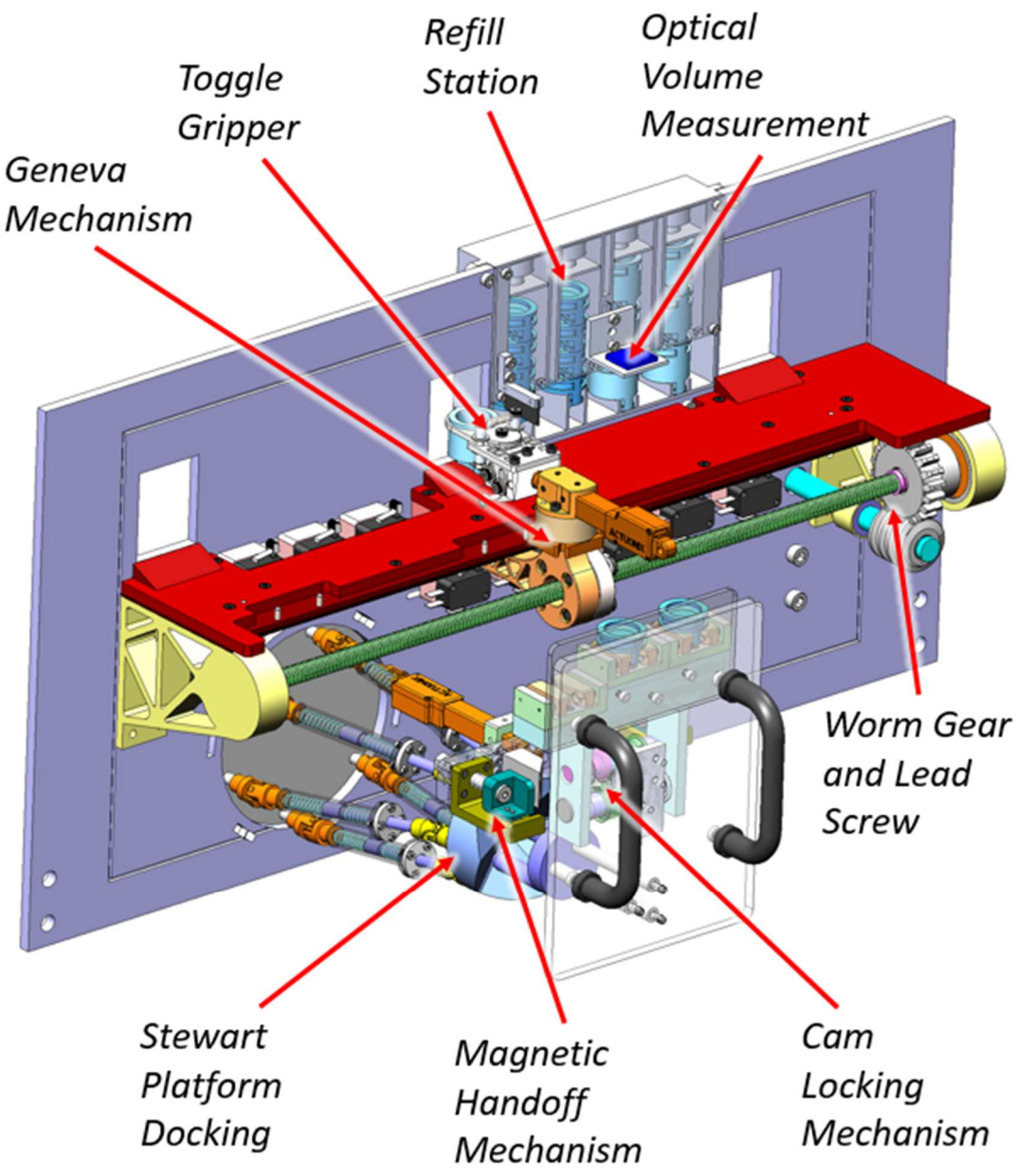


Figure 32: CAD of Developed Linear Concept

As the design team transitioned from Summer II into Fall, it was decided that the design process would be done in a different manner than how the preliminary research and design were carried out. During July and August, all parts of the project were primarily considered as individual components rather than acting in tandem with each other. This attitude led to research and preliminary design to be approached similarly, which made developing ideas about the integration of the entire assembly difficult.

Beginning in late August and early September a more holistic approach was taken. Within a week of classes starting, basic concepts of an integrated system were proposed by all group members. Although none of these ideas were fully fleshed out, discussion and questions lead to brainstorming and the exchange of research and ideas. Already it was evident that many designs shared key concepts and

features. As the second week of September began, four distinct concepts were presented to the capstone and industry advisors. With their assistance, similar concepts were combined until the number of designs was reduced to two. These two designs were rendered distinct primarily by the path they had the sample containers travel in: a linear path and a circular path.

With two designs to develop, group members had the opportunity to keep themselves thinking creatively and not develop "tunnel vision." By working on both designs the team was able to spot the triumphs and pitfalls of both designs as well as see where similar mechanisms and ideas could be employed on each design. As the end of the month drew near, however, a decision had to be made. After a lengthy discussion of concepts with the industry advisor, a thorough decision matrix with accurately weighted concerns was developed and employed to justify the final decision. Ultimately, the linear sample path was named more promising than the circular one; the team threw themselves into the further development of it immediately. Although the basics of all components had been considered, details such as the placement of motors, gear types, and mechanism geometry needed to be investigated. Several days later, the team presented their preliminary design to their industry advisor. This design review went positively for the team as the advisor approved all developments that had been made to the project, and offered up his final concerns to consider.

Team members then made any necessary alterations to their models, and began fabrication. For several components, physical representation allowed for design flaws to be caught and iterative designs to be made.

### 4.3.1. System Process Flowchart

Below, in Figure 33, is a flowchart that summarizes the processes that are performed. It details the path of a container from delivery to the system by the external robotic arm end effector to the scientific instruments beyond the vault doors. If a container is underfilled, it is returned to the container holder so that the robotic arm can bring it back to the surface for further filling. Once all containers have been processed, the flowchart indicates that empty containers will be delivered to the robotic arm so that the robotic arm can go collect more samples. This flowchart should be read as an overview, as it does not include all of the detailed edge cases or component-level actions. These will need to be later implemented in full in future software development.

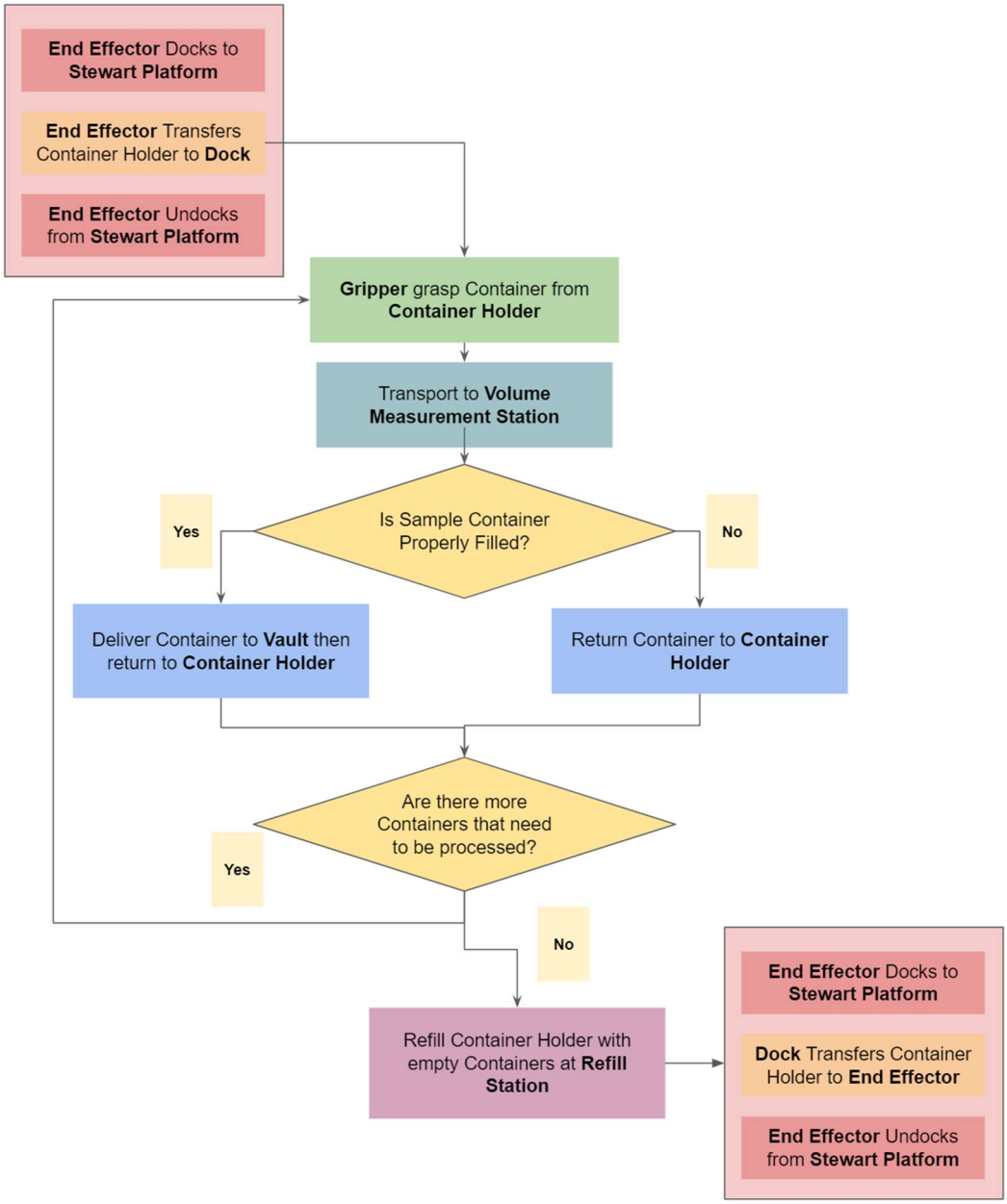


Figure 33: System Flow Chart

### 4.3.2. Sample Container

The sample container was developed in parallel with gripper and volume measurement systems. Throughout development, simplicity was valued over complexity. One important decision that affected total system development was that the system should not be responsible for division of sample into discrete containers. This eliminated the need for a sample separation process for the transfer system. It was also decided that the maximum holding volume of the containers should be the maximum sample volume with tolerances required by the scientific instruments. This eliminated the need for purging of sample.

As there will be fifteen sample containers that pass through the system (ten 1cc containers and five 5cc containers), one of the main drivers for the sample container design is mass. In addition to being light, the

sample container must have features to allow it to be gripped securely. In the case shown in Figure 36 34, the containers have an extrusion on the bottom that can be gripped by the bottom gripper, and a circular cutout around the middle that allows for it to be gripped by the fingers of a toggle gripper. The shape of the extrusion on the bottom allows for easy in and out movement through the bottom gripper; its upside down “T” shape prevents the container from being pulled upward out of the bottom gripper. The underside of this container can be seen in Figure 34. In addition to the bottom mating features, a small guide rail is located on the rear of the sample container. This feature keeps the containers aligned in the refill station.

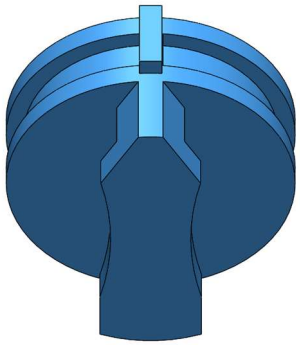

Figure 35: Mating extrusion on container bottom

While the small size of these features may yield a more challenging design, they are kept small to reduce mass. Since the same mechanism will grip each container, the outer geometry of the sample container that holds 5 cc and the sample container that hold 1cc will be the same. The only difference will be volume of the top opening, which will be sized to hold either exactly 5cc or exactly 1cc. Figure 36 shows both sample containers, the colors are not representative of the final design. The current material being researched for the sample container is alumina for its thermal properties.

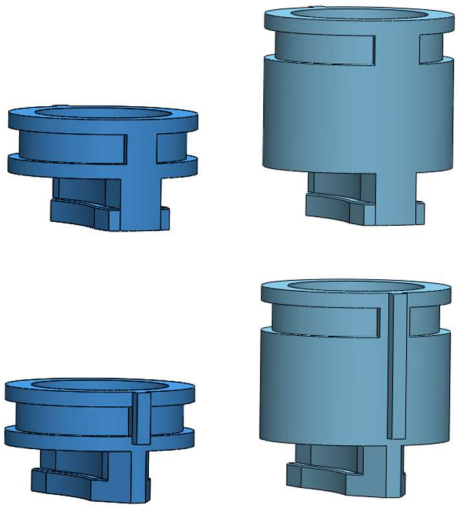

Figure 36: 1cc Sample Container (left) and 5cc Sample Container (right)

### 4.3.3. Docking Mechanism

The main goal of the docking mechanism is to correctly locate the robotic arm relative to the Lander body. This means the mechanism must deal with the arm dynamically by reacting to any inaccuracies in the positioning of the robotic arm, and must also statically interact with the arm to inhibit motion in six degrees of freedom.

A kinematic coupling is well-known fixture that exactly constrains two parts together. One example of such a fixture can be seen in Figure 37.

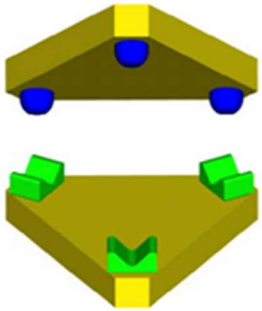

Figure 37: Three Groove Kinematic Coupling [42]

The top part has three semi-spherical features that fit into the three v-grooves on the part below it. Figure 38 shows the geometry of the fixture, where each groove points towards the coupling center. The design is based on the principle of Exact Constraint Design, where the number of degrees of freedom that are constrained should be equal to the number of points of constraint. In this case, each groove provides two contact points for the semi-spherical features, which constrains the top part in all six degrees of freedom.

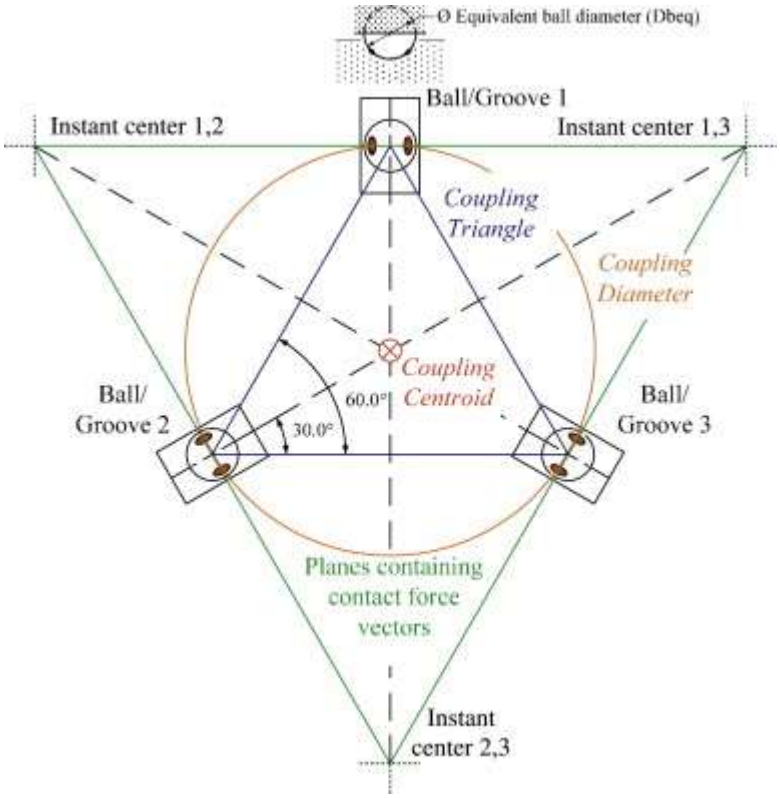


Figure 38: Geometric parameters for a Three Groove Kinematic Coupling [42]

The repeatability of a good connection between the v-grooves and the semi-spherical features is dependent on the angle of the v-grooves. Generally, a sharper angle is more repeatable, though it also increases the thickness and mass of the coupling. The shallowest angle at which the coupling is still considered to be "repeatable" is at 110 degrees [43]. Figure 39 shows a side view of the coupling design with the 110 degree angle. This geometry also informs the necessary deflection of the dock in response to the arm. In the worst-case scenario, when the arm is off target by 3 cm, the semi-spherical features, which can be seen in Figure 40, would contact the coupling about 17 mm away from the docked position in the normal direction. This would mean that the dock must be able to deform this amount in response.

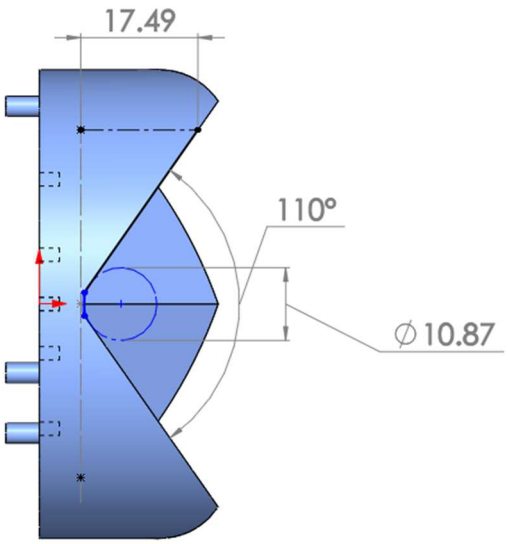


Figure 39: Side view of kinematic coupling design

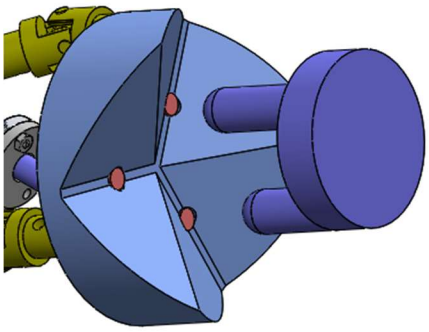

Figure 40: Semi-spherical end effector and kinematic coupling

The docking mechanism must be able to account for a translational inaccuracy of the arm of up to +/- 3 cm, and a rotational inaccuracy of +/- 2 degrees. The robotic arm is also currently being designed with 4 degrees of freedom, with a possibility for the addition of one more degree of freedom if needed. This means that the mechanism must be accountable for at least the degrees of freedom that the arm does not have. To summarize, the mechanism must behave dynamically to respond to any freedom of motion that the arm may or may not have.

One method to interact with such a system is with the use of a Stewart Platform. Pictured in Figure 41, a Stewart Platform uses "legs" assembled from universal joints and a piston, that when assembled correctly, allow for the motion of the moving platform in all six degrees of freedom.

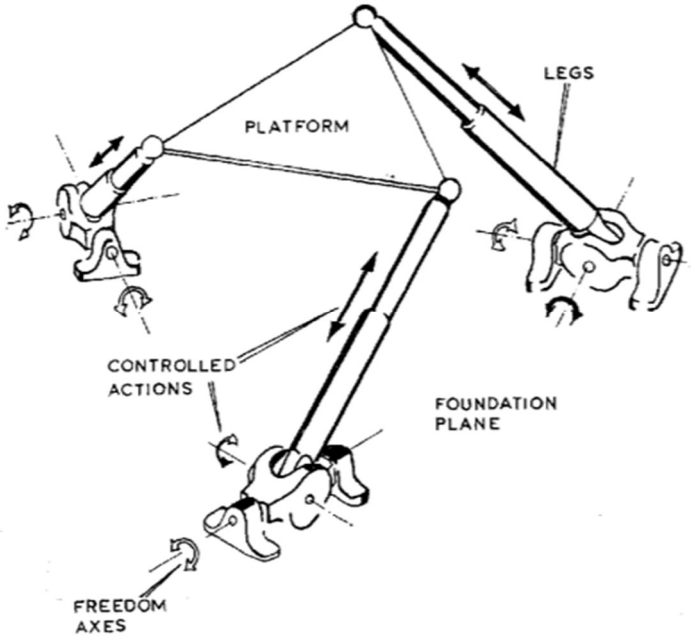


Figure 41: Generalized Stewart Platform [44]

This system can be described mathematically using Gruebler's equation, a version of which is seen in Equation 5 [45]. The equation relates *n*, which is the number of members, *g*, which is the number of

joints, and *f*, which is the number of degrees of freedom of joints, to *F*, the total resulting degrees of freedom of the system.

$$F = 6(n-1) - 6g + f \quad (5)$$

Figure 42 shows a potential configuration of a six leg Stewart platform system broken down into joints and degrees of freedom. Taking values from this configuration and inputting them into Equation 5 it is found that the system has six total resulting degrees of freedom.

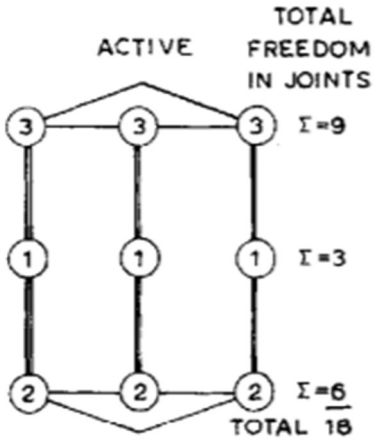


Figure 42: Six leg Stewart platform joint and DOF breakdown

This design for each leg is realized in Figure 43. In this case, only one degree of freedom is controlled, which is the axial motion of the piston.

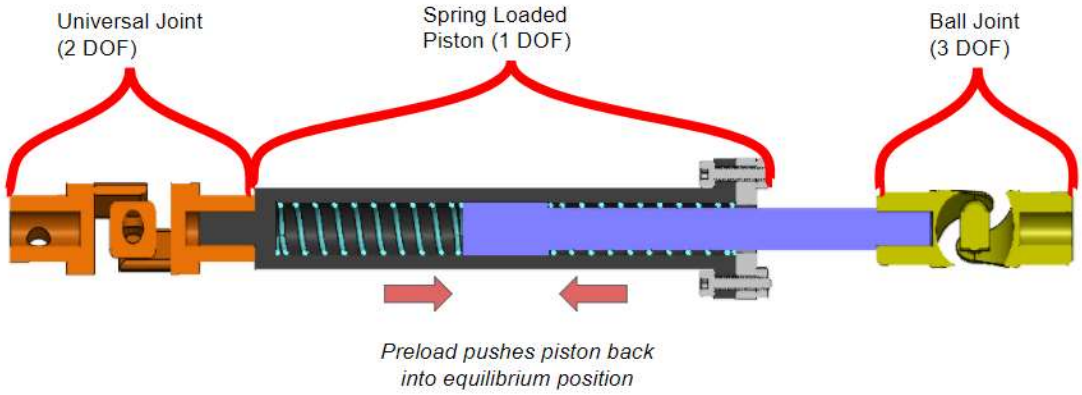


Figure 43: Labeled leg joint design

Combining the kinematic coupling and Stewart Platform yields a design for a docking mechanism that is viable for this application. Figure 44 shows a picture of this integrated design.

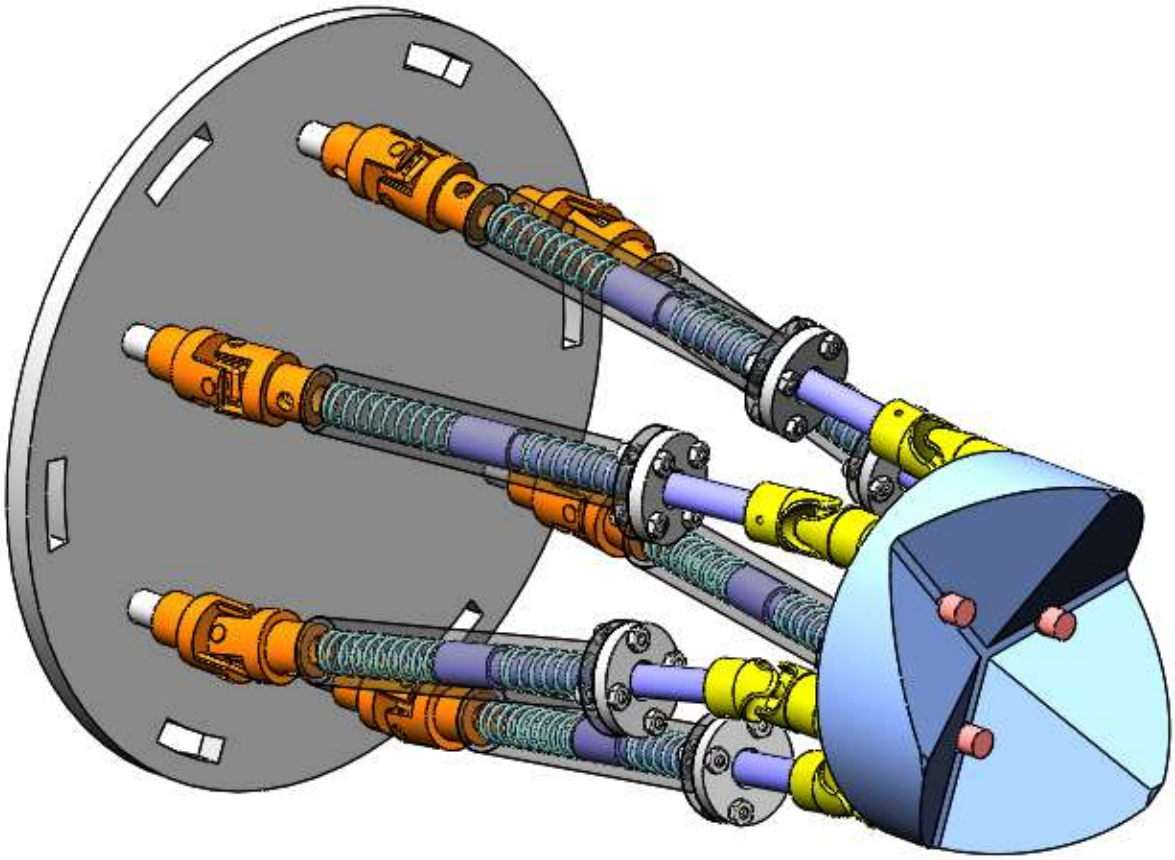

Figure 44: Docking Mechanism Design

When the robotic arm comes in toward the dock, ball features will contact somewhere on the kinematic coupling, which in this case is the moving platform of a Stewart Platform. The reaction forces on the V grooves from the robotic arm moving towards the Lander body will then cause the platform, which can move in any degree of freedom, to adjust. This will continue until the ball is located at the center of each groove, also known as the vertex of the coupling triangle. The end of the docking process may see the platform in a translated and twisted position.

Once the arm undocks and moves away from the system, the Stewart platform design must return to its equilibrium position, which is defined by the springs in each spring-loaded piston. However, each controlling each piston controls a total of three degrees of freedom, which leaves three degrees of freedom uncontrolled. This may mean that the platform may return to a position different than the original equilibrium. The solution to this issue may be found in Equation 6. Adding three more legs to the system with the spring-loaded pistons will change values to result in a total of zero free degrees of freedom. This solution will be further explored and validated with a physical prototype.

The mechanism also needs to be able to detect when docking is complete to continue to the next step. Placing a pushbutton switch at each vertex of the coupling triangle can detect when each ball feature is in the correct location. In the design shown in Figure 45, the pushbutton switches are threaded

through the back end of the kinematic coupling. The current switch being used in this design is an 8500 Subminiature Pushbutton Switch (Part Number: 8532MZQE2) from C&K Switches [46].

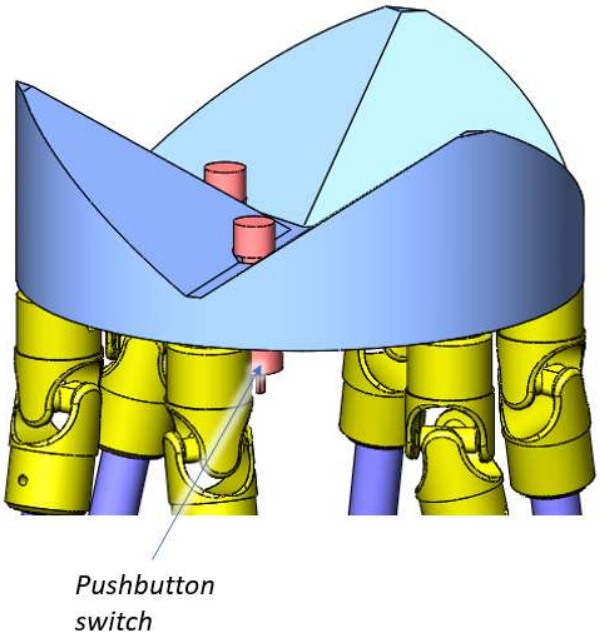


Figure 45: Pushbutton attached to kinematic coupling

### 4.3.4. End Effector to Dock Handoff

During transport of the collected samples to the docking station, the robotic arm must have the ability to securely retain the container tray as well as be capable of releasing the tray to the docking system during handoff. During the handoff process, however, the arm should only unlock from the container tray *after* it has been securely gripped by the next system, thus ensuring sample security. The transition between the locked and unlocked states should occur passively, and the same motion or action should trigger the switch between states.

To achieve this goal, a mechanism similar to the one found in retractable ballpoint pens can be used [47]. This pen mechanism involves a button on the end that, when pushed, toggles between extending and rotating the pen tip located at the other end. Inside this pen a cam drives an internal follower to rotate between two alternating tracks; these tracks correspond to the extended and retracted pen-tip conditions. In Figure 46, this mechanism can be seen, as well as the steps of the cam action that result in the extended and retracted positions.

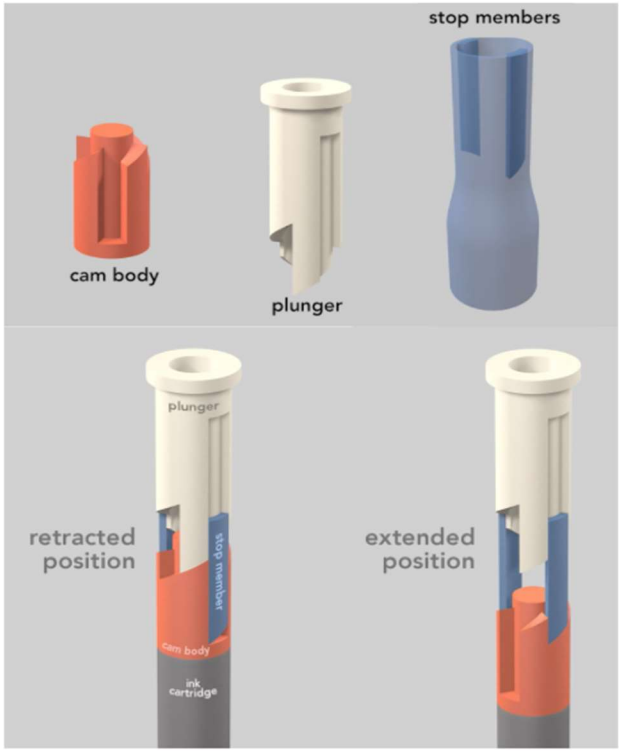


Figure 46: Pen-Tip Mechanism. Top: the Cam Body (orange) which rotates and moves up and down, the Plunger (white) which moves up and down, and the Stop Members which are stationary. Bottom: Cam Assembly positions at Retracted and Extended configurations. [48]

To apply this concept to the interface between the robotic arm and the tray, the arm shall be equipped with a member equipped with retractable cam following mechanisms, hereafter referred to as "retractable pens." The container tray itself has through holes which the extruding points of the retractable pens slide into when fully extended, which are highlighted in Figure 47. The container tray is also equipped with passive grippers capable of retaining three sample containers.

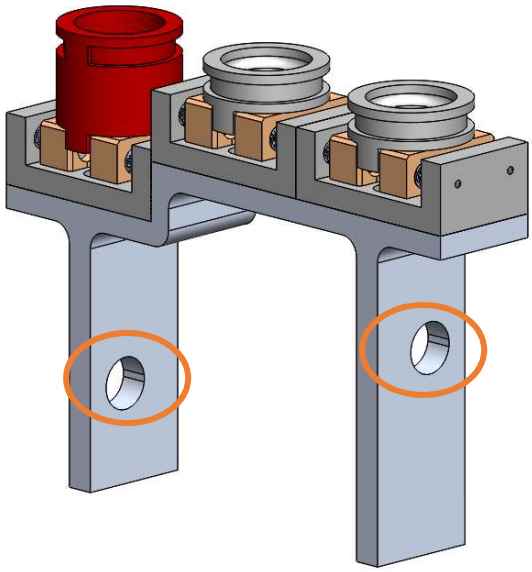

Figure 47: Sample Container Tray, Locking Pockets, Circled in Orange

Attached to the dock immediately adjacent to the passive grippers receiving the tray during handoff are two fixed ramp features which can be seen in green in Figure 48 and Figure 49. These ramps interact with the buttons of the retractable pens, which will switch between lock and unlocked positions.

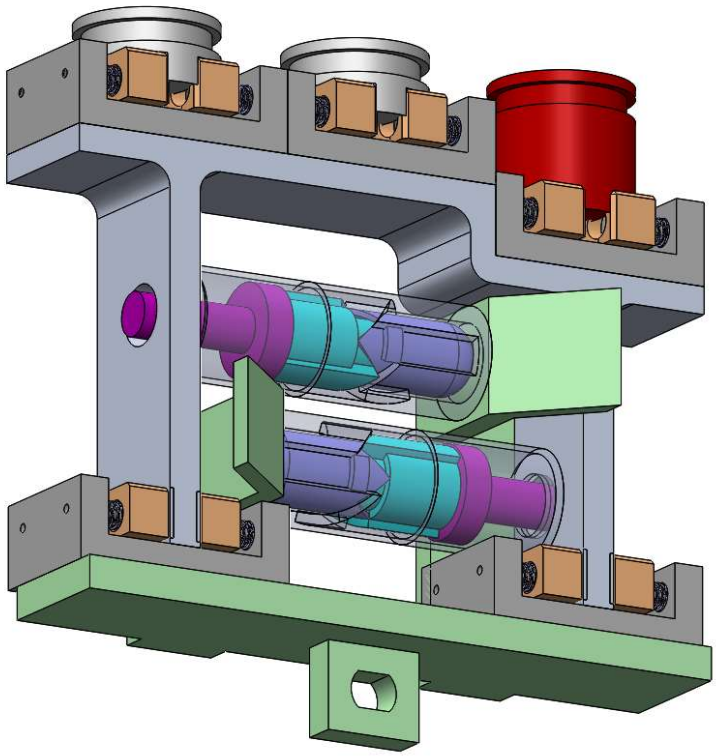

Figure 48: Full Assembly of Sample Container Tray in Locking Mechanism. Transparent/Pink/Blue/Purple are Retractable Pen Mechanisms Attached to Robot Arm; Gray is Sample Tray; Green is Dock's Actuating Ramps

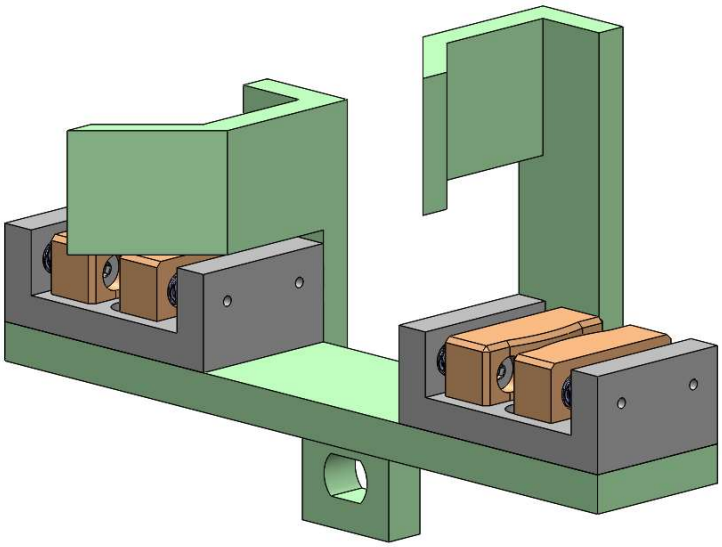

Figure 49: Dock with Ramp Features used for Actuating Retractable Pen Mechanism Buttons

A general timeline of sample container handoff and exchange would go roughly as follows:

The robotic arm approaches the tray and dock assembly, held in place by the retractable pens. Once the arm begins the docking and handing off process, actuators move the handoff grippers toward the tray.

As those handoff grippers grab the gripping features of the container tray, the ramp features on the dock begin to interact with the buttons on the pens. Eventually, the ramps actuate the buttons fully so that the pens switch from locked (points extended) to unlocked (points retracted). This process is illustrated in Figure 50. Once the points no longer interact with the pockets on the container tray's locking features, the robotic arm can back out and undock.

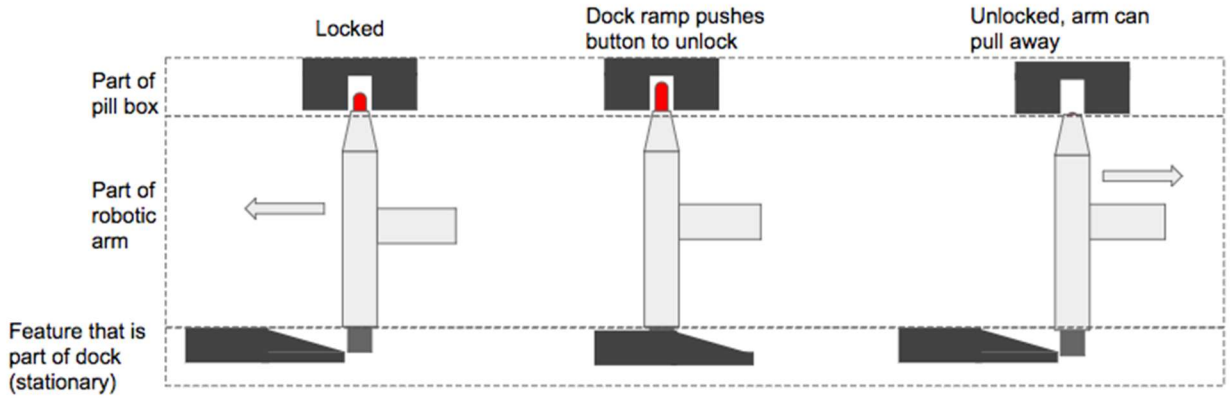


Figure 50: Process of Pen-Tip Locking Mechanism

When the arm re-docks to take back the container tray (either with previously delivered containers that need to be filled more, or with a set of new containers), it repeats the same process as it did to handoff the container tray to the dock. With the robotic arm's pen array lined up to the locking features on the container tray, the system actuates toward the dock so that the dock's ramp features interact with the pen buttons, actuating them again and switching them from unlocked to locked.

### 4.3.5. Container Cart

As the lead screw rotates, the container cart is driven along it axially. This container cart is responsible for grasping the sample at the docking site and securely holding the sample until it is time to release it.

To meet the requirement of maintaining secure control of the sample container throughout operation, the design team determined that a physical gripper should be used. To guide the design of an ideal gripper for this application, the team established several design goals that would work toward meeting the system-level requirements. First, the gripper design should allow for the container to be securely grasped at all times during system operation. This means that not only must it be secured during transportation, but it must also be firmly secured in the case of handoffs from one subsystem to another. Second, the gripper design should allow for some level of imprecision when attempting to grasp a container. Due to the multitude of moving components and the inherent limitations of external systems, there will likely be a tolerance stack-up that creates a range of relative positions between the gripper and the container. A gripper that can properly operate within the entire uncertainty range can ensure smooth and reliable system operation in a variety of circumstances. Finally, the design team determined that a gripper that can grasp and release the container passively would be very valuable to the system. Due to the weight, size, mass, and power limitations of the system, it is important to limit the number of powered actuators used. By designing a gripper that can grip and release by passively using other required motions of the system, the gripper design and functionality can be simplified and benefit the overall performance and characteristics of the system.

In Figure 51, a design for a cam joint gripper is shown. As the trigger of the gripper is pressed against a container, the gripper's fingers are closed around the container due to the cam joint interaction between the trigger and the fingers and a spring is compressed between the trigger and ground. When the trigger has been displaced the proper distance and the fingers are exerting the proper grasping force on the container, the trigger will lock into place due to a spring-lock mechanism protruding from the bottom of the trigger. This will allow the gripper to maintain a locked grasp on the container throughout any necessary transportation processes. When the gripper needs to release the container at a defined location, it will pass over an "unlocking ramp" geometric feature. By rubbing up against this feature through forward actuation, the spring-lock mechanism will unlock and relax the fingers' grips on the container. The compressed spring will then cause the trigger to push the container away from the gripper.

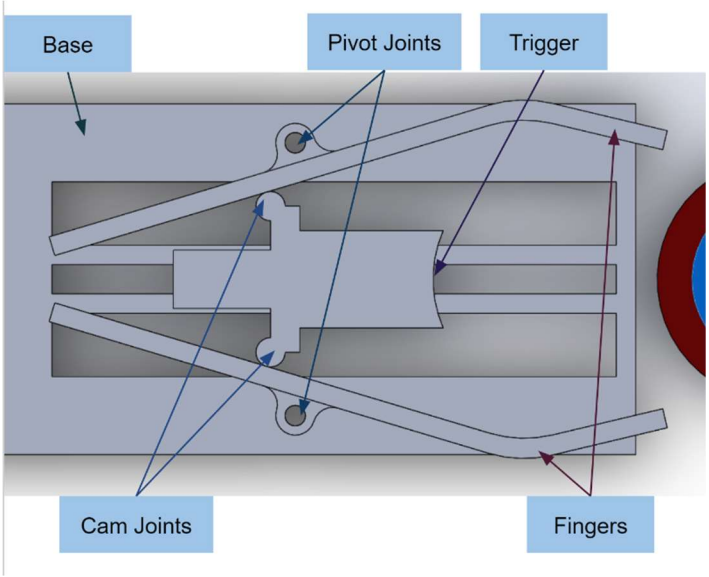


Figure 51: Passive Sample Gripper

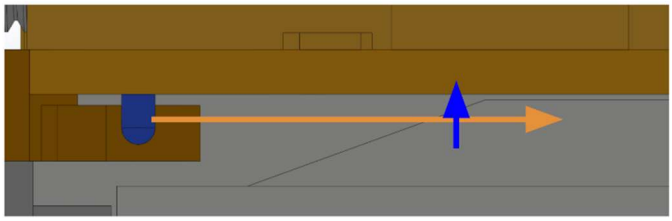

Figure 52: Passive Gripper Pin Unlocking Mechanism

Another gripper design is shown in Figure 52, described as the toggle gripper design. This design is based off of the toggle mechanism used widely in classical and modern mechanics. One familiar application of a toggle mechanism is in a vise grip. When two collinear jointed members are under compression, they are in an unstable state and will buckle in one of two ways. By applying a small perpendicular force at the joint, the user can bias which way that buckling will occur. Once buckling in one direction occurs, the system will not buckle in the opposite direction until there is another sufficient perpendicular force in that direction. By applying the proper geometric constraints to this mechanism, the toggle can be used as a stable lock that can provide a very high useful force, but requires very little force to change states (Figure 53). The toggle gripper uses this "over-center" principle to switch from its "open" unclamped state to its "closed" over-center state when the gripper is actuated in the forward direction and a container pushes against its trigger feature. A tension spring provides the compressive force between Point A and Point B

constrained in horizontal slots while Point C is allowed to rotate and constrained in a vertical slot. An adjustable ramped holding bar provides a surface for the buckled members to rest against while the gripper is in its grasping position (Figure 54). To relax the grip, the gripper must be actuated forward over a ramped geometric feature. This will raise the adjustable ramped holding bar and force the toggle mechanism to its opposite buckling state and relax the fingers' grip. After release is complete, a set of compression springs will return the adjustable ramped holding bar to its original position, readying the gripper to grasp another container.

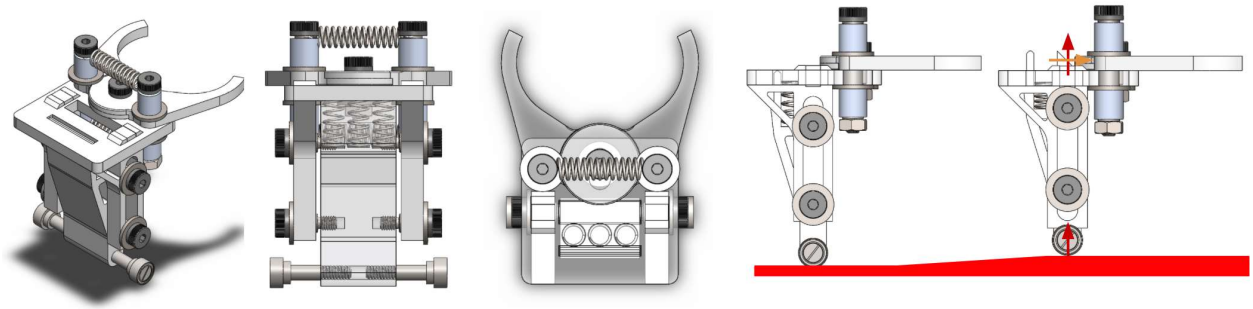

Figure 53: Toggle Gripper Design Overview

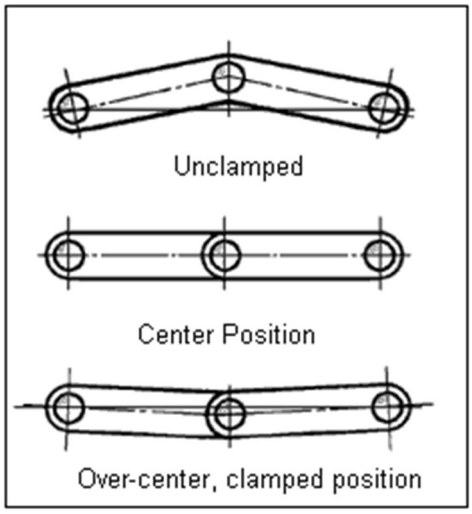


Figure 54: Toggle Action Principle [49]

The third gripper design, shown in Figure 55, uses two fingers with compression springs to grip around the base of a container. The unique shape of the container base and the grippers allows the grippers to slide around the cup easily with forward actuation. Once the container is fully in position, the concave features of the container paired with the convex features of the fingers cause the pull-out force to be much higher, thus securing the containers. To release the containers, a forward actuation against a wedge will spread the fingers apart and relax the grip on the container. While this design may not allow for as much control over the gripping process, its small footprint and simple design offer unique benefits.

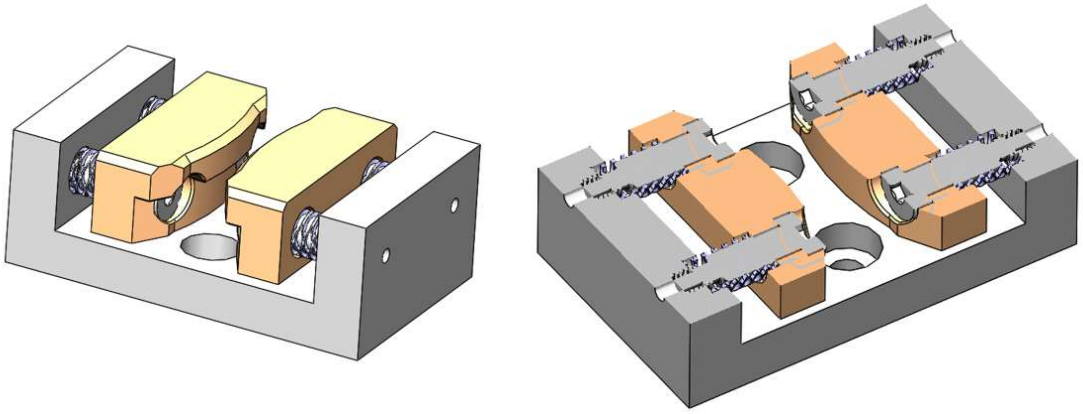

Figure 55: Passive Container Lower Gripper

The toggle gripper was chosen over the cam joint gripper because (1) the toggle gripper allowed for greater control of the container grip strength than the cam joint gripper based on geometry and spring choice and (2) the locking and unlocking mechanism of the toggle gripper was a simpler, surer and more well developed than the cam joint gripper design. The concave-convex spring based gripper is used as the passive container lower gripper and supports holding the containers in various stations in the system. In the final design, it will be shown that both the toggle gripper and spring gripper are used to complete the system's objectives.

To properly size the gripper's geometry and select the appropriate springs and actuators, a subsystem level force analysis is necessary. For the gripper level subsystem to work, a linear actuator must be able to provide enough force to actuate the passive toggle gripper. Once the toggle gripper grasps the container, the linear actuator will attempt to pull the container away from the lower gripper. This means that the toggle gripper "pull-out" force must be greater than the lower gripper retaining force. For this analysis, it is assumed that the toggle gripper design values are fixed and that the lower gripper and linear actuator requirements are based off the toggle gripper design. It should be noted that all analysis below is idealized and does not include friction in the calculations.

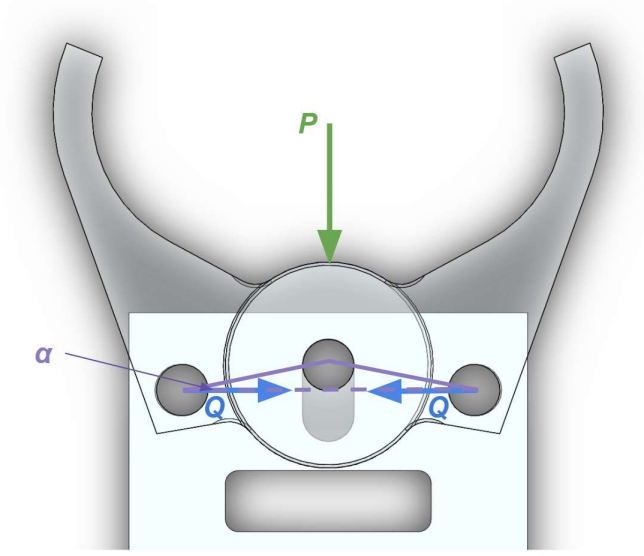


Figure 56: Toggle Gripper Grasping Diagram

The container grasping motion is shown in Figure 56. The linear actuator is providing the applied force $P$ in the vertical direction and the extension spring is applying $F_{spring}$ in the horizontal direction (Eq 6,7).

$$\frac{F_{Spring}}{P} = \frac{\cos\alpha}{2\sin\alpha} = \frac{1}{2\tan\alpha} \quad (6)$$

$$for\ \alpha = 10°, P = 0.352F_{Spring} \quad (7)$$

The extension spring is modeled as a preloaded linear spring (Equation 8).

$$F_{Spring} = n_{springs\ in\ parallel}(k(x - x_0) + F_{unstretched}) \quad (8)$$

As angle α decreases from $\alpha_0$ to 0°, the force ratio of vertical forces to horizontal forces reduces to zero. This means that the force required to move the toggle gripper forward and close its grip decreases as it is further actuated. Once α decreases past 0°, the vertical force switches signs so that the spring force pulls the toggle gripper into position without the assistance of the linear actuator. Figure 57 shows how the applied force $P$ is at a maximum in the gripper's initial position, zero at the toggle position, and minimum at its grasped position. Figure 58 shows that once the gripper has been actuated to the toggle point at α=0°, the gripper requires no more energy to properly grasp the container.

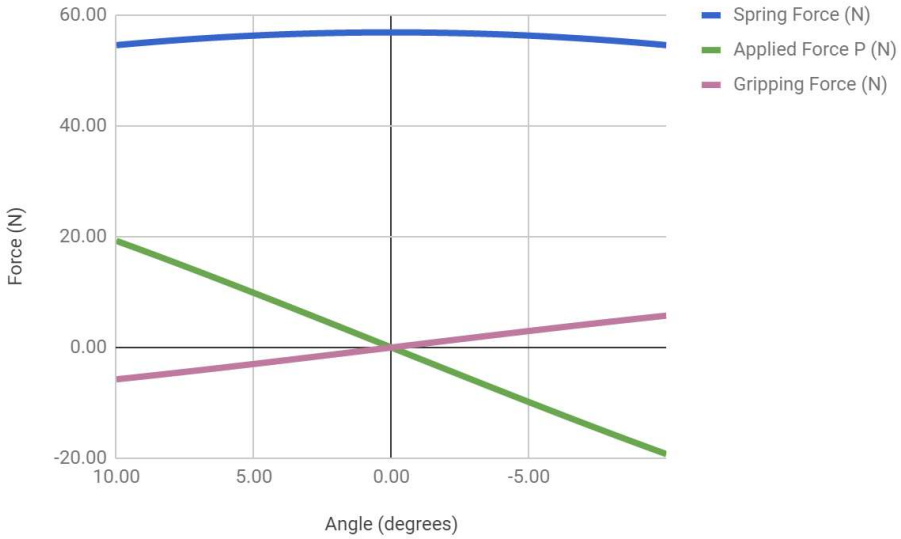


Figure 57: Toggle Gripper Grasping Forces

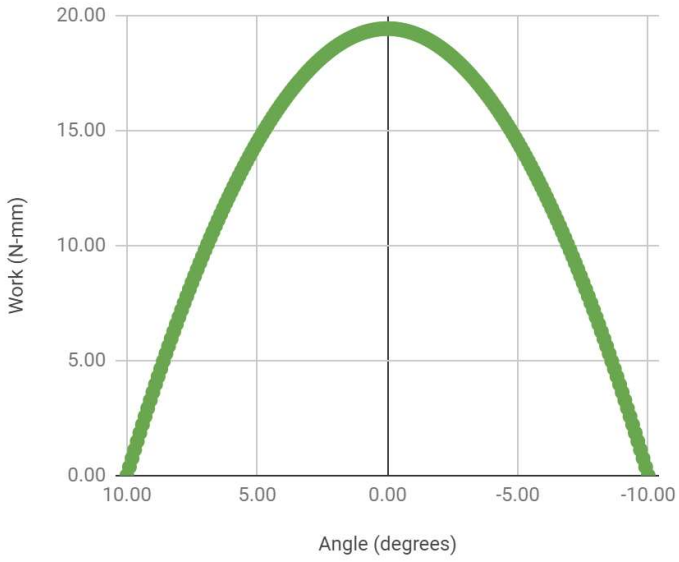


Figure 58: Toggle Gripper Applied Energy

After the gripper has grasped, reaction force *R* in the vertical direction is used to differentiate between the force applied by the linear actuator. Force *R* is equal in value and opposite in direction to *P* (Equation 9).

$$R = 2F_{Spring} \tan \propto = P \quad (9)$$

To determine the gripping force on the container (see Figure 59), it is necessary to sum the moments around the outer joints (Eq 5-6).

$$\left(\frac{R}{2}\cos \propto\right) b = F_{Grip} a \quad (10)$$

$$F_{Grip} = \frac{Rb \cos\propto}{2a} \quad (11)$$

It should be noted that the grasped gripper position is designed to have only a very small interference fit with the container. This will provide a secure and repeatable fit without providing excess hoop stress on the sample container. Gripping force is also plotted for comparison in Figure 57.

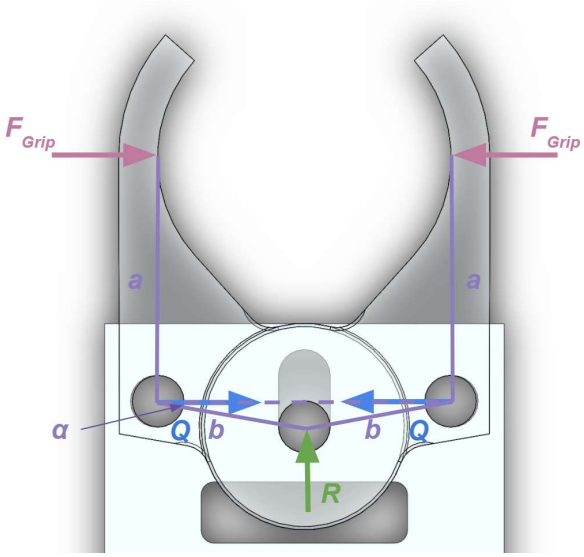


Figure 59: Toggle Gripper Grasped Diagram

Figure 60 shows the gripper in its grasped position as it attempts to remove the container from the bottom holding gripper.

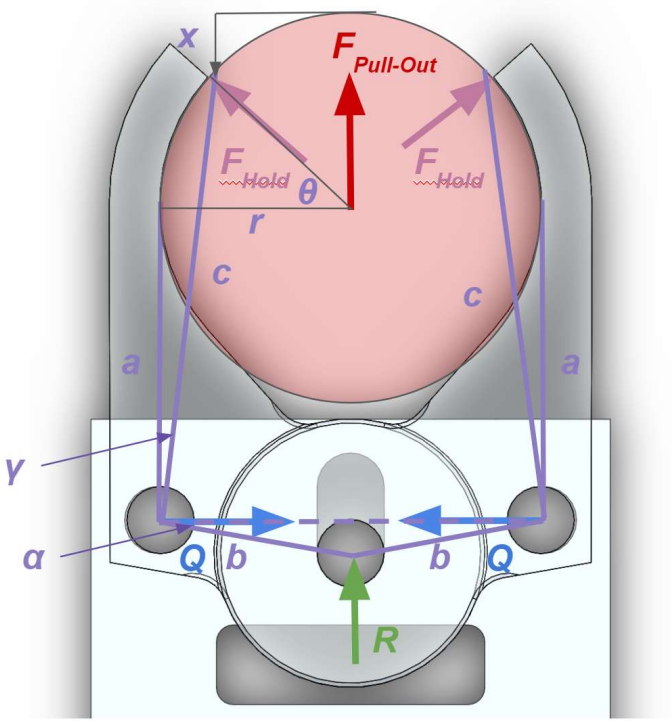


Figure 60: Toggle Gripper Pull-Out Diagram

The "pull-out" force provided by the toggle gripper must be greater than the holding force of the bottom gripper. The calculation to find the pull-out force is as follows (Eq 12-16).

$$r = b\cos\propto_0 \quad (12)$$

$$x = r - c\sin\gamma \quad (13)$$

$$\theta = \cos^{-1}\frac{x}{r} \quad (14)$$

$$F_{Holding} = \frac{Rb\cos\propto}{2c\cos(\theta-\alpha)} \quad (15)$$

$$F_{Pull-Out} = F_{Holding}\sin(\theta) \quad (16)$$

Figure 61 shows that the pull-out force decreases as the gripper fingers slip down the side of the cup, so the maximum pull-out force occurs only when the fingers are fully secured around the container.

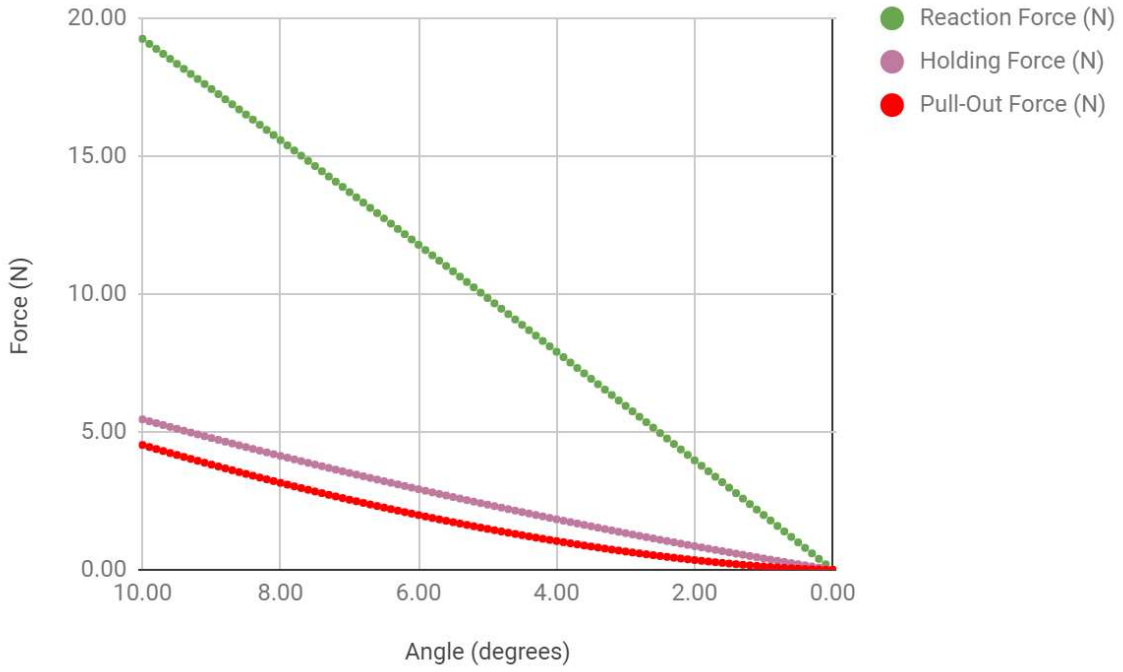


Figure 61: Toggle Gripper Pull-Out Force

By balancing the relations that the previous analysis provides with the remainder of the system's overall design needs in regard to size, fit and mass, the gripper's geometry can be assigned and the force properties deduced. Assuming the gripper geometry holds the values dictated in Table 6:

Table 6: Gripper Geometry

| Variable | Value |
|---|---|
| $\propto_0$ | $10°$ |
| $a$ | $18.14\ mm$ |
| $b$ | $11.47\ mm$ |
| $c$ | $28.73\ mm$ |
| $\gamma_0$ | $10°$ |

Properties of the selected spring can be found in Table 7:

Table 7: Spring Selection

| Variable | Value |
|---|---|
| $n_{springs\ in\ parallel}$ | 2 |
| $k$ | $3.31\ N/mm$ |
| $x_0$ | $19.05\ mm$ |
| $F_{unstretched}$ | $2.31\ N$ |

Then the resulting forces (shown in Table 8) can be determined to be:

Table 8: Gripper Forces

| Variable | Value |
|---|---|
| $F_{Spring,Max}$ | $56.92\ N$ |
| $P_{Max}$ | $19.26\ N$ |
| $F_{Grip,Max}$ | $5.75\ N$ |
| $F_{Holding,Max}$ | $5.46\ N$ |
| $F_{Pull-Out,Max}$ | $4.53\ N$ |

With these results, the linear actuator must be sized to be greater than $P_{max}$ (it is currently sized to provide 80 N) and the bottom gripper must be sized to provide less than $F_{Pull\text{-}Out,Max}$. As shown in Figure 62 below, the bottom gripper holding force is determined by the friction force, spring force, and concave feature angle.

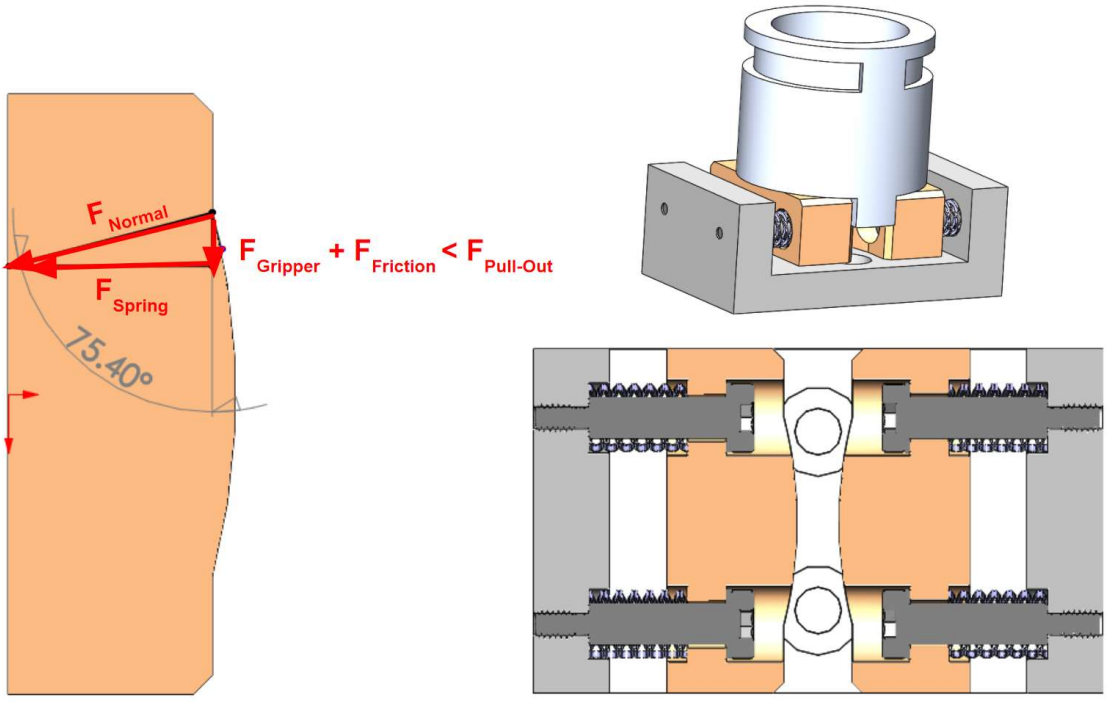


Figure 62: Bottom Gripper Force Diagram and Design

One of the primary challenges in transporting the sample was changing the orientation of the gripper. The gripper was designed so that capture and release are facilitated by the same mechanism; rotation is needed

to allow for the containers to be picked up and deposited on opposite sides of the gripper's initial, neutral position in front of the docking station. Actively turning the gripper was briefly considered, then discarded in favor of being conservative with regards weight and power supply. Thus, a passive system of ensuring the proper amount of rotation became the design goal.

From its neutral position to any of the vault windows/measurement/refill stations, the gripper is never required to exceed 180 degrees of rotation. Further rotation would require modification of sample measurement plans, as well as introduce opportunities for the over-constraint of the system and tolerance stack ups. In order to hit the 180-degree mark and go no further, some method of indexing the gripper position was deemed necessary. Mechanisms such as a rack and pinion were explored, but concerns about over gear teeth binding were being raised. Ultimately, the team found its biggest source of inspiration while researching Geneva drives.

The Geneva drive is a mechanism that converts continuous rotation into intermittent rotary motion. The driven wheel contains some number of slots that interface with the driving wheel via a pin the same diameter as the slots. As the driving wheel spins, the pin moves into the driven wheel's slots and turns the driven wheel one step at a time, as seen below in . When not in direct contact with the pin, the driven wheel's position is constrained by a round mating feature that runs between each set of slots. Due to their inherent looser constraints, slots are less likely to cause binding than gears. Additionally, slots can be sized to offer enough clearance to compensate for possible lead screw backlash. Thus, it was determined that a slot and pin indexing mechanism suited the needs of the design best.

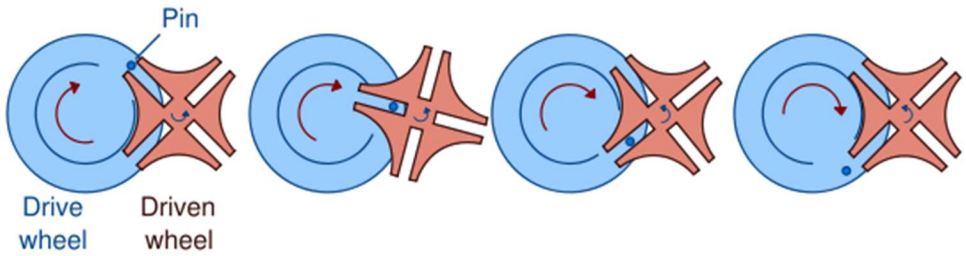


Figure 63 Geneva Mechanism [50]

This stands in contrast to the Geneva drive mechanism currently designed, a timeline for which can be seen below in .

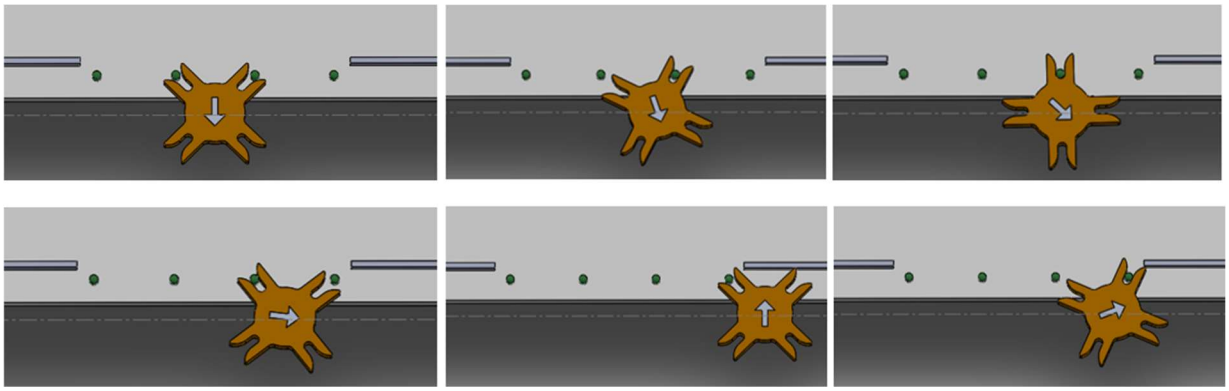

Figure 64: Geneva Mechanism for Transport Subsystem

In this timeline, the mechanism is pictured with no attachments in order to make its function clearer. The arrow indicates the position the gripper would be facing, with down being toward the docking station. In

the first image, the driven wheel is seen in its neutral state, with the gripper facing outward. As the lead screw moves the gripper assembly to the right of the image, the pins push the driven wheel to rotate about its central axis, the path of which is represented by the dashed line. After passing through the pins, the driven wheel's rotation is halted by a low guide rail. When in contact with the rail, the driven wheel has rotated 180 degrees, and is kept from rotating any more. The gripper can then face the wall as the lead screw moves it about the system. Running the lead screw in the opposite direction forces the same process to happen in reverse.

While this rotary motion mechanism draws heavy inspiration from the Geneva drive, it is not a "true" or typical one. A typical Geneva drive involves two rotating bodies; the driven wheel in this design only rotates when one of its four slots interface with one of four stationary pins. Additionally, there is no rounded mating feature as it would not constrain the driven wheel in a helpful manner and add mass to the overall system. At its core however, this mechanism relies on the same principles employed by Geneva drives, and will serve well as a passive rotator. The final iteration of this Geneva mechanism has a cross member between alternating prongs to resist deflection of the prongs.

### 4.3.6. Drive System

To find the sample container transport design best suited to the overall subsystem, the team identified several goals that an ideal design would strive to achieve. First and foremost, the transport subsystem shall be able to deliver the sample containers to all necessary points. This includes transportation to the docking station, the volume measurement station, the container refill station, and each of the three vault wall doors. Furthermore, the transport design must be dynamic enough that it can adjust the container's route based on the process circumstances. For example, if Container 2 does not have enough sample for it to be delivered to Vault Door 2, the subsystem must be capable of returning the sample to the dock so that the robotic arm can send the container out for refilling. It should be noted that a design that requires the opening of a vault door the container is not being delivered to is non-ideal, as the unnecessary opening of vault doors exposes the sample to unwanted radiative heat. An ideal transport system should also use the least amount of motors necessary to power the system to reduce the burden on system weight, volume, and energy requirements. This may involve creating some transport systems that can be passively drive by another system, as seen in the passive gripper designs. An ideal transport design should strive to minimize the number of handoffs required in each container delivery process. Each handoff is another opportunity for an error resulting in harm or loss of sample to occur and these opportunities must be minimized. Lastly, since the transport subsystem will likely be one of the largest subsystems in the integrated design, low weight and small footprint are also highly valued characteristics of a successful transportation design.

One method considered to transport the samples was via carousel, wherein the path of delivery is roughly circular and its motion can be directly run by a motor at the rotational axis of the pathway. Arranging the instrument ports in a circular array along the delivery path of the carousel would allow for the carousel to deliver to each vault window once per full rotation. However, since the carousel's pathway traverses over each instrument port, delivery of containers to the correct location in the correct order is crucial to functionality, and presents many design challenges. Ultimately this design was deemed unfeasible.

One commonly implemented method of container transportation is through linear actuation. In linear actuation, rotational motion from a driving motor is translated into linear motion. Two popular methods of linear actuation applicable to this system lie within the categories of belt and chain actuators versus ball and lead screw actuators.

With belt and chain actuators, the belt or chain is held in tension by two pulleys or sprockets while one of the pulleys or sprockets is driven by a rotary motor. A cart could be mounted to the belt or pulley so that the cart experiences translation when the motor is powered Belt and chain actuators are very simple in design and can transmit payloads long distances efficiently. However, they tend to have low displacement precision [51].

Ball and lead screw actuators, sometimes referred to as spindle actuators, utilize the operating principle of a screw in Figure 65.

Figure 65: Lead Screw and Lead Nut Mechanism

In a lead screw actuator, a motor drives the rotation of a lead screw and as a result, a lead nut travels linearly down the shaft if the lead nut's rotation is fixed. While there is some backlash in these actuators, lead screw systems can offer very high precision displacements and can be very tightly controlled. Lead screws and ball screws operate on the same principle however they differ in their nut/screw interface. Lead screw systems rely on geometric properties of helical wedges contacting each other while ball screws use a sophisticated mechanism that is essentially a continuous ball bearing in a helical pattern. Because of this mechanism, ball screws encounter far less friction than lead screws and have higher efficiencies of 80-90% versus 25-50% for lead screws. Because of this, lead screws generate more heat than ball screws and run more slowly. However, because ball screws are more complex, then tend to be more delicate than lead screws. Ball screws need to be regularly lubricated, can jam easily if they encounter debris, and typically require an active braking mechanism. Due to the need for precision, reliability, resilience to the environment, and a tight footprint, the team has determined that the lead screw actuator best fits the need of the linear transport system [51].

After numerous iterations and component spec'ing, the team designed a finalized linear transport assembly, seen below in Figure 66. Design of components is discussed below.

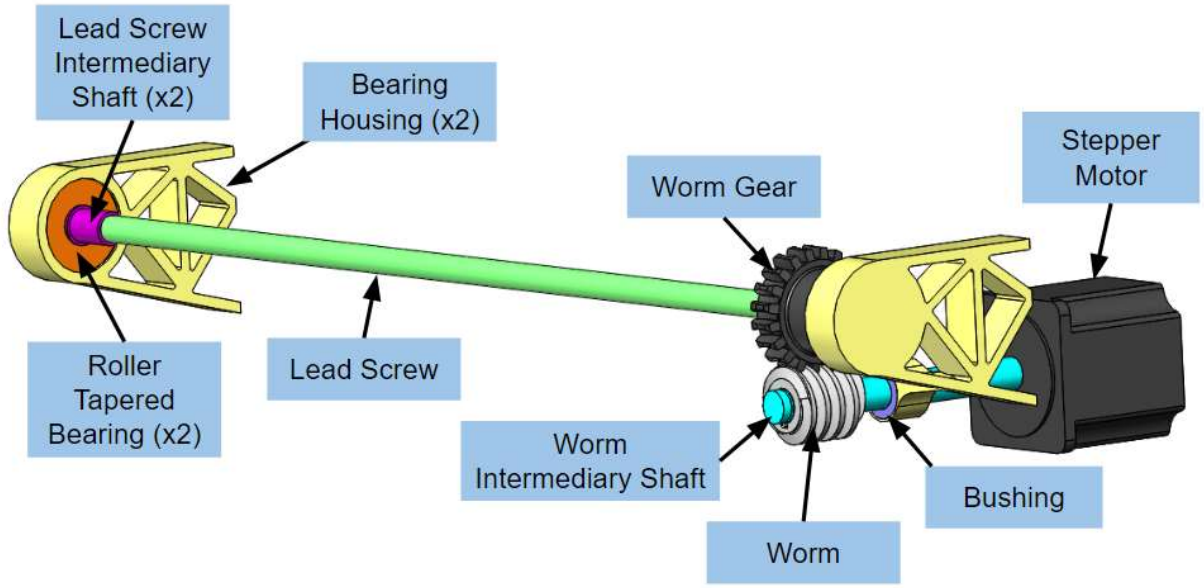


Figure 66: Linear transport assembly

In choosing a lead screw, top concerns included precision and weight. As the lead screw needs to extend the length between the two furthest vault windows, small increases in diameter result in a sizable weight increase. At the same time however, any appreciable deflection could cause binding, and a too-thin lead screw might not be able to support the weight of the carriage (the payload being transported by the lead screw, in this case the assembly carrying the sample container). For the purpose of creating a prototype, only off the shelf parts were considered. Metric lead screws were examined as it would make calculations and conversions simpler. Given an assumed carriage mass of .25kg, the density of steel (the material all considered lead screws were made of), and an assumed maximum length of 250 mm, four different lead screw sizes and their respective masses and max deflections were found. Maximum deflection was approximated using beam theory of a three-point bend. Also considered was the lead, or mm of linear motion per revolution. The smaller this number, the more precision the system could achieve [51].

Ultimately, it was decided that a 10M lead screw, with a diameter of 10 mm and lead of 2 mm per revolution, offered the best tradeoff between lead and mass. To ensure it would be able to withstand its load without deflecting, a static simulation study for deflection was run in SolidWorks. Applying a point load of 0.25 kg in the center of the shaft resulted in a maximum deflection of 0.01226 mm, as seen in Figure 67. Such a small deflection would be negligible in the operation of the system and thus it was determined that a 10M lead screw would suit the team's needs.

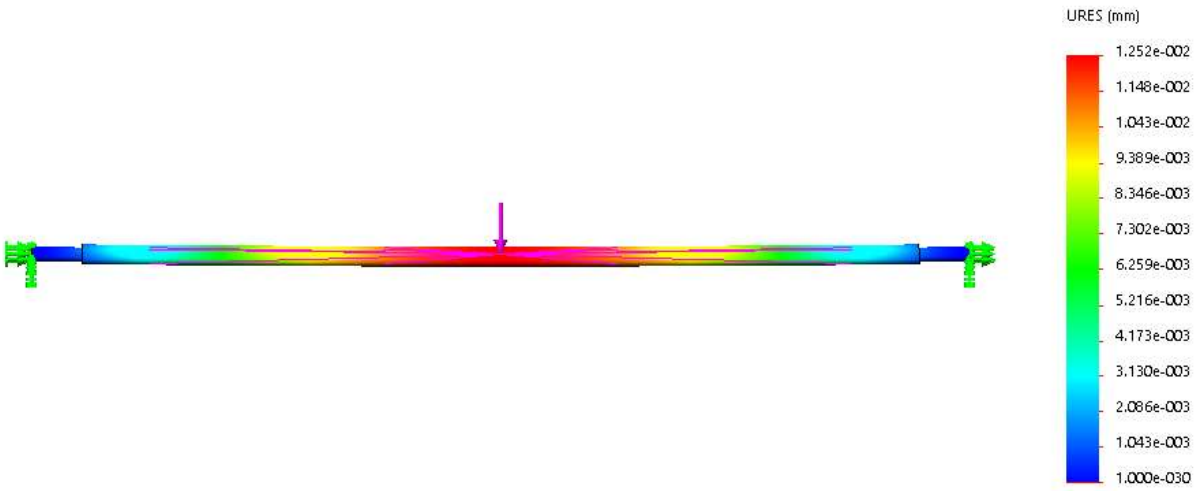


Figure 67: Lead screw deflection study

With the lead screw chosen, bearing selection was possible. Only roller tapered bearings were considered, as they support both axial and radial loads in a compact package. For sizing purposes, roller tapered bearings with an outer diameter of 35 mm and inner bore of 15 mm. These bearings were rated for a dynamic loading of 18.5 kN and static loading of 14.6 kN, as well as speeds up to 20,000 rpm. As these loads and speed were far greater than the 0.25 kg mass or motors under consideration could possibly impart, the bearings were considered acceptable. It should be noted that fatigue did not factor into calculations, as the system will undergo very few cycles [51].

To ensure proper function of any motor powering the transport system, sans special design features such as heating elements, the driving motor will be placed inside the vault wall with a powered output shaft protruding through the wall. This orientation necessitates power transmission at a right angle from the motor shaft to the lead screw.

Both a bevel gear (the right image in Figure 68) and a worm gear were considered for accomplishing right angle power transmission. The main advantages of a bevel gear lie in its ability to transmit high powers at high speeds and low gear ratios.

Figure 68 Worm Gear and Bevel Gear

However, this type of gear suffers from backlash concerns that would further contribute to a system-wide decrease in precision. Worm gears in contrast tend to transmit power at high gear ratios, thus amplifying the torque transmitted while decreasing the output speed. Being able to amplify torque in the gear train also allows a smaller motor to drive the system. Their design also makes them nearly impossible to backdrive, making them ideal for high precision applications where motor braking is not desired. As speed and lower gear ratios are not important concerns for this design in comparison to precision and low amount of backlash, the worm gear was chosen by the team as the ideal right angle power transmission candidate [51].

In choosing a worm gear, the team was primarily concerned with size and weight. In order to achieve an optimal transmission ratio, the gear in a worm gear assembly are often quite large, especially considering the design envelope and weight restrictions. After looking at OTS components available, the team decided on a worm and gear that offered a transmission ratio of 20 with pitch diameters of 1" and 1.67" respectively. This ratio means the worm connected to the motor shaft rotates 20 times for every 1 revolution of the gear coupled with the lead screw, causing the lead screw to turn more slowly but with more torque than if it were directly driven by the motor. Although the use of components with imperial measurements was not desirable, their relatively small size made them an optimal choice.

There was some concern over the stresses the worm gear teeth would be subjected to. Worm gear teeth are much weaker than that of the worm due to their unique geometry. To check for failure, the allowable tangential force was found as seen in Equation 17:

$$(W^t)_{all} = C_s D_m^{0.8} F_e C_m C_v \quad (17)$$

Where $C_s$ is the materials factor, $D_m$ is the mean gear diameter, $F_e$ is the effective gear face width, $C_m$ is the ratio correction factor, and $C_v$ is the velocity factor. The allowable force of 395.5 lbf was then compared to the actual tangential force, found using Equation 18 below:

$$W_G^t = \frac{33{,}000 n_d H_o K_a}{V_G e} \quad (18)$$

Where $n_d$ is the design factor, $K_a$ is the application factor, $H_0$ is the output horsepower, $V_G$ is the tangential gear speed, and $e$ is the efficiency. The tangential force seen by the gear was calculated to be 250 lbf. As this force is less than the allowable force, the gear mesh will survive. To get a sense of the actual stresses the gear would experience under load, a static simulation was run in SolidWorks wherein $W_G^t$ was applied to one tooth. The effects of this study can be seen below, in Figure 69.

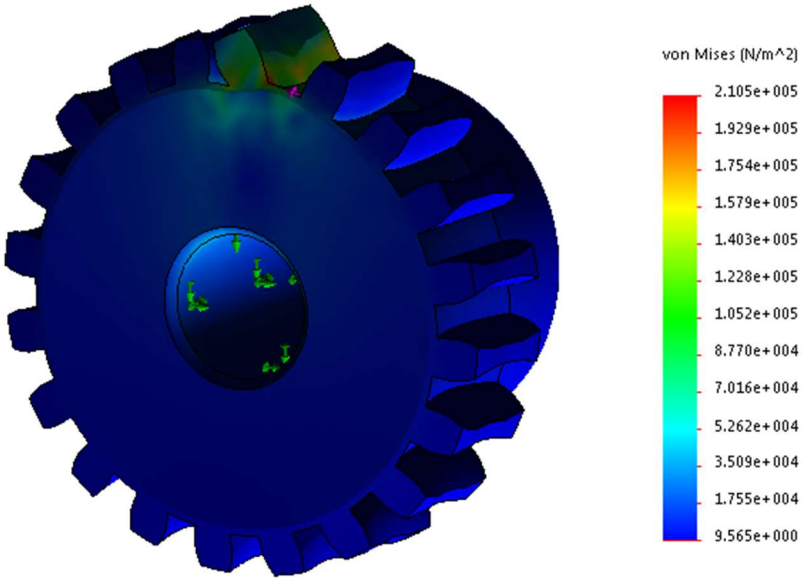


Figure 69: Worm gear teeth von Mises stresses

As seen in the figure above, the maximum von Mises stress experienced by the tooth was 210,500 N/m$^2$. As the yield strength of the gear material, iron, is 50 MPa, the gear teeth will not experience nearly enough stress to yield or otherwise cause problems within the assembly [51].

With the lead screw and power transmission components decided upon, motor selection was possible. The team considered various motors such as brushed DC, brushless DC, servo, and stepper, ultimately deciding on using a stepper motor to drive the system. A stepper motor is a type of brushless DC motor that divides one full rotation of the motor shaft into steps of equal size; the motor can be controlled to move by a certain number of steps and thus a certain degree of rotation on the output shaft. When connected to a lead screw through a gear drive, this step to revolution value is further decreased. The result is that through combining a lead screw with a stepper motor, a high degree of accuracy in position can be known at all times. The error in stepper motor position is about 3-5% of a step, but this is non-cumulative meaning that having a slightly inaccurate payload position in one spot does not negatively affect the motor's positioning of the payload to the next spot. Precision can be further increased by microstepping, or using a controller to smooth the shocks of applying steps to the motor. Equation 19 below can be used to determine steps per mm, an important metric for determining lead screw precision [52].

$$steps\ per\ mm = \left(\frac{revolution}{mm}\right)_{lead\ screw} * \frac{1}{microstep} * \left(\frac{step}{revolution}\right)_{motor} \quad (19)$$

In choosing a motor, first the torque required must be considered. In order to drive a load, the stepper motor must overcome the torque due to acceleration as well as friction, which can be summed up by the relationship seen below in Equation 20:

$$\tau_{motor} \geq \tau_f + \tau_A \quad (20)$$

$\tau_f$, the torque due to friction, results from both the carriage sliding along the lead screw, as well as the frictional force acting at the worm and gear. Combining the two sources of friction, the equation for finding total torque due to friction can be seen below in Equation 21:

$$\tau_f = \frac{\mu W}{2\pi Pe} + \frac{f W_G^t D_m}{2(f sin\lambda - cos\emptyset_n \, cos\,\lambda)} \quad (21)$$

Where $\mu$ is the coefficient of friction of the lead nut and lead screw, $W$ is the weight of the carriage, $P$ is the pitch of the lead screw, $e$ is the efficiency of the lead screw, $f$ is the coefficient of friction between the gear and worm, $W_G^t$ is the tangential force acting on worm gear, $D_m$ is the mean gear diameter of the worm gear, $\lambda$ is the lead angle of the worm, $\emptyset_n$ is the normal pressure angle of worm. The torque due to friction was calculated to be 0.711 N.

Next the torque due to acceleration was calculated. This is directly related to the inertial load reflected back to the motor through the gear train. The inertial load of the worm gear, lead screw, and carriage is multiplied by the inverse of the worm and gear transmission ratio squared, plus the inertial load of the worm and motor. This relationship can be seen in Equation 22:

$$J_{tot} = J_m + J_w + [\left(\frac{N_w}{N_g}\right)^2 (J_{ls} + J_g + J_{lin})] \quad (22)$$

Where $J_{tot}$ is the total inertia, $J_m$ is the motor inertia, $J_w$ is the worm inertia, $N_w$ is the number of leads on worm, $N_g$ is the number of gear teeth, $J_{ls}$ is the lead screw inertia, $J_g$ is the worm gear inertia, and $J_{lin}$ is the inertia of the carriage.

The total inertial load is then related to the torque due to acceleration as seen in Equation 23 below:

$$\tau_A = \frac{J_{tot}\alpha}{e} \quad (23)$$

Where $\alpha$ is the angular acceleration and $e$ is the overall efficiency. Without choosing an angular acceleration, the torque due to acceleration becomes $7.94*10^{-7}\alpha$. Thus the torque the motor must be able to produce must be equivalent to $0.711+7.94*10^{-7}\alpha$ [51].

The torque produced by a motor can be shown by the relationship shown in Equation 24 below:

$$\tau = \frac{P}{\omega} \quad (24)$$

Where $P$ is the power supplied to the motor, and $\omega$ is the angular velocity of the motor. This relationship demonstrates that by adjusting the voltage or current supplied to the motor, as well as the speed the motor is running out, the torque output can be varied. Stepper motors are unique in that they output higher torque at lower speeds rather than faster ones like most motors. The maximum amount of torque the motor can supply is determined by the holding torque, or torque required to turn the motor shaft while current is applied to the motor [52].

Ultimately a stepper motor was chosen that offered a holding torque of 0.883 Nm and a step resolution of 100 steps per mm, as well as a max speed of 108 rpm. This holding torque is close to the required torque due to friction and acceleration, however by adjusting the angular speed and acceleration as well as current and voltage, the initial torque acting against the motor can be overcome and the carriage propelled forward.

The bearings selected were the smallest readily available, however their inner bore was still 5 mm larger than the major diameter of the lead screw. An intermediary shaft was needed between the lead screw and

bearing to account for this difference in diameters. To achieve this, two intermediary shafts were designed as seen below in Figure 70 and Figure 71.

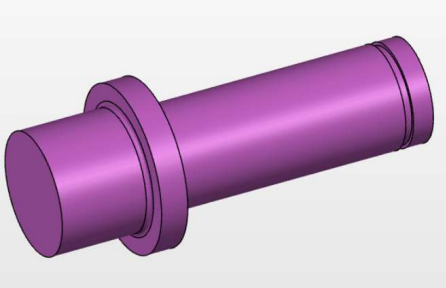

Figure 70: Intermediary shaft 1

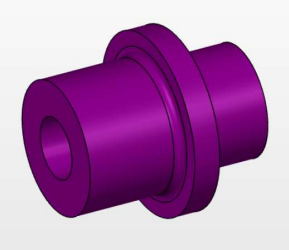

Figure 71: Intermediary shaft 2

By making these intermediary shafts out of aluminum and correctly sizing the bore to have an interference with the turned-down end of the lead screw, the shafts could be shrunk-fit onto the lead screw at a tight enough fit to transmit all torque. Intermediary shaft 1 has a slightly oversized diameter on the skinnier portion so that the worm gear will have an interference fit onto it; a retaining ring groove serves to further constrain it. Shoulders on both shafts constrain the movement of the bearings to keep them from falling out of the bearing cups.

Another intermediary shaft is necessitated by the short shaft length of the stepper motor. Although the chosen motor's shaft is 35 mm in length, the worm it must rotate is centered above the lead screw at 80 mm from the shaft wall. Although not ideal, this distance from the wall is needed to allot for the arc the linear actuator sweeps as it makes a revolution. The third intermediary shaft connecting the motor to the worm is shown below in Figure 72.

Figure 72: Intermediary shaft 3

Shaft 3 was made of aluminum and pressed onto the motor shaft. A milled keyseat and two retaining ring grooves will constrain the worm on the shaft. Two set screws along the axis secured the intermediary to the motor's shaft further.

To suspend the entire lead screw assembly, two bearing housings will be manufactured from aluminum. These bearing housings, seen below in Figure 73, are placed so as to hold the bearings and thus lead screw at the required 80 mm from the vault wall, as well as support the carriage at the correct height.

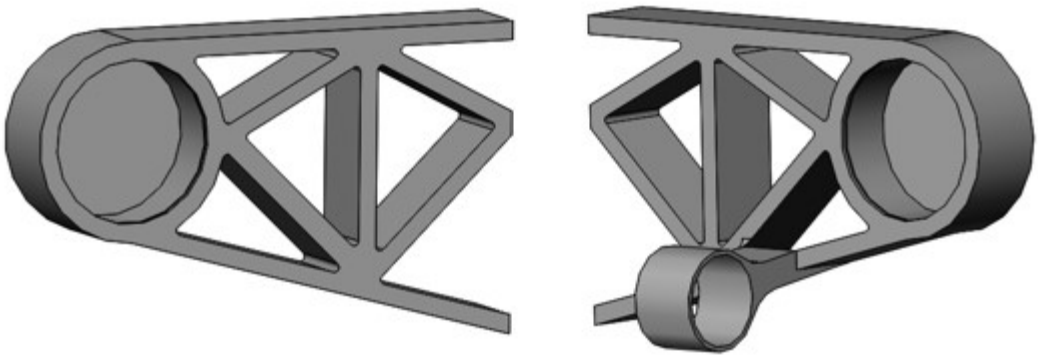

Figure 73: Bearing housings

Rather than have straight cantilevered beams supporting the lead screw and its bearings, the lower leg of the housing were angled. To save material weight while maintaining structural integrity, triangular trusses join the upper and lower legs of the housings. An extrusion was added on the right bearing housing in order to hold the bushing supporting the intermediary motor shaft; without this support the worm gear could become significantly cantilevered and system function would not be optimal.

To determine just how well these bearing housings would fare under load, a SolidWorks simulation was carried out and point loads were applied in the bushing holder as well as the main cup of the housing. The results of this study can be seen below in Figure 74.

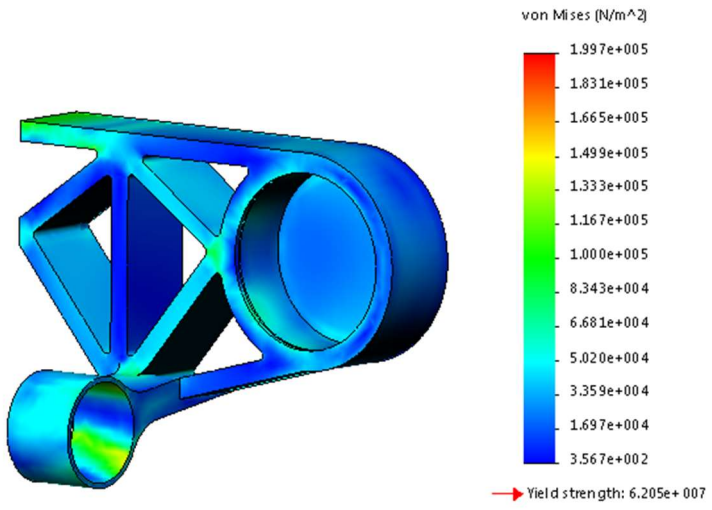


Figure 74: von Mises stresses of right bearing housing

According to this study, the maximum von Mises stress were found to be about 200,000 $N/m^2$. The yield stress of aluminum, however, is 290 MPa, well above this threshold. Thus, the bearing housings will perform to standards.

As the prototype's bearing housings were to be 3D printed, a bearing cup needed to be designed to allow for a tight, controllable fit between the bearing and its housing. These bearings were made of aluminum and correctly sized to stop any relative motion of the outer ring of the bearing.

### 4.3.7. Volume Measurement

After reviewing considering system requirements and available technology, the team decided that an optical measurement system would be the best option for determining volume. An optical measurement system would not interfere with the sample physically, and preliminary reviews suggested that any radiation from a light source would not affect the sample temperature enough to move it out of the required temperature range. Because sample security is one of the bigger concerns for this subsystem, it was imperative that a non-disruptive solution be implemented.

After looking through several potential optical measurement sensors, an infrared (IR) proximity sensor was selected. IR sensors work in a wide range of temperature applications, critical for a system such as this where the sensor must operate at cryogenic temperatures but also survive the 56 day, 125°C bake-out procedure. IR sensors are simple and low profile, allowing for easy integration with the system without any threat to mass or space occupancy. The VL6180X "time of flight" sensor from Adafruit was chosen for closer investigation. Figure 75 below shows a picture of the IR proximity sensor. Its footprint is suitably small at 18mm x 16.5mm by 3.75mm. The sensor operates on a "time of flight" principle, meaning that it calculates distance based on the time it takes for an IR light to travel from and back to the sensor. This type of sensor was selected due to its independence of material reflectance. Other IR proximity sensors operate using an amount of light reflected. Because the reflectivity of the surface sample is unknown, it was decided that this would be a better option for the subsystem. The IR sensor was also selected because of its ability to take measurements through transparent materials. Preliminary particle simulations suggest that the sample containers will need a cover in order to prevent sample material from exiting the sample container.

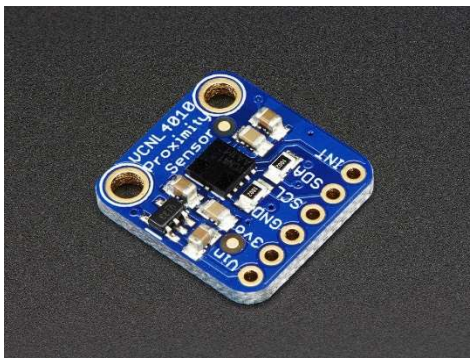


Figure 75 Adafruit IR Proximity Sensor

For the measurement to work with a transparent cover, the top of the lid must be clear. This lead the team to include a surface scraper to scrape the top surface of the sample container, clearing it of any sample. For this scraping, the team considered 2 options: a flap-type scraper similar to a window squeegee, or a brush with bristles. The primary concerns with a brush design were that the sample could accumulate within the bristles of the brush. This may lead to particles to fall back onto the cover, which would lead to inaccurate measurement. For this reason, a flexible flap was selected. The current station design can be seen in Figure 76.

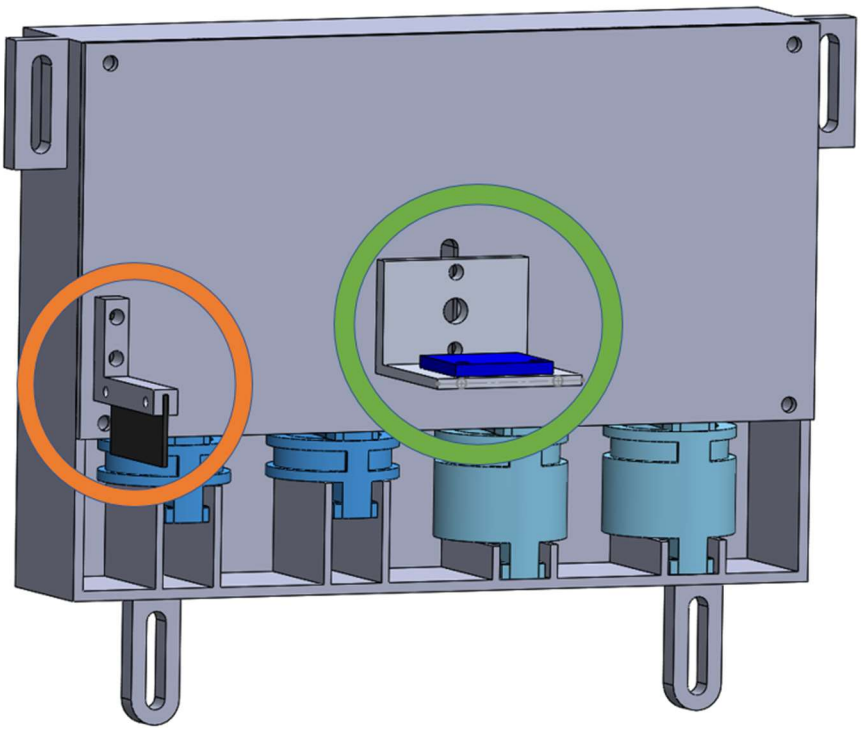

Figure 76: Optical Measurement Station

The blue chip circled in green is the IR proximity sensor, which is oriented downward in order to read the volume of a sample container located below this assembly. A flexible flap for scraping the top of sample containers is a separate component located to the side of the refill station, seen circled in orange. To attain a volume measurement, the cup will then sit below the IR sensor and the sample inside will be measured. If the cup has sufficient volume, it will be passed on to the corresponding scientific instrument. If the cup does not have sufficient volume, it will be transported back to the excavation arm for further sample collection.

One of the most important aspects of implementing the IR sensor is the calibration of the device. To get the best measurement possible, the sensor needs to detect only the surface of the sample material. Because the sample container has a cover on it, this will be more difficult. The IR sensor selected for this project has a range of calibration tools in order achieve the most accurate measurements for this application. It is important to note that the IR sensor is a "time of flight sensor" which means that its distance measurements are done based on the amount of time it takes for the IR light to leave and travel back to the sensor. This time will then give a distance from the sensor to the surface that reflected the IR light. The sensor has the ability to block out IR readings within a certain specified distance. Because the cover is transparent, light from the sensor will pass through it, although some will be reflected back, which would cause a bad reading. In order to get an accurate reading of the sample height within the container, this prematurely reflected light will need to be ignored. To do this, the sensor will first take a reading without any filters. This will give a distance from the sensor to the top of the cover. This is useful because it will give the volume measurement a starting height. Once the height is determined, the sensor will then be able to filter out any IR light that would read a distant of that reading, plus the thickness of the cover. This in turn, gives a point for the bottom of the cover (which is also the top of the container). Knowing how far away the bottom of the cover is, is key to calculating the distance of the sample from the bottom of the cover. The sensor will then flash another IR light, ignoring any premature IR readings from the

cover glass. The reading received by the IR sensor will be from the sample material inside the container. This height will then yield a volume of the sample using Equation 25.

$$V = \pi r^2 h \quad (25)$$

Where V is the volume of the sample container, r is the radius of the inner wall of the sample container and h is the height of the sample material in the sample container. h can be described by the following Equation 26.

$$h = l - d \quad (26)$$

Where l is the height of the sample container's inner cavity to the top of the container, and d is the distance from the bottom of the cover to the top of the surface, which is found using the sensor. This will then give the sample container's volume, which can then be used to determine if the sample container can be sent to the scientific instrument.

The volume measurement was a fairly unique challenge presented by this project, as most industries dealing with fine powders measure volume based on mass. But this system requires a specific sample volume, not mass. The team needed to come up with a solution that would measure volume without risking the purity of the sample, leading to the time of flight sensor being selected.

### 4.3.8. Refill Station

The refill subsystem shall also be the site for the collection of new sample containers to replace the used ones. Once the excavation arm docks and all of the cups it has filled are verified and sent to the scientific instruments, three new sample containers are required to continue sample collection. For this, the team decided to use the gripping cart to collect a new sample container and bring it back to the arm for reloading. There are many examples of container replenishing mechanisms, most notably a cup dispenser. Cups are typically stacked vertically in a cup dispenser, with one of the cups suspended outside of the containing device. When a cup is taken, the next cup moves into its place, either by gravity, a spring, or some sort of connecting feature between cups. This stacked cup technique is well suited to the needs of the project, as it can be designed so that the cups are always in the same position when they are ready to be used.

Since there are two types of container cups, 1 cc and 5 cc, the dispenser was designed to have two sections dispensing each size. Due to the limited vertical space, it was decided to have four columns of stacked cups, with two columns of four 1 cc cups and two columns of 5 cc cups stacked two high. This design is based off the assumption the robotic arm will be responsible for holding the first set of three container cups. This cup distribution allows for five full sets of sample collections, or fifteen containers in total. Upon consultation with JPL, this decision was approved.

In order to bias the cup stacks toward the bottom of the dispenser where they can be accessed, compression springs were used. Gravity could not be relied on for assistance due to low gravity on Europa. Four springs, one for each stack, were included in the design, as can be seen in Figure 77. The springs push down on a platform resting on top of the cup stack. This prevents the springs from coming in contact with the sample containers as well as distribute the spring force over the upper surface area of the sample container, removing worry of localized pressure points. The container will be attached to the vault wall and situated between the rightmost door and the center door.

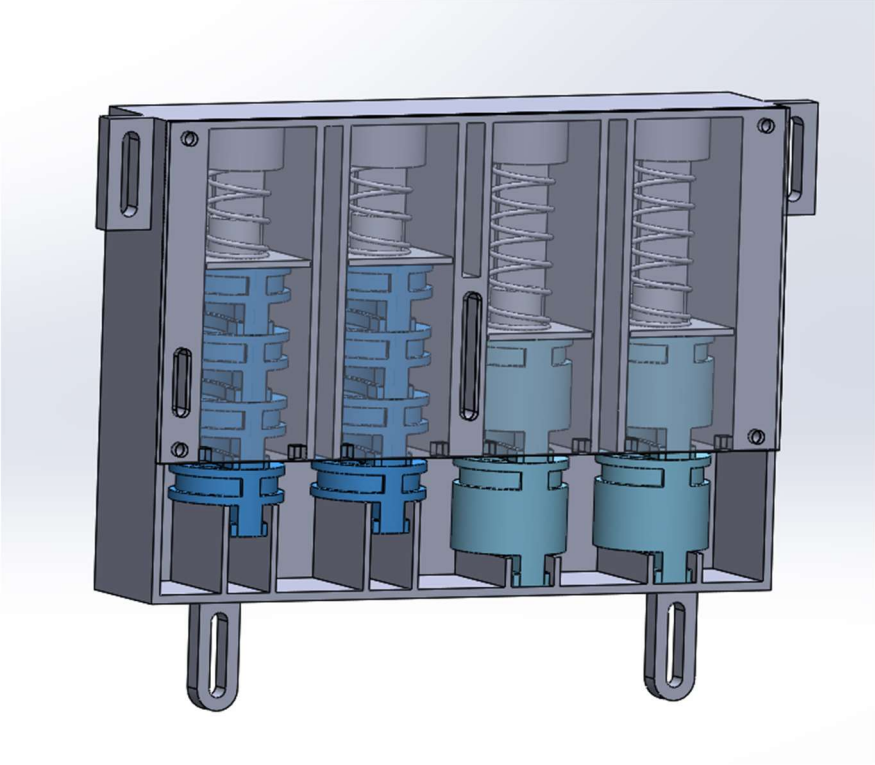

Figure 77: Refill Container

One concern with this design is that as a cup is being moved out of the ready position, the cup above it may want to fall at an angle, which may jam the system. The inner wall was designed, however, to be very close to the stack, limiting the amount of tilt the cup might experience upon removal. Additionally, two guide rails placed in the bottom of each container stack help the cup sit in the correct orientation while waiting for the gripper. As seen in Figure 78 , a guide feature in the back of the refill station wall was included to mat with cup geometry and to keep containers from rotating out of proper alignment.

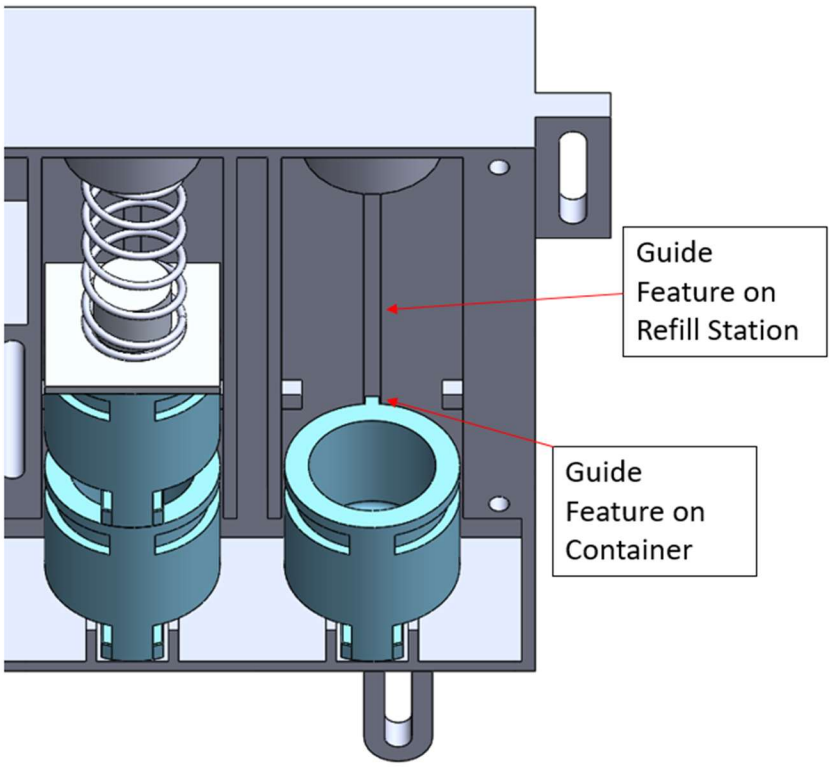


Figure 78: Guiding features on containers and refill station

Although jamming did not prove to be a problem for the prototype, several solutions were developed and are easily implemented. One solutions to prevent jamming is to implement a spacer between cups. This spacer would prevent cups from tipping over, however it would need to be removed from the refill station without traveling with the container. Another possible solution would be to implement a ratchet mechanism that will only allow the platform retaining the spring to move when the ready cup is removed from the refill station. It should be noted, however, that these plans would add possibly unnecessary weight to the system.

In order to avoid interference with the transportation cart and gripper, the cup container was situated so that its front plane was flush with the vault wall. Four mounting features, located at each corner, allowed the container to be attacked to the vault wall.

### *4.4. Design Review*

Review of the design was given by Chris Yahnker, the industry advisor from JPL. The solution presented was concluded to be sound and its design viable, green lighting further development of the system. The takeaways of this review and team responses are discussed as follows.

One concern brought up was the number of handoffs of the sample container. Each handoff adds risk to sample handling, which is very important since any small sample is considered precious. Sample security is a major criterion that was a major reason for why the Linear Concept was chosen over the Carousel Concept. However, it currently seems the design requires each handoff to meet other criteria. For example, two extra handoffs are added with the docking subassembly to account for inaccuracy of positioning of the robotic arm, since the gripper cannot grab each container if it is in an unknown position. The team will answer this concern by designing for each handoff to be reliable.

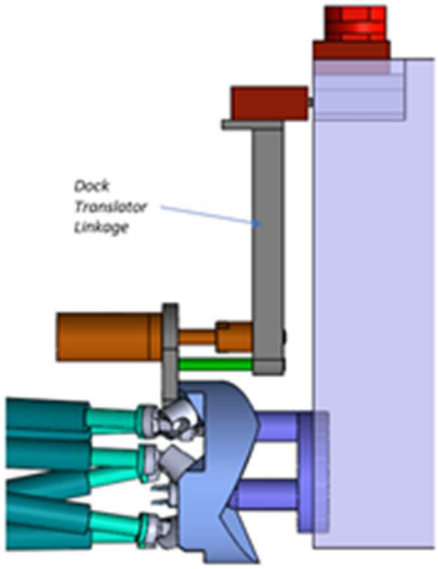


Figure 79: Robot Arm End Effector On Docking System

Another concern brought up was the length of the dock translator piece, seen in Figure 79. The mass on the end of the long part can create a cantilever effect that can cause binding during motion by the spindle drive. This was mitigated by rearranging the assembly to be able to shorten the piece.

The Geneva mechanism was also identified as a potential issue. The combination of linear translation from the lead screw and rotation of the Geneva wheel over constrains the design, and allows for the possibility of binding. This can be addressed by taking into account any inaccuracy in the lead screw translation and factor that into the tolerances between the extensions of the Geneva wheel and the posts that it rotates about.

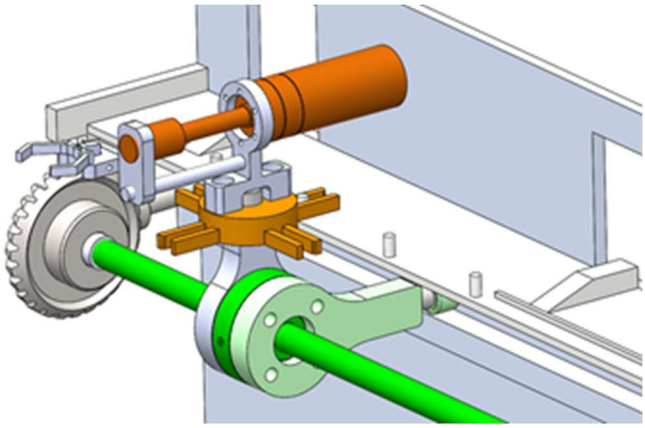

Figure 80 Linear Transport Mechanism

The lock and unlock mechanisms for retaining and releasing the Container Set subassembly was also brought up as an area of concern, since the sliding and rotating of several small parts means that friction will play a big role in the design. The careful tolerancing of parts and material selection will help mitigate this concern.

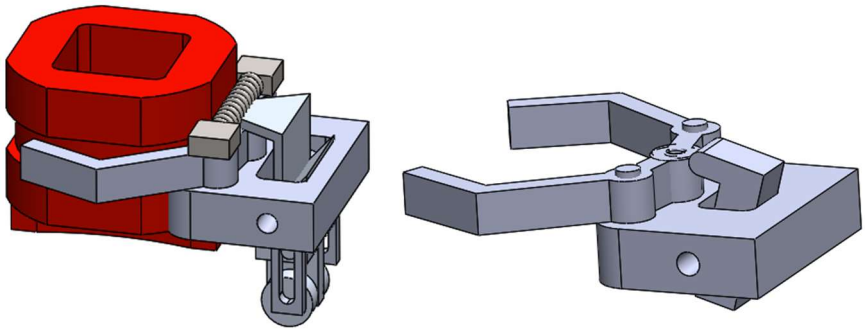

Figure 81 Sample Cup in Pivot Gripper

At the time of the design review, there was a lever on the gripper mechanism, seen in Figure 81, meant to return the gripper to the open position. This was also a point of worry, since the design would have to consider changing contact angles and sliding. This was addressed by modifying the design to have a ramp and slider mechanism replace the lever. This redesign made sure that the release force was more controlled and based more on position than force, which resulted in a more predictable system.

One other change that made the final design after the review was a change from a bevel gear to a worm gear reduction to transfer torque. This was because a worm gear design is less back-drivable, reducing possible backlash in a system where accuracy and consistency is important.

### *4.5. Fabrication*

Due primarily to the timeline and manufacturing limitations such as skill set and cost, much of the system was custom created using 3D printing and laser cutting technologies. This had many positive impacts on design, as it allowed for rapid prototyping and numerous iterations of complex components such as the toggle gripper, Geneva mechanism, and docking mechanisms.

3D printing also allowed for custom bearing housings to be incorporated into the design, which made desired geometries feasible. The rest of the drive system assembly, on the other hand, was machined in house by one team member. In order to account for machining tolerances, extensive tolerance calculations were performed, a table of which can be seen in Table 9. This allowed the team to be confident that the components would work together correctly.

Table 9: Drive system component tolerance calculations

| Part | Place of Concern | Desired Fit | Connected Components | | Basic Size (mm) | | Tolerances | | | |
|---|---|---|---|---|---|---|---|---|---|---|
| | | | | | | | Shaft (mm) | Hole (mm) | Shaft (in) | Hole (in) |
| Shaft 3 | motor shaft | interference (P7/h6) | shaft: | motor shaft | 6.35 | lower: | 6.342 | 6.33 | 0.2497 | 0.2492 |
| | | | hub: | intermediary | | upper: | 6.35 | 6.342 | 0.2500 | 0.2497 |
| | worm | clearance (H7/h6) | shaft: | intermediary | 12.7 | lower: | 12.689 | 12.7 | 0.4996 | 0.5000 |
| | | | hub: | worm | | upper: | 12.7 | 12.718 | 0.5000 | 0.5007 |
| Shaft 1 | lead screw | interference (H7/s6) | shaft: | lead screw | 7 | lower: | 7.023 | 7 | 0.2765 | 0.2756 |
| | | | hub: | intermediary | | upper: | 7.032 | 7.015 | 0.2769 | 0.2762 |
| | worm gear | interference (H7/s6) | shaft: | intermediary | 12.7 | lower: | 12.728 | 12.7 | 0.5011 | 0.5000 |
| | | | hub: | worm gear | | upper: | 12.739 | 12.718 | 0.5015 | 0.5007 |
| | bearing | clearance (H7/h6) | shaft: | intermediary | 15 | lower: | 14.989 | 15 | 0.5901 | 0.5906 |
| | | | hub: | bearing | | upper: | 15 | 15.018 | 0.5906 | 0.5913 |
| Shaft 2 | lead screw | interference (H7/s6) | shaft: | lead screw | 7 | lower: | 7.023 | 7 | 0.2765 | 0.2756 |
| | | | hub: | intermediary | | upper: | 7.032 | 7.015 | 0.2769 | 0.2762 |
| | bearing | clearance (H7/h6) | shaft: | intermediary | 15 | lower: | 14.989 | 15 | 0.5901 | 0.5906 |
| | | | hub: | bearing | | upper: | 15 | 15.018 | 0.5906 | 0.5913 |
| Bearing Housing | bearing | interference (S7/h6) | shaft: | bearing | 35 | lower: | 34.987 | 34.952 | 1.3774 | 1.3761 |
| | | | hub: | housing | | upper: | 35 | 34.973 | 1.3780 | 1.3769 |

The entire assembly was mounted onto a quarter-inch thick sheet of aluminum which had been custom machined to put in bolt holes and openings for mechanisms and vault windows; numerous fasteners were used to hold everything in place.

# 5. Analysis

## *5.1. Steady State Heat Transfer*

One requirement of the system is to ensure the temperature of the sample is maintained below 150 K until it is delivered to the scientific instruments. What makes this requirement challenging is the fact that any motor that is used outside of the Lander body must be heated to a temperature of 223 K to operate. The current design employs two motors outside of the Lander body; the actuator attached to the docking mechanism and the actuator operating the toggle gripper. The actuator that is closest in proximity to the sample container and is the most concerning in terms of heat transfer is the one operating the toggle gripper. This subassembly was simplified and run through SolidWorks thermal analysis software to test the feasibility of the design to prevent the overheating of the sample. Figure 82 shows the results of this analysis, as well as the material of each labeled part and the boundary conditions involved.

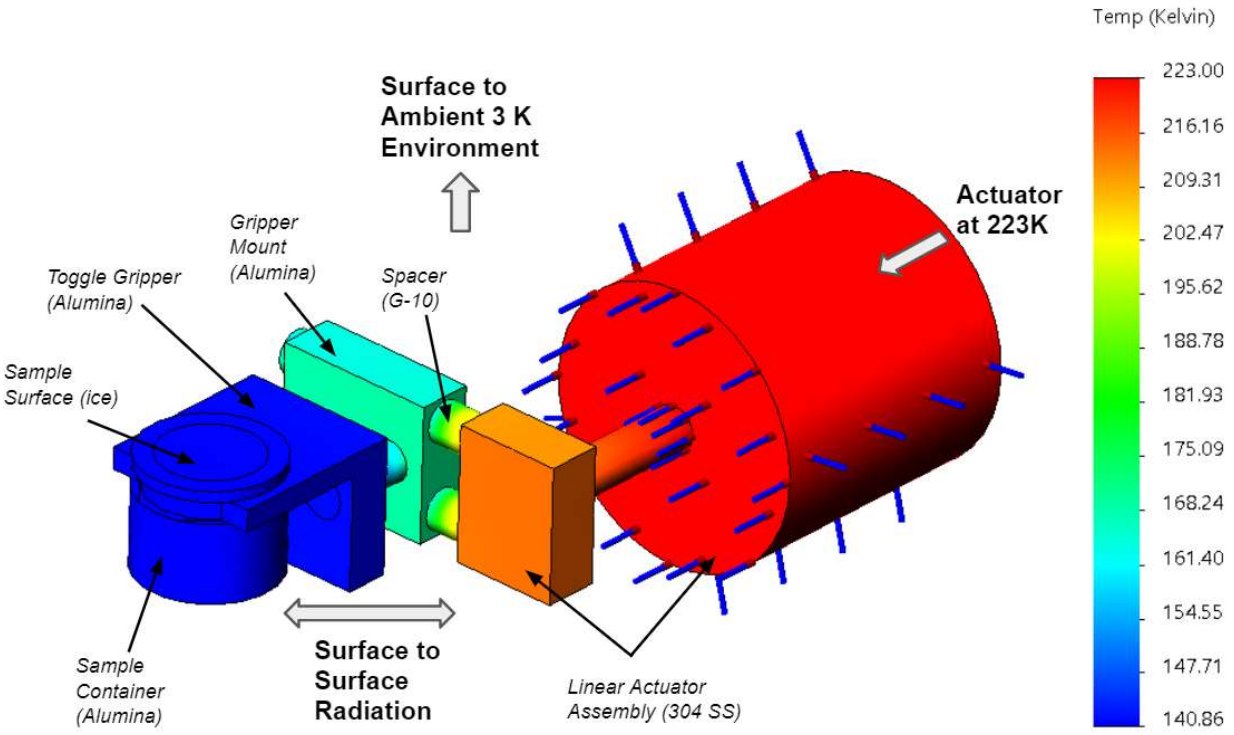


Figure 82: Heat Transfer Analysis for Simplified Toggle Gripper and Actuator Subassembly

Due to the low atmosphere environment of Europa, the two thermal pathways from the linear actuator to the sample container are conduction and surface to surface radiation. Each part is also radiating out into a 3 K environment, which plays a significant part in cooling down the subassembly.

Figure 83 shows the same model but with the sample floating and out of contact from the sample container. This means there is no conduction path to the sample, and it is only heated by radiation from the heated surfaces of the surrounding parts. This illustrates the significance of surface to surface radiation in the model, which may not be intuitive, as the sample is heated all the way from 3 K to 89 K just from radiation. However, this also makes clear that conduction is the driving contributor to heating up the sample, as the temperature of the sample container, 140 K, is much higher than the temperature of the floating sample, 89K. It is important to note that a major reason for this result may be the configuration of the assembly, which intentionally reduces the view factor between the heated actuator and the top of the sample container.

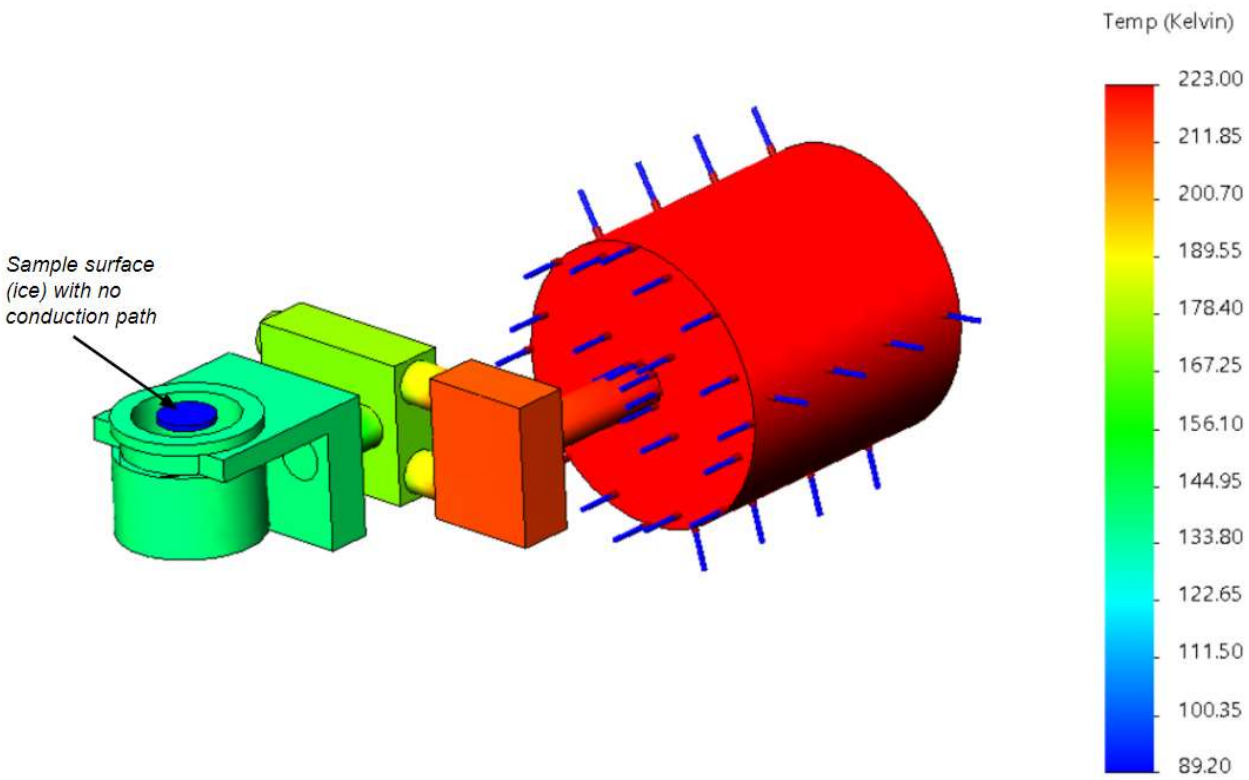


Figure 83: Heat Transfer Analysis to Review the Significance of Surface to Surface Radiation

To evaluate the validity of this model, the assumed conditions of the subassembly are assessed. The driving material properties are thermal conductivity for conduction and emissivity for radiation, both of which are temperature dependent. This dependence can be rather significant, one example of which is seen in Figure 84, which shows the emissivity of G-10 as a function of temperature. In the model shown, the G-10 spacers would have a range of values for emissivity since there is a large range in temperature.

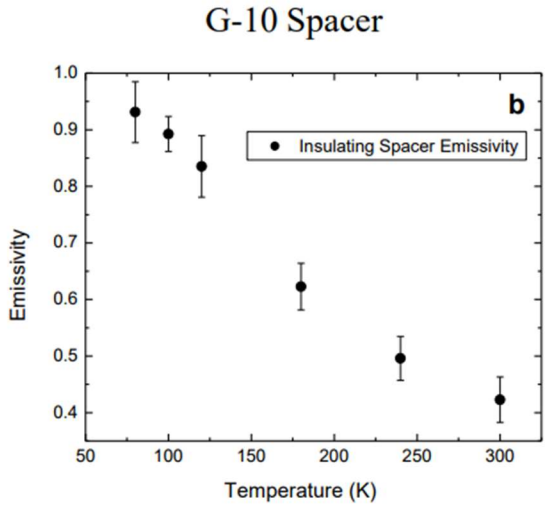


Figure 84: Emissivity versus Temperature of a G-10 spacer [4]

One major challenge of this model is that values for these properties are not always well researched for such low temperatures, which amplifies the importance of empirical testing for this case. To avoid results that conclude a false positive result, reasonable worst-case values are selected for material properties

where there is uncertainty. This means using higher than expected emissivity and thermal conductivity properties. Table 10 displays these chosen values.

Table 10: Values for Thermal Conductivity and Emissivity of Modeled Materials

| **Part** | **Material** | **Thermal Conductivity (W/m-K)** | **Emissivity** |
|---|---|---|---|
| Linear Actuator | 304 SS | 16.2 [53] | 0.05 [54] |
| Spacer | G-10 Fiberglass Epoxy | 0.6 [55] | 0.93 [56] |
| Screw | Modeled as G-10 | | |
| Gripper Mount | Alumina | 18 [57] | 0.8 [58] |
| Gripper | | | |
| Sample Container | | | |
| Sample Surface | Ice | 3.48 [59] | .98 [60] |

Another important note is that thermal contact resistance between components is challenging to correctly model. It is dependent on several factors such as the surrounding pressure, the contact pressure, the materials of the parts, and the roughness of the surfaces. To again take the worst-case scenario, thermal contact resistance is also taken to be zero for all contacts.

The major takeaway from this analysis is that the design is feasible in terms of thermally isolating the sample from a temperature of higher than 150 K. The worst-case values for material properties used in the model mean that a lower temperature would be expected of the sample in an empirical test, even taking into account the simplified geometry used.

### *5.2. Transient Heat Analysis*

Another area of interest is the heating of the sample container while it is being presented to the inside of the lander. Radiation from inside the lander body is the primary method of heat transfer in this scenario; a worst-case scenario has the inner temperature to be 313 K with an emissivity of 0.3. Figure 85 below illustrates the situation for the prototype design, as well as the simplified model used for analysis. Assumptions made for the steady state analysis remained in place for this analysis. Starting temperature of sample and sample container were taken to be 140 K, the steady state result of the previous analysis.

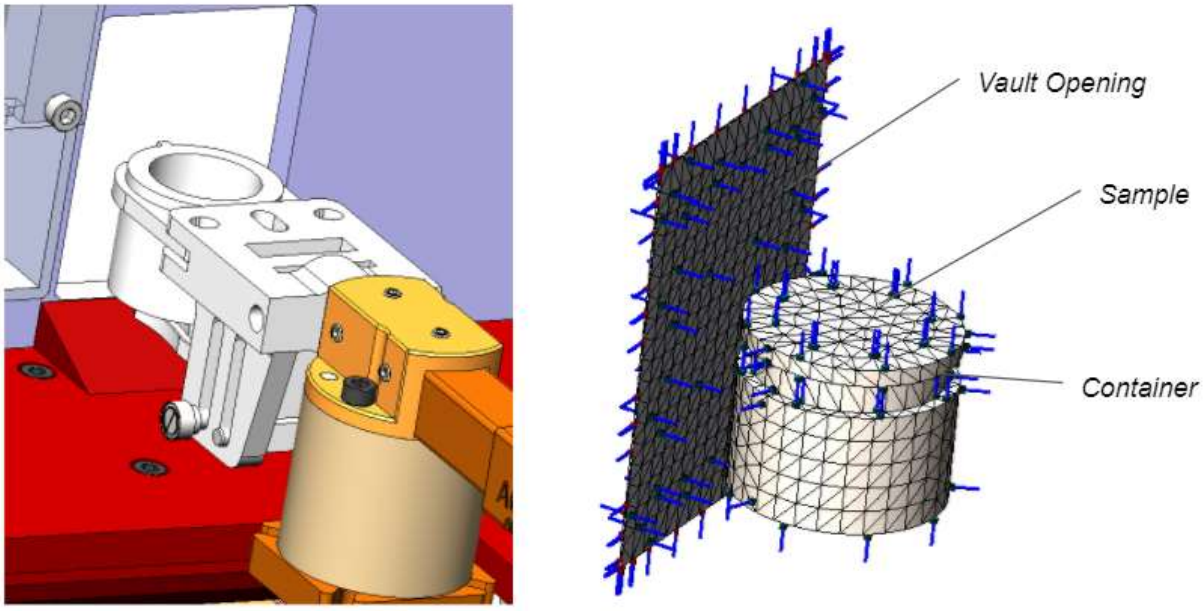


Figure 85: Scenario of interest (left) and simplified model (right)

Figure 86 shows the steady state result of the vault opening analysis. It is apparent the sample reaches a temperature greater than 150 K.

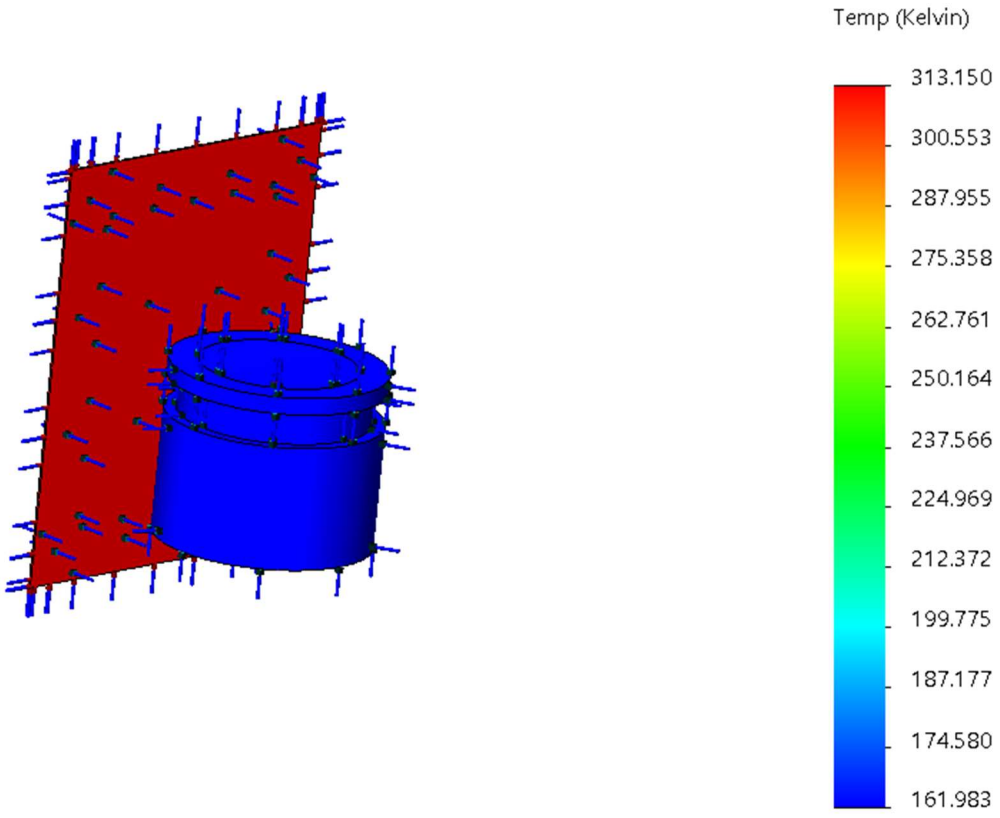


Figure 86: Steady state result of heat transfer

Figure 84 shows the transient result, or how long it takes to reach steady state.

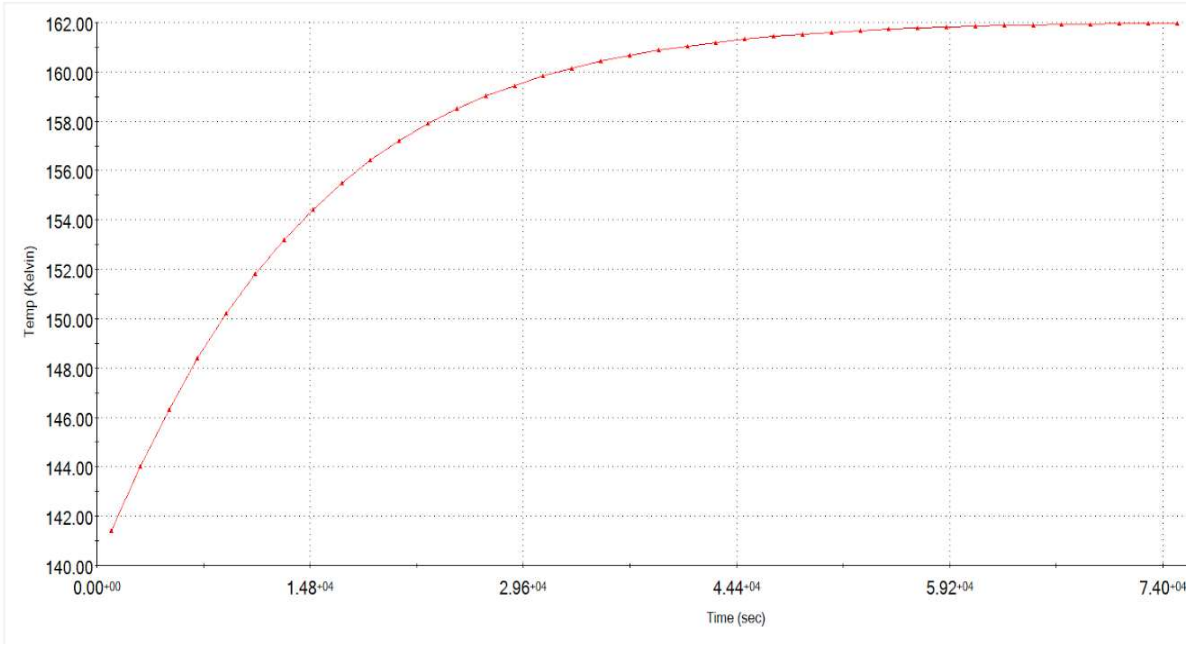


Figure 87: Open door transient response of heat transfer

The time to steady state is in the order of hours, which is much longer than the amount of time the sample would be exposed to radiation. This suggests the steady state result may not be indicative of what would occur. This was further investigated by placing the sample and sample container inside the vault with the vault door still open. Figure 88shows the steady state result of this analysis.

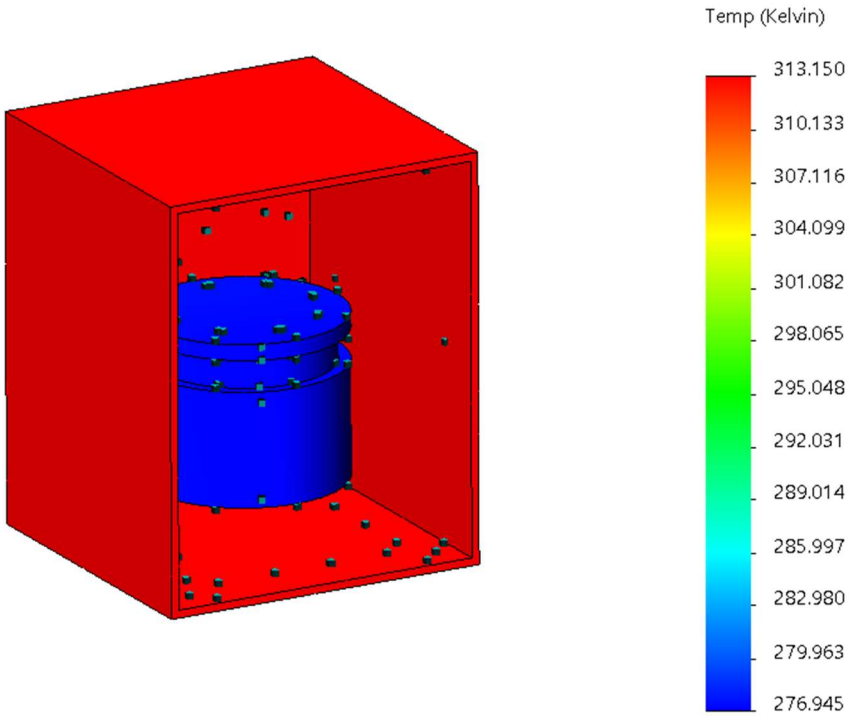


Figure 88: Steady state result of heat transfer inside vault

The sample reaches a much higher steady state temperature in this scenario, which was expected. Figure 89 shows the transient response, and how long it takes to reach steady state.

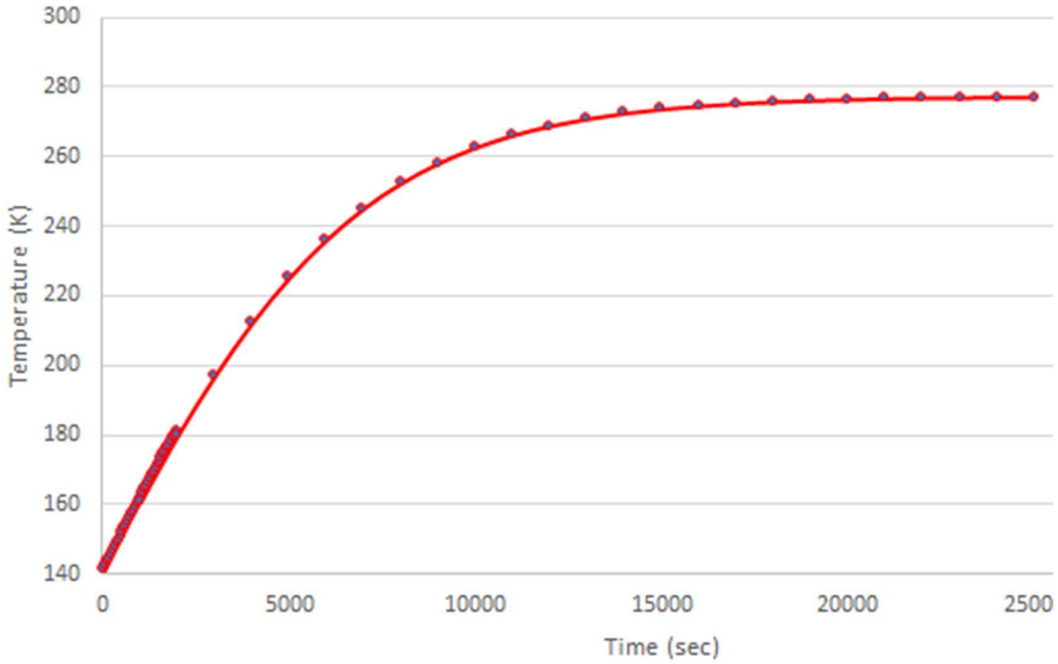


Figure 89: Transient response of heat transfer inside vault

The data shown is a combination of two analyses, one with a large time interval and large step time that shows the full curve, and another with a shorter time interval and shorter step to capture the linear portion of the response. This was done to lower computation time. The results of both analyses are shown in Table 11.

Table 11: Transient heat transfer results summary

| Condition | Emissivity | Starting Temperature (K) | Ending Temperature (K) | Time Constant (min) | Time to 150 K (min) |
|---|---|---|---|---|---|
| Outside Vault | 0.3 | 140 | 162 | 250 | 150 |
| Inside Vault | 0.3 | 140 | 277 | 83 | 8.3 |

As expected, the sample container heats up much faster inside the vault, and the time to 150 K is an order of magnitude smaller. However, the time values for both scenarios are greater than expected, as the sample was predicted to heat up within a matter of minutes from outside the vault. This was confirmed in discussion with JPL, which has experimental data that may indicate a faster thermal response.

The results of this analysis indicate that the solution is plausible, since the container is expected to be delivered in a matter of seconds after the opening of the doors. However, it can also be concluded that the model is heavily oversimplified and not comprehensively indicative of the energy transfer occurring. Some of the more prominent details not included in the model are the gripper holding the container, the wall of the lander body, as well as sample characteristics such as granularity. These features may add to the validity of the model, but also would have significantly increased complexity. Discussion with JPL directed the group to not go beyond the scope of the project and carry out only simplified analyses to validate initial designs.

### *5.3. Particle Simulation*

The low gravity vacuum environment on Europa provides some challenges in particle handling when compared to the environment of Earth. It is unclear how particles of various sizes will behave and if their behavior could negatively impact this sample delivery system. While this may present several opportunities of concern, one important area of focus is the addition or neglect of a lid on the sample container. While neglecting a lid would simplify several steps of the process both collecting and receiving Europan sample, neglecting a lid may also result in partial loss of sample. It's possible that some portion of the sample may fly away if properly excited by an impulse force or vibration. To better understand this behavior, an effort was made to develop a particle simulation to compare particle behavior on Europa vs particle behavior on Earth and understand some of the worst-case scenarios that particles may encounter.

The goal of the particle simulation was to numerically model the behavior of five particles in one dimensional vertical space and observe their dynamic behavior after an impulse force is applied to the ground. In both environments, attractive van der Waals forces, repulsive collision steric forces, and downward gravitational forces were modeled between each particle. Viscous drag was modeled for the particles in an Earth-like atmosphere. These forces were summed and the kinematic dynamics were recalculated ten million ($10^7$) times per second of simulated time.

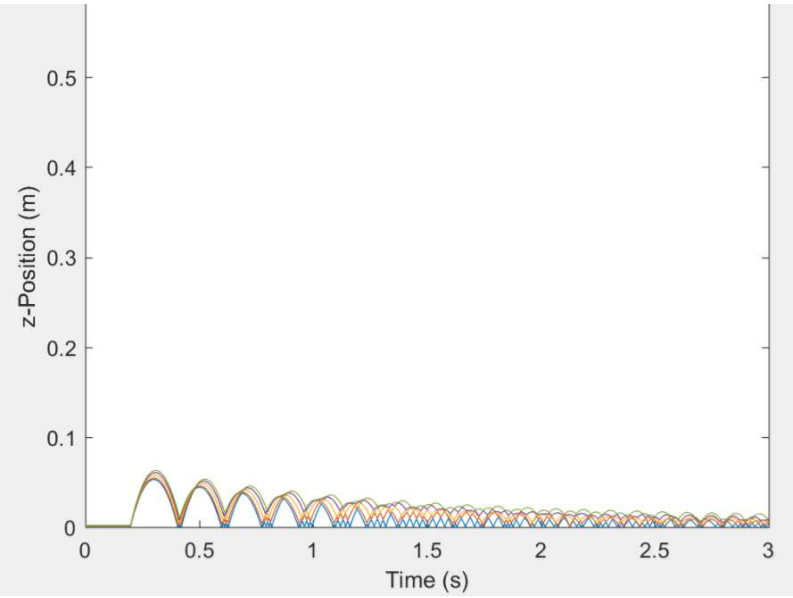


Figure 90: Earth particle simulation results for particles with a radius of 250 microns

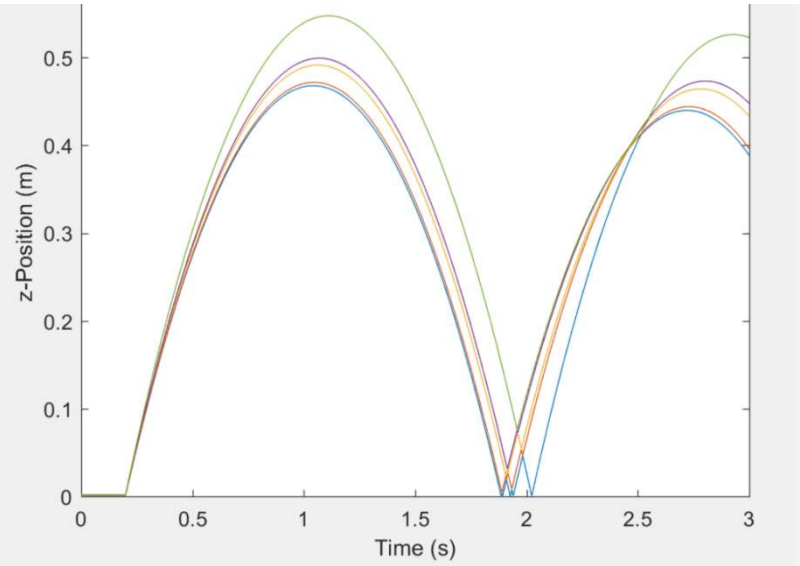


Figure 91: Europa particle simulation results for particles with a radius of 250 Microns

The results were displayed in both an animation and static graphs. The displacement vs time plots for the two simulations analyzing particles with a 250 micron radius are shown in the figures above. Figure 90 and Figure 91 shows the results of particles on Europa and shows the results of the same particles on Earth. The plots have the same y-axis scale, making it clearly visible that Europan particles can experience much greater displacement than similar particles with a similar force would experience on Earth due to the significant difference in gravity. It should also be noted that Europan particles have a much longer settling time than particles on Earth because there is no damping drag caused by the particles' interaction with the atmosphere.

This simulation does have its limitations. As mentioned before, this one-dimensional simulation is designed to be a worst-case scenario. Particles operating in a three-dimensional world would have much more opportunity to dissipate their energy in a variety of directions and with many other particles, so it is unlikely that an observer would witness the extreme oscillating behavior shown with this simulation. Dissipation of collision energy in the form of heat is also difficult to accurately model and is not factored into this simulation effort. To successfully model a greater number of particles in more dimensions accurately would require a finer time step to reduce computational artifacts and errors in the results. Taking these steps would also greatly increase simulation run-time and computational power needed to beyond the current resources of this capstone team.

With the results and limitations in mind, it still appears to be reasonable to conclude that there is a significant risk in assuming that particles on Europa in an open sample container will stay put as they are transferred around the system. To avoid loss of valuable Europan sample in this environment, it is the suggestion of this capstone design team that transparent covers should be placed on all sample containers at the time of sample collection by the sample collection mechanism.

### *5.4. Volume Measurement*

As mentioned in the design section, the volume measurement component of the subsystem uses an IR light to the measure distance between the sensor itself and the surface of the sample material in the container. The sensor is a time of flight (ToF) sensor, meaning that it measures the time it takes an IR pulse to leave the sensor, bounce off of a surface, and return to the sensor. Manufacturer's specifications of the sensor said that the time of flight concept of measurement would be independent of surface material reflectivity. Because of this feature, as well as the IR's lack of physical interaction with the sample material, the ToF concept of distance measurement a viable option. To prove the plausibility of

this, a variety of tests were conducted. This test aimed to test several variables that may affect the accuracy of the sensor. The variables tested were: accuracy of reading at varying distances, number of data points collected to calculate an average, time between IR readings of the sensor, effects of light and dark surroundings, and different materials to test different reflectivities.

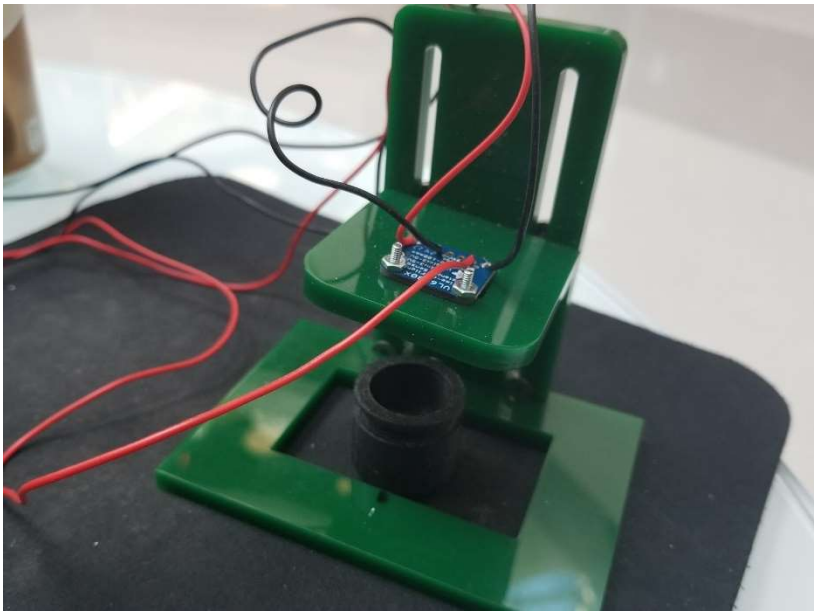

Figure 92: Volume measurement test fixture

Figure 92 above shows the test fixture used in the following tests. The fixture is designed to vary the height of the sensor to the different containers in order to get data for those varying heights. The wires are plugged into an Arduino Uno board which is plugged into a laptop for data acquisition.

The first test that was conducted was varying the distance between the sensor and a solid surface. The surface was a black piece of construction paper. To get a measured distance, 13 data points were collected from the sensor at a rate of 1 reading per 100 ms. Table 12 below shows one of the tests conducted at a distance of 25 mm, which is the medium value of the furthest and shortest distance required of the sensor to measure within the subsystem.

Table 12: Output of volume sensor at 25 mm distance

| Set Dist: | 25 | Readings |
|---|---|---|
| Average: | 25.15385 | 24 |
| Off: | -0.15385 | 27 |
| Percent Error | 0.615385 | 26 |
| Standard Dev | 1.344504 | 24 |

The test was conducted at a static distance, and even though this was the case, the sensor still outputted different values, showing a lack of accuracy in the sensor. Although the values were off, the average value of the readings was fairly close, being off by -0.15 mm. This same test was conducted at varying distances, and the averages were plotted in Figure 93 below.

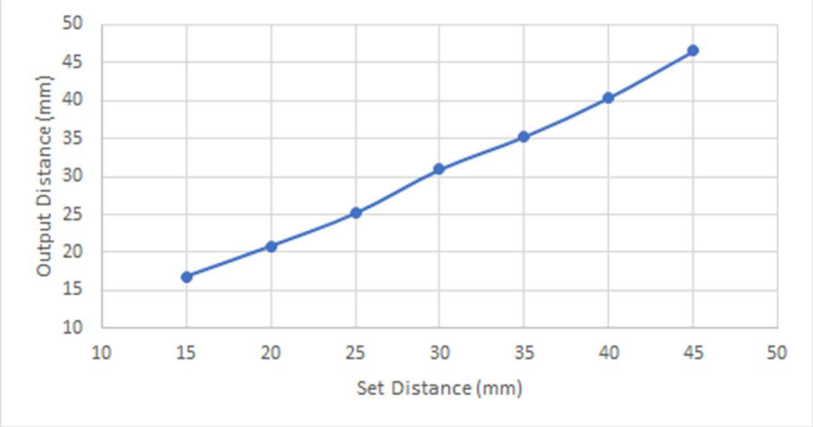


Figure 93: Average output of volume sensor at varying distances

The graph shows that the measurements are close to the set distances, although not entirely correct. The average standard deviation for the different tests was 1.56, which is reasonable giving the sensors output of millimeter increments.

The next test conducted was varying the reading rate at a set distance of 35 mm. The test was conducted similarly to the test above. 20 data points of a static black paper were recorded at the varying read rates. This test was conducted for several other pulse rates. Those pulse rates are 5 ms, 20 ms, 100 ms, 250 ms, 500 ms, 1000 ms, and 2000 ms. To determine if pulse rate would affect the average distance measurement, the different tests were compared to each other, looking at the average distance and the standard deviation. Comparing the results shows that pulse rate had no significant effect on the accuracy of the sensor. This is shown in Figure 94 below, which compares four of the noted pulse rates. The 35 mm distance had varying distance readouts for each read frequency. Increasing the frequency had no significant effect on the accuracy of the volume sensor.

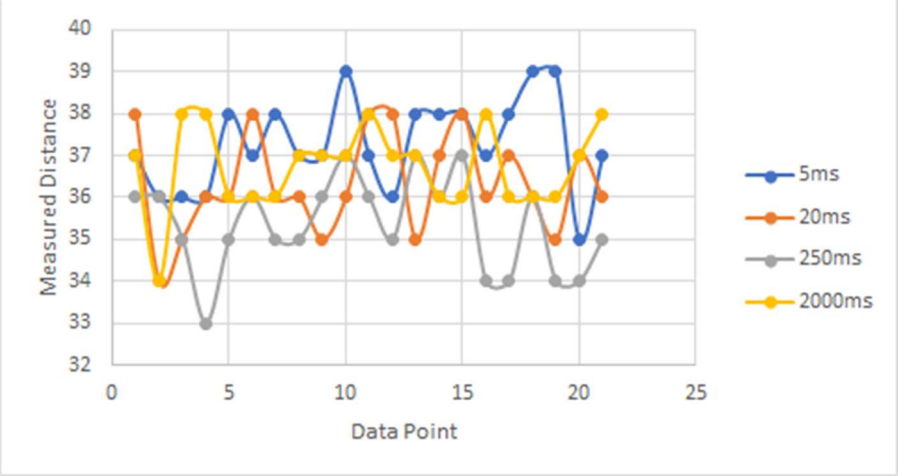


Figure 94: Average distance measurements with varying pulse rates

The next variable tested was number of data points used to calculate an average distance. Although the sensor is not accurate for individual data points, generating an average using multiple points seemed to bring the sensors readout closer to the set target distance. A static black target was fixed at a distance of 50mm away from the sensor and the sensor's pulse rate was set to 1 reading per 200ms. Table 18Table 13 below shows averages and standard deviations for reading counts of 20 readings, 50 readings, 100 readings, and 250 readings.

Table 13: Average distance output with varying read count averages

| Reading | 20 | 50 | 100 | 250 |
|---|---|---|---|---|
| Avg | 50.95 | 51.19 | 51.52 | 51.16 |
| Std Dev | 1.465 | 1.183 | 1.11 | 1.206 |

With these preliminary tests completed in order to get a feel for the accuracy of the sensor, the next tests conducted will be done with 2 different materials, salt and pepper. These materials were selected for the different colors and reflective particles. Salt is very light and very reflective like snow, and pepper is darker and less reflective. This will test the sensor's ability to handle two extremes of materials. The first material tested was the salt. Salt is white and shiny, which is closer to what is expected on Europa. The container is set a distance away from the sensor close to what would be expected on the prototype. The prototype is set to allow for varying the sensor distance to the container for optimization. In this test, the bottom of the 5cc container is set a distance of 48mm away from the sensor with surrounding lights on. Table X below shows the measured distance of the container being incrementally filled with salt at 1 cc intervals, the deviation between the 20 readings used to calculate the average at a read rate of one reading per 200ms, and the calculated volume based on the geometry of the cup (3.72 mm = 1 cc of material). Test results can be seen in Table 14 and Table 15.

Table 14: Salt sample in volume measurement fixture

| | Empty | 1cc | 2cc | 3cc | 4cc | 5cc |
|---|---|---|---|---|---|---|
| Avg Reading (mm) | 48.19048 | 50.9 | 50.28 | 51.47 | 48.8 | 46.9 |
| Standard Deviation | 1.569 | 0.831 | 0.784 | 0.98 | 0.814 | 1.14 |
| Calculated Volume (cc) | 0 | -0.78 | -0.6 | -0.94 | -0.178 | 0.37 |

Table 15: Black pepper sample measured in volume measurement fixture

| | Empty | 1cc | 2cc | 3cc | 4cc | 5cc |
|---|---|---|---|---|---|---|
| Avg Reading (mm) | 49.14 | 46.86 | 42.62 | 40.52 | 38.24 | 35.29 |
| Standard Deviation | 1.388 | 1.014 | 1.117 | 1.078 | 0.889 | 0.956 |
| Calculated Volume (cc) | 0 | 0.69 | 1.979 | 2.615 | 3.309 | 4.2 |

This test shows that the sensor operated better with the darker pepper than the salt. The accuracy of the readings was less than ideal, and fell out of the +/- 10% tolerance of sample material measured specified by the industry advisor. Upon recalibration, however, the following results occurred.

Table 16: Salt measurements with calibration

| | Empty | 1cc | 2cc | 3cc | 4cc | 5cc |
|---|---|---|---|---|---|---|
| Avg Reading (mm) | 61.04762 | 57.90476 | 54.66667 | 50.04762 | 48.47619 | 40.90476 |
| Standard Deviation | 1.321975 | 0.995227 | 1.583924 | 1.07127 | 1.327368 | 0.995227 |
| Calculated Volume (cc) | 0 | 0.99 | 1.01 | 2.73 | 3.12 | 4.87 |

The results show that with the calibration and the system in darkness, that the volume measurement is fairly accurate and a plausible solution for the volume measurement component of this subsystem. But these tests were performed without a cover on the sample containers. The next tests done test the sensor's ability to read distance through a glass cover on the sample container. The sensor does have a calibration procedure that was followed prior to the following tests.

A sample container was covered with a thin glass lid and distance was measured. The test was conducted with only two states: an empty sample container and a salt filled one. This was done in order to see if the sensor would read any differently. The sensor was again placed at a distance representative of the distance it would see while implemented in the subsystem. The test concluded that the sensor was only reading the distance to the cover glass. This was shown to be the case when the pepper was tested as well. To see if

this held true at different distances, a test was conducted with the sensor as close to the sample container as it could get. This height was about 3 mm above the sample container, due to the limitations of the test fixture. The results show that once again, the accuracy decreases with the salt. But with the pepper the results are better. Table X below shows the average distance measurements of the pepper in the sample container covered by the glass cover.

Table 17: Pepper measurements with calibration and cover glass

| | Empty | 1cc | 2cc | 3cc | 4cc | 5cc |
|---|---|---|---|---|---|---|
| Avg Reading (mm) | 26.38095 | 25.66667 | 22.47619 | 20.14286 | 17.09524 | 14.09524 |
| Standard Deviation | 1.20317 | 0.912871 | 1.589147 | 1.014185 | 0.94365 | 0.70034 |
| Calculated Volume (cc) | 0 | 0.99 | 1.01 | 2.73 | 3.12 | 4.87 |

The sensor was able to accurately calculate the volume of the pepper through the cover glass when the sensor is closer to the sample container. This proves that the use of an IR distance sensor is a plausible solution for volume measurement for the Europa Lander mission. It is able to measure distances with an accuracy near the range required for the given tolerances. It is also able to read through cover glass that would be on the sample containers.

## 6. Outcomes and Conclusions

At the conclusion of the Capstone project, a full-scale prototype of the system was manufactured and assembled, as seen in Figure 95. This prototype allowed the team to identify any more weaknesses in the design as well as test all systems and definitively determine viability of design concepts. The conclusions drawn from this implementation are as follows:

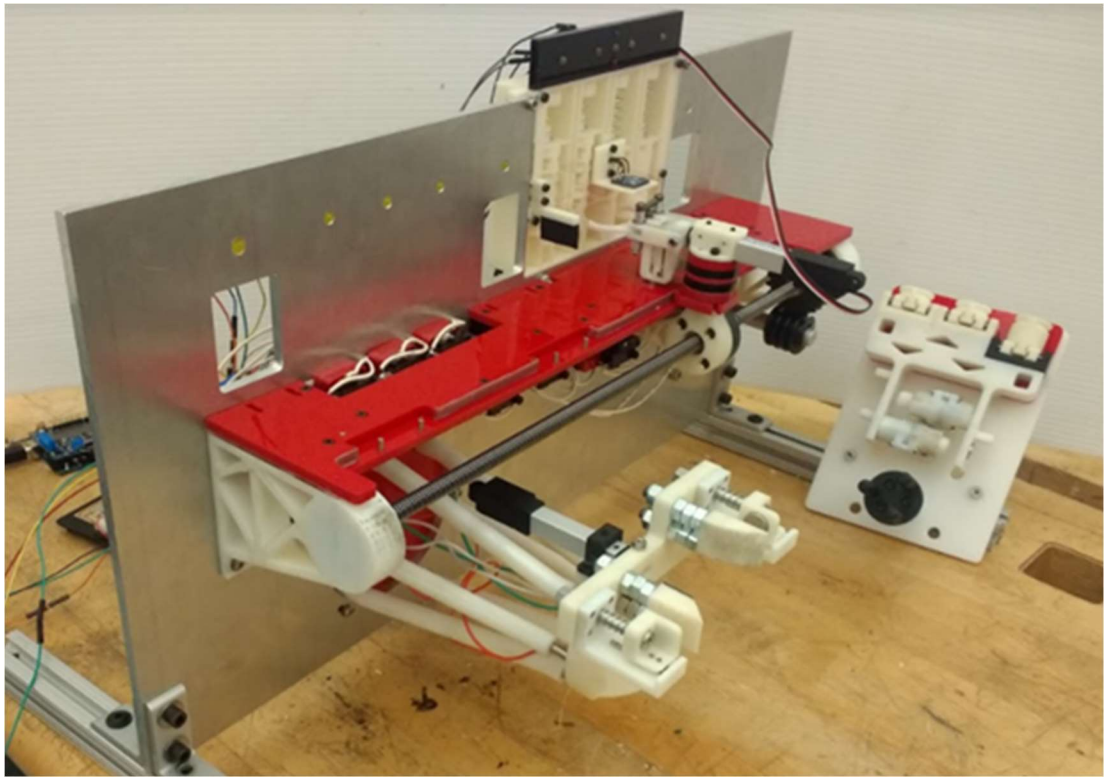

Figure 95: Completed prototype

### *6.1. Sample Container*

Key decisions and recommendations for determining container sample geometry were that the system should not be responsible for division of sample into discrete containers, and that the maximum holding volume of the containers should be that of the maximum tolerance of sample volume required by each of the scientific instruments. These recommendations reduce complexity of the system and container design. Particle analysis suggest that the sample container requires a lid to hold sample material without risk of sample loss. As this was determined later in the development of the system, a removable lid was not designed for this prototype.

For cryogenic applications, indium seals are often used. According to a paper written by C.C. Lim titled "Indium seals for low-temperature and moderate-pressure applications" it is noted that indium seals work in temperatures around 2 K, which is far below the surface temperature of Europa. [61] Another important recommendation for JPL was using two distinct container sizes for the two different required volumes, with the same diameters but different heights, visible in Figure 77.

Since the container was developed in parallel with other subsystems like the grippers and container refill station, its interacts well with these systems. Points of concern are that some of the features of the container are underdeveloped, such as the lid and container material. Although some heat transfer analysis was carried out, a wholly comprehensive study cannot be investigated yet as the only defined properties of the sample container is its geometry.

### *6.2. Docking Platform*

A picture of the docking platform can be seen in Figure 96. When assembled as seen in the CAD model, the tight angle makes translating the kinematic coupling parallel to the bottom platform difficult.

Figure 96: Prototype of docking platform

Additionally, the kinematic coupling has free range motion about equilibrium which means it is not fully constrained. This means the coupling can be in an unpredictable position simply due to the force of

gravity. A test fixture was created to investigate the effect of larger angles of the legs. Ultimately an angle of 45 degrees was found to be optimal. However, this angle still allowed for free motion, though it was significantly reduced. An angle of 60 degrees was found to fully constrain the assembly, however the preload from the shear springs sheared the set screws from the 3D printed legs. Additionally, the bottom u-joints were at the maximum allowable angle in equilibrium, which did not allow the motion of the coupling down along the symmetric axis.

Increasing the platform angle negatively impacted the footprint on the lander body to well outside the design envelope. To account for this a fixed, stand in docking platform has been printed and assembled for mounting on the prototype, allowing for the testing of the surrounding mechanisms. This stand in platform is seen in Figure 97.

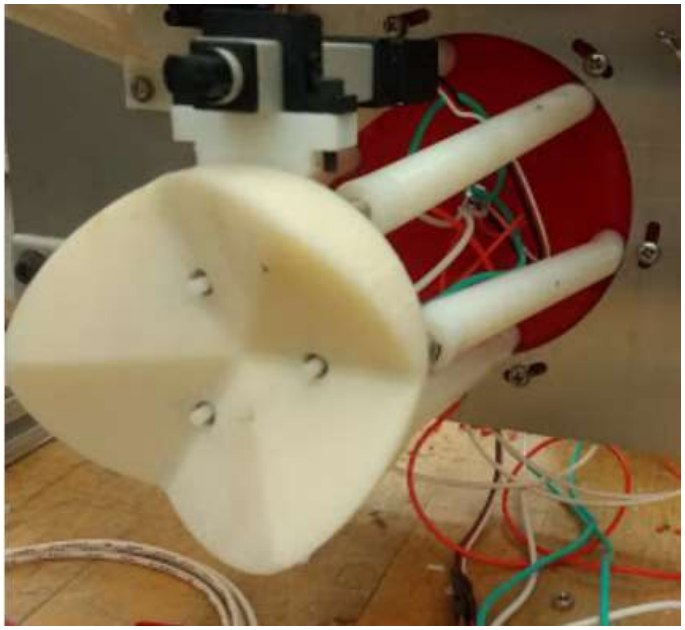

Figure 97: Fixed, stand in docking structure

The design of the kinematic coupling proved to be viable, though it could be improved with custom push buttons with a rounder profile, which would improve contact forces. In addition, a lower friction material for the coupling would be favorable.

The general takeaway from this design is that it can be a functional, unique solution that is worth exploring further. This exploration could involve simple design changes such as looking at the effect of changing leg orientation to an asymmetric design. It should be noted that this design is inherently complex and will mostly likely be heavy and with a large footprint. One suggestion is requiring one less degree of freedom from the docking platform, and requiring the robotic arm to make up for it instead.

### *6.3. End Effector to Docking Handoff*

The locking cam mechanism, seen as part of the assembly in Figure 104 proved itself to be a good proof of concept, but too large on the current scale. However, the concept of “mechanical memory” as illustrated by the cams is a useful concept that could be implemented in many other parts of an assembly, and should be developed further with more precise manufacturing techniques.

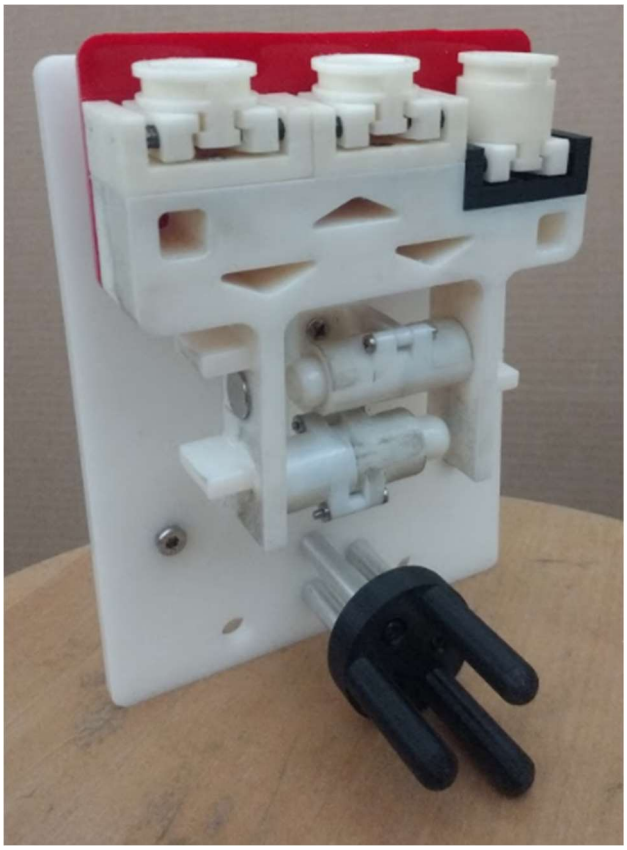

Figure 98: Robotic end effector with lock cam mechanism retaining container tray

Regarding the magnet handoff seen in Figure 99, the rail and spring mechanism works well, as it provides a degree of motion that does not require too much force. The use of two magnets as a grip force is a weakness of the design, as it does not constrain rotation for the container tray very well, and take a lot of force to slide apart. A major improvement to this design would be to have three magnets, staggered, so there would be no rotation.

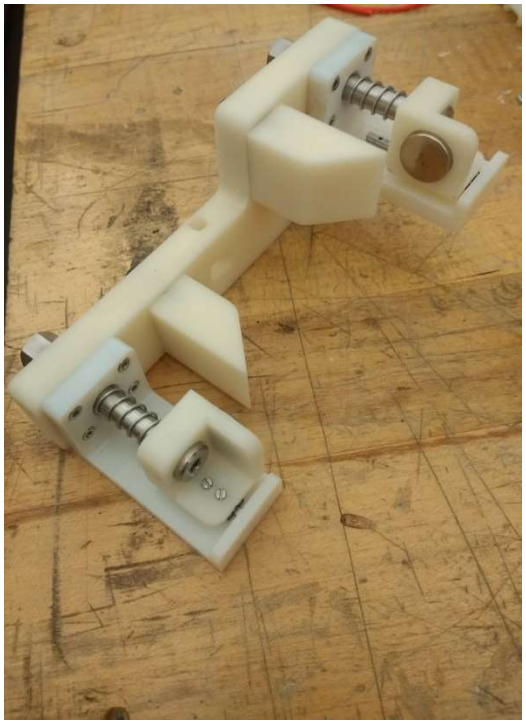

Figure 99: Assembled magnet handoff mechanism

### *6.4. Container Cart*

The toggle gripper seen in Figure 100went through several iterative designs to attempt to maximize the gripping force (pull-out force), minimize the finger activation force and minimize the release wedge activation force. Varying the toggle angle, wedge angle and wedge displacement as well as trying several materials and off the shelf components was necessary to fine-tune the design.

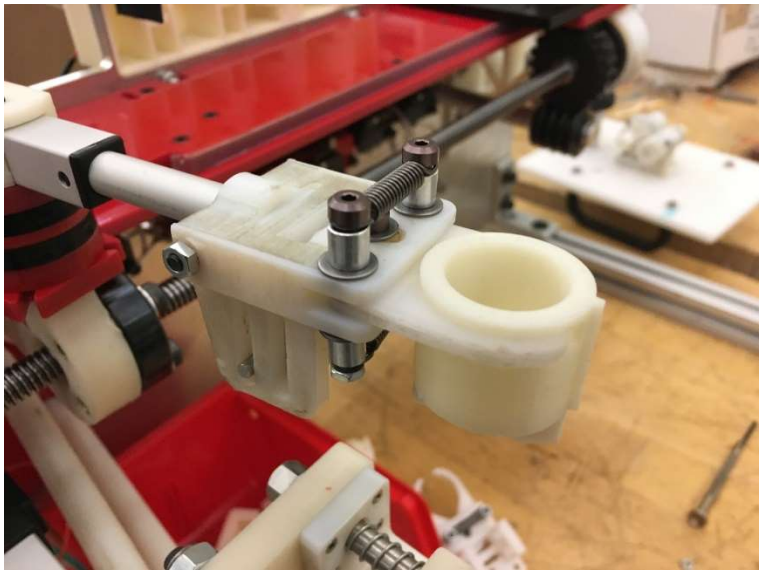

Figure 100: Fabricated toggle gripper

The gripper strived to achieve three principle functionalities; gripper activation, gripper retention during handoff with bottom gripper, and gripper release. The gripper was able to successfully activate its passive grasping mechanism when it presses against a container with a force of approximately 20 N. The gripper

was also able to show that it could maintain a grasp on the container strong enough to pull it out of the bottom gripper's teeth at a force of 6 N. Unfortunately, the final iteration of the release wedge was unable to be successfully demonstrated in the integrated full prototype, as friction acting played a greater role than expected in mechanism actuation.

Improvements could be made to improve the interaction between sliding joints. Components that were 3D printed proved to be low precision and high friction which led to both jamming and unwanted free play. The constant radial force on the shoulder bolts from the extension springs also provided high friction that could have been mitigated with specialized bearings. The connection between the toggle gripper and the off-the-shelf linear actuator proved to be far too compliant for the mechanism to operate consistently without unwanted deflection; a fault that could be easily solved with a more robust linear actuator. The toggle gripper also ended up being bulky and fragile in the vertical direction due to the spiral extension springs employed. A custom designed flex spring could provide a more elegant and controllable actuating force.

One function that was not realized in the fabricated design is the release of the toggle gripper when delivering an empty refill container to the container tray for new sample collection. A potential solution is shown in Figure 101 that depicts a wedge ramp fixture that is attached to the container cart. By adjusting the position of the container tray with its linear actuator, the toggle gripper linear actuator will either extend an additional distance that can engage the release wedge when desired. For the current docking mechanism to have full successful integration with the toggle gripper, further development and implementation of this concept would also be necessary.

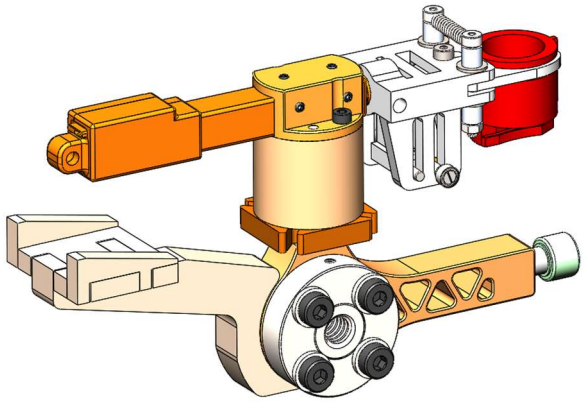

Figure 101: Container tray release ramp concept

The toggle gripper mechanism is a strong candidate for further development in future system development. It's a well-functioning passive gripper that doesn't require any active actuator to hold the sample and it has relatively low activation and release forces while maintaining a small footprint on the system.

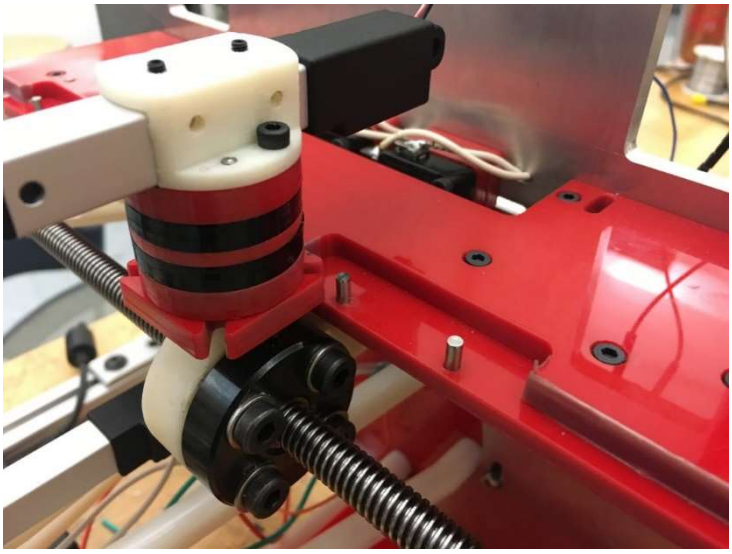

Figure 102: Fabricated Geneva drive and transport cart

The Geneva mechanism, shown as part of the cart assembly above in Figure 102, demonstrated tremendously successful functionality both as a stand-alone test fixture and integrated into the full assembly. When testing the Geneva mechanism operation on a test fixture uncoupled to the lead screw, the Geneva mechanism can be seen obtaining very smooth and consistent low and high-speed operation. When integrated into the assembly the mechanism can also be successfully demonstrated, however there is sometimes an issue of alignment between the Geneva platform and the lead screw. This could be countered by applying a small amount of preload to the drive. The mechanism currently operates at very low friction with acrylic parts, but it is possible to reduce the friction even further with implementation of specialized bearings on contact surfaces.

### *6.5. Drive System*

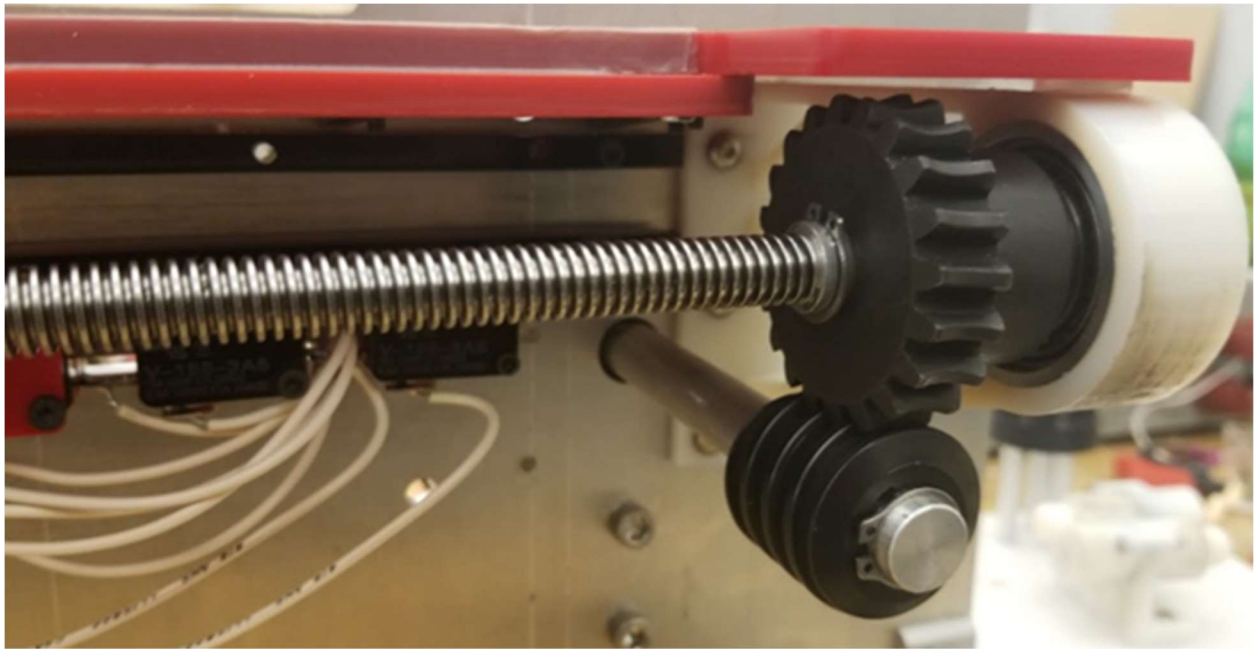

Figure 103: Drive system fabrication

The drive system, a closeup of which can be seen in Figure 103, functioned as intended as a linear transport system that was able to provide high resolution positioning of the transport cart. In future iterations, higher tolerances should be used when machining or purchasing off the shelf shafts in order to limit rotation based vibration and to eliminate wobble of the transport cart. A flexible coupling may also provide useful where applicable to make up for any shaft misalignment. Custom components with space grade materials can optimize weight and environmental resistance. Other improvements can be made by adding covering components to protect the lead screw and surrounding components from damage due to particles. Additionally, a more powerful motor would assist in running the lead screw more quickly.

### *6.6. Volume Measurement*

The current design for the prototype does not allow the sensor to get close enough to the sample container to bypass the cover glass. Future designs would want to include a sensor that is able to get closer to the cover glass of the sample container. Overall, the results of the sensor were decent, but a better accuracy sensor along with a better design to optimize the sensor would make this form of volume measurement a decent area to proceed with research.

### *6.7. Refill Station*

The functionality of the refill station was good, and functioned as intended. One area of concern is the springs. The current prototype used off the shelf springs which proved to be stiffer than needed. Most off the shelf springs did not have the force to length ratios that would have optimized this system. Although this was the case, the stiffer springs worked, and could be seen as a good way of securing the containers during turbulent parts of their journey. The stiffer spring made it hard for the toggle gripper to pull the container out of the station. This was resolved by shortening the spring slightly. The drawback to this solution was the last container in the 1 cc container sleeve was not experiencing any normal force from the spring, and could potentially fall out if the lander receives any sudden force while the last 1 cc container is awaiting retrieval. Another flaw is that the refill station exceeds past the allotted envelope by about 32 mm. This was required to give the springs enough space to compress. Future development may want to concern a different stacking geometry, or different placement of components to have this fit into the envelope. The last modification is that the refill station is currently held within the vault wall. This was not the original design but was changed to allow room for the toggle gripper / lead screw assembly to move along the vault wall without crashing into the refill station. This may be modified in the future as well.

### *6.8. Motor vs Mechanism*

One of the largest drivers of design was the reduction of the number of actuators used in the system. This led to a more passive solution where an actuator performs multiple functions. In the case of the Geneva and lead screw integration, this was a more positive implementation of this concept, as the Geneva rotated well with the linear actuation of the lead screw. This additional motion eliminated the need for another actuator, which reduces power consumption.

In a couple components, this was not necessarily the case. Spring loaded passive mechanisms such as the toggle gripper and the magnet handoff mechanism require extra power from an actuator to operate and deflect the springs. Without careful consideration of force requirements and friction, the passive system can negatively impact the power consumption of the system. In the case of the toggle release mechanism and magnet handoff, both forces are impossible to actuate with the off the shelf actuator used.

The design of the handoff mechanism is largely based on the reduction of actuators used as well. The “mechanical memory” of the pen cam and resulting magnet handoff mechanism yields a complex solution. It includes many moving parts and requires a delicate balance of forces. Figure 104 summarizes this force hierarchy, as well as the successes, unknowns, and failures of the prototype.

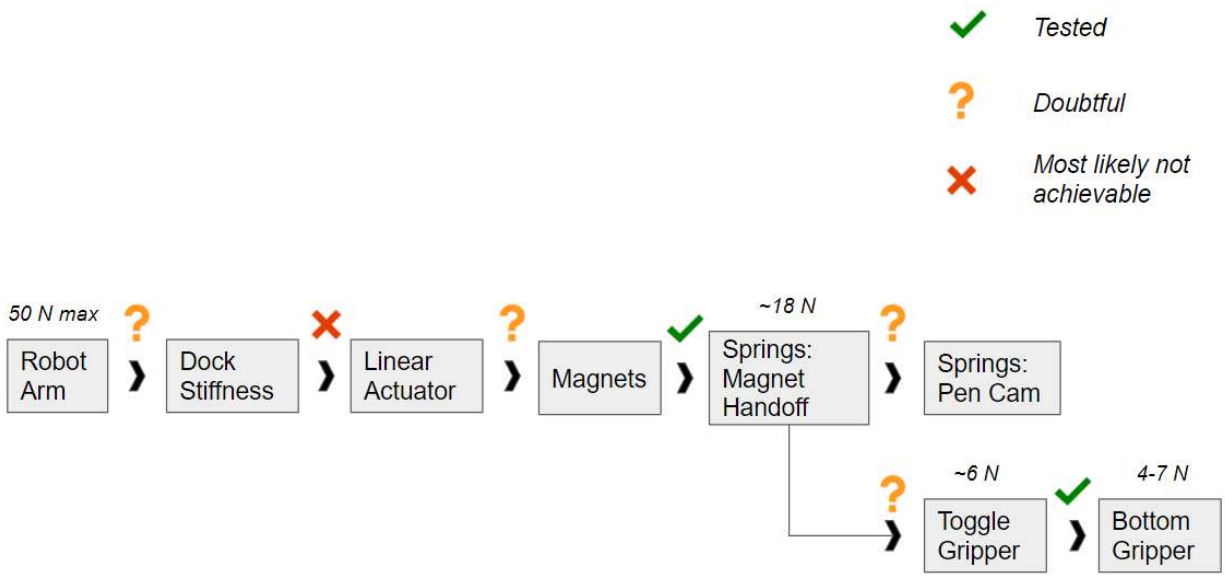


Figure 104: Force hierarchy of docking and handoff integration

### *6.9. Mass*

The measured mass of the prototype with the wall and wall components came out at about 6.5 kg. Taking away the estimated mass of the wall and wall components yields a system mass of about 3.9 kg. As expected, the prototype exceeds the mass requirement for the system. However, this value is not significantly higher, and there are several points of reduction that would most likely allow the mass to be reduced to 2 kg. The major mass improvements would be to use lightweight, flight materials for any of the heavier components, such as the steel lead screw, gear and worm gear. Many support components, such as the Geneva platform and bearing housings can also be optimized with material selection and cutouts to reduce mass. In terms of system level design, a less sophisticated dock and dock handoff design can also cut out mass. The general conclusion is that 2 kg is not unreasonable for a flight design.

### *6.10. System Control*

After successful system integration, the final step to system autonomy is the implementation of a control system. A logic tree was developed, seen in Figure 105, was implemented using an Arduino Mega microcontroller that sensed the system's surroundings and mapped where the sample was in the delivery process. Button sensors were used on the kinematic coupling to sense the robotic arm and activate the docking procedure. Limit switches along the lead screw's path were used for closed loop control of the transport cart via the stepper motor while the toggle gripper's linear servo actuator operated on position based open loop control. LEDs were used above each of the eleven sensed stations to visualize system status and provide insight for troubleshooting.

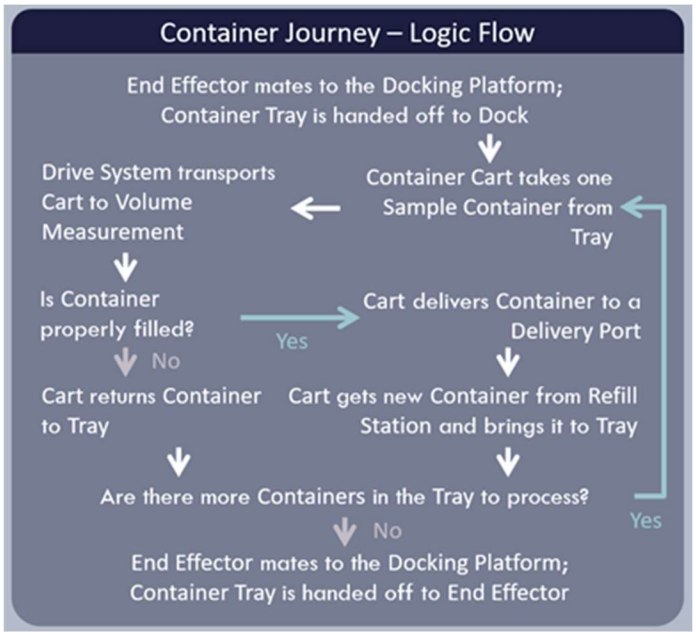


Figure 105: System operation logic tree

Successful implementation of the automated system was demonstrated on a breadboard separated from the fabricated assembly. System generated outputs verified the status and progress of the system as the user manually activated each limit switch to indicate that the transport cart reached each required destination. The stepper motor and linear actuators were activated and deactivated in a system representative manner during this test. Unfortunately, due to last minute hardware failures of the linear actuator and the stepper motor driver board, the team was unable to conduct a full system test of autonomous operation.

Even with the inability to run a full autonomous test with mechanical hardware, there were still some clear takeaways. While limit switches are very useful for consistent closed loop testing, the implementation of a switch at every station adds a lot of mass and volume and wiring to the system that may not be necessary. As lead screws are not actually meant to be driven with limit switches except for a rehoming switch, significant weight could be cut. Alternatively, the inclusion of individual limit switches for each cart stop can also allow for the easy control of a faster and more powerful motor for quicker system operation. Both options are viable and should be considered in future control system iterations.

### *6.11 JPL Response*

Upon reaching out to JPL for feedback, the team received very positive responses. The industry advisor stressed that their project was purely investigative; by producing a proof of concept they were achieving all JPL had hoped for. Any and all suggestions, advice, or lessons learned will assist the future of the Europa Lander project.

## 7. Conclusion

The project has been finalized with a fully integrated design modeled, built, and tested as the result of several months' effort. Previous contact with JPL, in addition to research into the Europan environment and the lander mission, had yielded a comprehensive problem definition and an exploration of past sample collection missions, sample handling technology, potential mechanisms, and material considerations, all of which laid the foundation to produce useful initial designs. The project focus then shifted towards design development and the selection and conceptualization of mechanisms that could mechanically accomplish the required actions of the system: docking the robotic arm, gripping the

sample, measuring the sample, and delivering the sample to the instrument ports. Though two potential concepts of such integrated systems arose as options, ultimately a linear concept, featuring a lead screw paired with a passive rotary mechanism, was chosen.

This concept was developed into a CAD model of a prototype, with each mechanism undergoing relevant force analysis and design using principles of mechanical engineering. Heat transfer analysis was conducted to further assess the viability of the design. A particle simulation was modeled to compare the behavior of particulates in a Europan environment versus an environment on Earth, which led to the conclusion of a lid for the sample container. The volume measurement system was calibrated to show functionality.

Various methods of fabrication were carried to build a full-scale prototype of the design. Most components were assemblies of off the shelf, 3D printed, and lasercut parts. Some parts for the lead screw and vault wall were machined. Assembled prototypes and component iterations highlighted weaknesses and challenges of the design. The final assembly was wired and programmed to function autonomously, though full autonomy was not achieved as several mechanical components were found not to work due to the limitations of rapid prototyping and delicate force hierarchy of the design.

Overall, the design concept presented is a great first look at a complex subsystem and the environment around it. The results and conclusions serve as a reference point for a more educated definition of the subsystem requirements, and a useful first step towards the development of more designs.

# Works Cited


[1] Europa Lander Mission Concept Team, "Europa Lander Science Definition Team Report," 2016.

[2] E. Howell, "Europa: Facts About Jupiter's Icy Moon and its Ocean," June 2013. [Online]. Available: https://www.space.com/15498-europa-sdcmp.html. [Accessed 28 July 2017].

[3] NASA, "About Europa," [Online]. Available: https://solarsystem.nasa.gov/europa/overview.cfm. [Accessed 20 July 2017].

[4] "Europa: Facts about Jupiter's Moon, Europa," [Online]. Available: https://theplanets.org/europa/. [Accessed 17 August 2017].

[5] P. P. R. Schenk, "Topographic variations in chaos on Europa: Implications for diapiric formation," *Geophysical Research Letters,* vol. 31, no. 16, pp. 1-5, August 2004.

[6] M. Kramer, "Jupiter's Moon Europa May Have 'Spikes of Ice'," 25 March 2013. [Online]. Available: https://www.space.com/20356-jupiter-moon-europa-ice-spikes.html. [Accessed 3 August 2017].

[7] R. e. a. Carlson, "Europa's surface composition," *Europa,* pp. 283-316, 2009.

[8] N. e. a. Ligier, "VLT/SINFONI observations of Europa: new insights into the surface composition," *The Astronomical Journal ,* vol. 151, no. 163, 2016.

[9] J. Alton, "Catalog of Apollo Lunar Surface Geological Sampling Tools and Containers," Houston, 1989.

[10] N. JPL, March 2005. [Online]. Available: https://stardust.jpl.nasa.gov/tech/aerogel.html.

[11] A. e. a. May, "OSIRIS-REx Touch-and-Go (TAG) Mission Design for Asteroid Sample Collection," in *65th International Astronautical Congress*, Toronto, 2014.

[12] B. e. a. Rizk, "OCAMS: The OSIRIS-REx Camera Suite".

[13] A. Joshi, "LITHIUM ALUMINIUM ALLOYS–The New Generation Aerospace Alloys," Bombay.

[14] National Research Council, Technology for Small Spacecraft, Washington, DC: Washington, DC: The National Academies Press., 1994.

[15] N. G. A. W. R. Prasad, Aluminum-Lithium Alloys: Processing, Properties, and Applications, Oxford: Butterworth-Heinemann, 2013, pp. 58-62.

[16] H. Flower, High Performance Materials in Aerospace, Dordrecht: Springer Science & Business Media, 1995, pp. 7-10.

[17] T. Woods, 2011. [Online]. Available: https://www.nasa.gov/topics/technology/features/aerogels.html.

[18] NASA JPL, [Online]. Available: https://stardust.jpl.nasa.gov/aerogel_factsheet.pdf.

[19] Aerogel Technologies, [Online]. Available: http://www.aerogeltechnologies.com/about-aerogels.

[20] A. Hurlich, "Low Temperature Metals," in *Chemical Engineering*, McGraw-Hill Publishing, 1963.

[21] "Steel properties at low and high temperatures," May 2001. [Online]. Available: http://www.totalmateria.com/page.aspx?ID=CheckArticle&site=kts&NM=48.

[22] A. Woodcraft, "Aluminium thermal conductivity at cryogenic temperatures," 17 December 2005. [Online]. Available: http://reference.lowtemp.org/alkappa.html.

[23] B. Best, "Physical Parameters of Cooling in Cryonics," [Online]. Available: https://www.benbest.com/cryonics/cooling.html.

[24] D. a. Q. Y. Zhou, "Understanding Material Properties in Pharmaceutical Product Development and Manufacturing: Powder Flow and Mechanical Properties," *Journal of Validation Technology,* 2010.

[25] Joseph D Lewis, "Level Measurement of Bulk Solids in Bins, Silos, and Hoppers," Monitor Technologies, 2004.

[26] S. Shanmugam, "Granulation techniques and technologies: recent progresses," *Bioimpacts,* vol. 5, pp. 55-63, 2015.

[27] "One Docking Ring to Rule Them All," 3 June 2014. [Online]. Available: http://www.esa.int/Our_Activities/Human_Spaceflight/One_docking_ring_to_rule_them_all/(print).

[28] International Docking System Standard, 20 November 2013. [Online]. Available: https://web.archive.org/web/20131216200055/http://internationaldockingstandard.com/download/IDSS_IDD_Rev_C_11_22_13_FINAL.pdf.

[29] N. M. 2020. [Online]. Available: https://mars.nasa.gov/mars2020/mission/rover/sample-handling/ .

[30] G. e. a. Monkman, "Introduction to Prehension Technology," in *Robot Grippers*, Weinheim, Wiley-VCH, 2007, pp. 1-14.

[31] M. (. Mossage, BinMaster, 27 July 2017. [Online]. Available: https://www.binmaster.com/_resources/dyn/files/75417343ze1be1acb/_fn/TT%20Technology%20to%20Measure%20Fertilizer.pdf.

[32] S. a. H. S. Lanka, "How to implement liquid-level measurement using capacitive sensing technology," *Core & Code,* 2017.

[33] S. e. a. Sherrit, "Compact sensitive piezoelectric mass balance for measurement of unconsolidated materials in space," 2017.

[34] NASA Mars 2020, 2017. [Online]. Available: https://mars.nasa.gov/mars2020/mission/rover/arm/. [Accessed 05 Aug 2017].

[35] Massachusetts Institute of Technology,, 2002. [Online].

[36] N. Sclater, "Chain and belt devices and mechanisms," in *Mechanisms and Mechanical Devices Sourcebook*, 5th ed., New York, McGraw Hill, 2011, pp. 262-277.

[37] M. e. a. Plooij, "Review of locking devices found in robotics," *IEEE Robotics and Automation Magazine,* vol. 22, no. 1, March 2017.

[38] B. Dunbar, "Technology Readiness Level," 4 August 2017. [Online]. Available: https://www.nasa.gov/directorates/heo/scan/engineering/technology/txt_accordion1.html.

[39] Properties and Selection: Nonferrous Alloys and Special Purpose Materials, Vol. 2 10th Edition, ASM International, 1990.

[40] J. F. e. a. Poco, "Synthesis of high porosity, monolithic alumina aerogels," *Journal of Non-Crystalline Solids,* vol. 285, no. 1, pp. 57-63.

[41] T. L. Bergman, Introduction to heat transfer, John Wiley & Sons, 2011.

[42] A. Slocum, "Kinematic couplings: A review of design principles and applications," *International Journal of Machine Tools and Manufacture 50.4,* pp. 310-327, 2010.

[43] "Vee Block Design and Mounting Techniques for Kinematic Applications," Bal-tec, [Online]. Available: http://www.precisionballs.com/vee_block_design.php. [Accessed 3 11 2017].

[44] e. a. Ramesh Kumar P., "Variable Gain Super Twisting Controller for the Position Stabilization of Stewart Platform," in *Advances in Control and Optimization of Dynamical Systems*, Kanpur, Kanpur, India, 2014.

[45] D. Stewart, "A Platform with Six Degrees of Freedom," *Proceedings of the Institution of Mechanical Engineers,* vol. 180, no. 1, pp. 371-386, 1965.

[46] C. Switches, *8500 Series: Subminiature Pushbutton Switches.*

[47] K. R. Nolan, "Writing instrument". USA Patent US 3205863 A, 14 September 14 1965.

[48] engineerguy, Director, *How a Retractable Ballpoint Pen Works.* [Film]. YouTube, 2015.

[49] M. V. Company, "How Toggle Action Work," M.J. Vail Company, [Online]. Available: http://www.mjvail.com/destaco/intropage3.html. [Accessed 29 September 2017].

[50] "Geneva Drive," Wikipedia, [Online]. Available: https://en.wikipedia.org/wiki/Geneva_drive#/media/File:Geneva_drive.svg. [Accessed 29 September 2017].

[51] J. N. R.G. Budynas, Shigley's Mechanical Engineering Design, New York, NY: McGraw-Hill, 2015.

[52] Valvano, "Industrial Circuit Application Note: Stepper motor and driver selection," University of Texas.

[53] "Matweb," 2017. [Online]. Available: http://www.matweb.com/. [Accessed 3 11 2017].

[54] T. J. D. R. S. J. Y. S.I. Woods, "Emissivity of silver and stainless steel from 80 K to 300 K: Application," *Elsevier,* pp. 44-48, 2014.

[55] NIST, "Material Properties: G-10 CR (Fiberglass Epoxy)," Cryogenics Technologies Group, [Online]. Available: http://cryogenics.nist.gov/MPropsMAY/G-10%20CR%20Fiberglass%20Epoxy/G10CRFiberglassEpoxy_rev.htm.

[56] T. M. J. G. L. J. Y. S.I. Woods, "Cryogenic Emissivity Calibration of Highly Reflective Materials," National Institute of Standards and Technology.

[57] W. X. H. C. Y. H. Z. Xie, "Mechanical and thermal properties of 99% and 92% alumina at cryogenic temperatures," *Elsevier,* 2011.

[58] K. Timmerhaus, "Advances in Cryogenic Engineering," in *Proceedings of the 1966 Cryogenic Engineering Conference*, Boulder, Colorado, 1966.

[59] "Ice - Thermal Properties," Engineering Toolbox, 2017. [Online]. Available: https://www.engineeringtoolbox.com/ice-thermal-properties-d_576.html.

[60] "Emissivity Coefficients for some common Materials," Engineering Toolbox, 2017. [Online]. Available: https://www.engineeringtoolbox.com/radiation-heat-emissivity-d_432.html.

[61] C. Lim, "Indium seals for low-temperature and moderate-pressure applications," *Review of Scientific Instruments,* vol. 57, no. 108, 1986.

[62] D. a. Q. Y. Zhou, "Understanding Material Properties in Pharmaceutical Product Development and Manufacturing: Powder Flow and Mechanical Properties," *Journal of Validation Technology,* 2010.

[63] D. L. Smith, "The Effect of Cryogenic Treatment on the Fatigue Life of Chrome Silicon Steel Compression Springs," e-Publications@Marquette, 2009.

# Appendix A – System Requirements

Table 18: Requirements

| Europa Lander Docking and Sample Transfer Subsystem - Requirements Summary | | | | |
|---|---|---|---|---|
| **Field** | **Constraint** | **Requirement** | **Specification** | **Success Criteria Fulfilment** |
| **Basic Functional Capabilities** | *Robotic Arm Docking* | Subsystem shall provide a docking mechanism to secure the Robotic Arm/Sample Cup | Requires a mechanical locking dock mechanism | Test |
| | | | Requires electrical/mechanical docking detection and signal | Test |
| | | | Requires ability to release robotic arm and sample cup | Test |
| | | | Shall tolerate robotic arm accuracy of +/- 3 cm | Test |
| | *Container Gripping Mechanism* | Subsystem shall securely grip container to transfer sample | | Test |
| | *Volume Measurement Device* | Subsystem shall measure and verify volume of three containers per sample | Three sample volumes: 5cc, 1cc, 1cc to within +/- 5% | Test |
| | | | Assume a +10% -0% tolerance on the sample volume delivered | Test |
| | | Volume measurement shall not alter properties of sample | Consider effects of heat, compression | Test/Analysis |
| | *Sample Transfer Mechanism* | Subsystem shall transfer sample to three scientific instruments | Assume scientific instruments are linearly arranged and 20 cm apart | Test |
| **Performance Capabilities** | *Thermal Management* | Sample shall be kept within specified temperature range. | maximum of (<150 K, or 10 degrees above surface temperature) | Analysis |
| | | | shall be insulated from <40C vault | Analysis |
| | | Subsystem shall survive bake-out process | >125 C for 56 days | Analysis |
| | *Sample Handling* | Subsystem shall be able to properly handle a range of Europan sample materials | Assume <2mm size chips/grains | Test/Analysis |
| | *Autonomy* | Subsystem shall function entirely without user input | | Test |
| | | Subsystem shall respond to faults and errors without user input | | Test |
| | | Subsystem shall independently begin task when signaled | Signal - robotic arm triggers subsystem | Test |
| | *Purge Capability* | Subsystem shall be able to dispose of excess sample and/or unwanted samples | Samples shall not be dumped internal to the vault | Test |
| | Container Storage | Subsystem shall store all containers for sample transfer | | Test |
| | *Subsystem Life* | Subsystem shall perform task multiple times | 5 times | Test |
| | | Subsystem shall survive mission length | 20+ days | Analysis |
| | *Time* | Subsystem shall complete task in allocated time | 60-90 minutes | Test |
| **Environment** | *Temperature* | Subsystem shall be able to perform in Europan environment temperature range | 80 - 130 K | Analysis |
| | *Gravity* | Subsystem shall perform under Europan gravity | 1.35 m/s^2 (13.4% of Earth's gravity) | Analysis |
| | *Atmosphere* | Subsystem shall perform in Europan atmosphere | High Vacuum (0.1 μPa of O2) | Analysis |
| | *Radiation* | Subsystem shall perform in Europan high radiation environment | Electronics rated to 300 kRad | Recommendation |
| | *Corrosivity* | Subsystem shall not corrode in Europan environment | Materials shall be resistive to sulfiric acid (H2SO4) and magnesium sulfate (MgSO4) | Recommendation |
| | *Orientation* | Subsystem shall be tollerant of variable landing orientations | +/- 30 degrees from gravity vector | Test |
| **Physical Properties** | *Mass* | Subsystem must not exceed specified mass | 2 kg | Test |
| | *Structural* | System must survive vibration and loads from ascent and descent | Assume that system can have load locks in the design. | Test/Analysis |
| | *Connection* | Subsystem must securely mount to side of lander body | Assume this system will be mounted to a plate that bolts onto the lander vault | Test |
| | *Electrical* | Subsystem shall operate within voltage and current limits | 24 or 48 VDC | Test |
| | | | <1 amp | Test |
| | | Subsystem shall operate below energy allocation | 5% of 45 kWh (25% of 20% sample acquistion energy) | Test |